**Supporting Information for the article**

# Stabilization of the Pd-NHC framework with 1,2,4-triazol-5-ylidene ligands toward decomposition in alkaline media

Andrey Yu. Chernenko,[†] Alexander V. Astakhov,[†] Vadim V. Kutyrev,[†] Evgeniy G. Gordeev,[‡] Julia V. Burykina,[‡] Mikhail E. Minyaev,[‡] Victor N. Khrustalev,[‡] Victor M. Chernyshev,*[†] Valentine P. Ananikov*,[†,‡]

[†]Platov South-Russian State Polytechnic University (NPI), Prosvescheniya 132, Novocherkassk, 346428, Russia
[‡]Zelinsky Institute of Organic Chemistry, Russian Academy of Sciences, Leninsky Prospect 47, Moscow, 119991, Russia
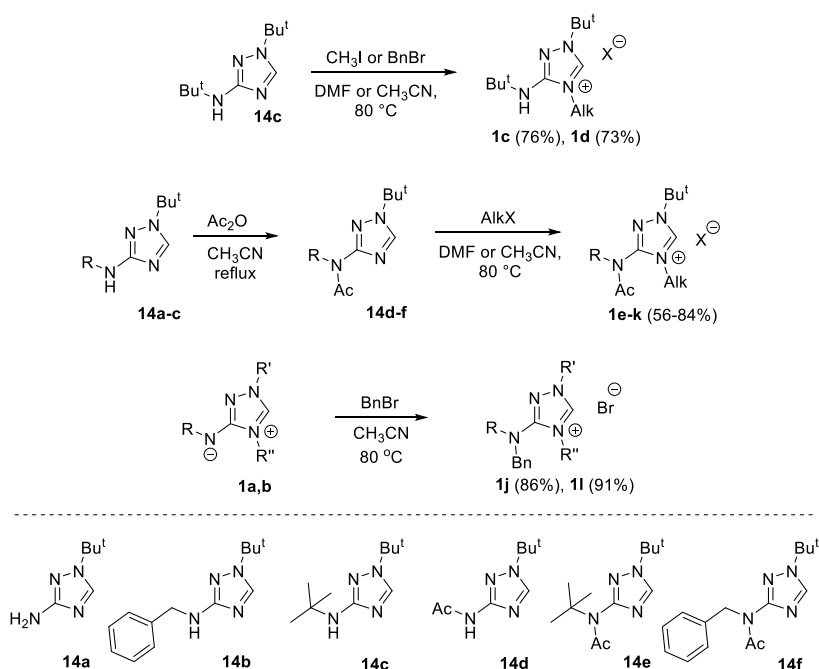*Corresponding authors: chern13@yandex.ru (Victor M. Chernyshev), val@ioc.ac.ru (Valentine P. Ananikov)*

## Table of contents

# S1. Additional experimental data on Pd/NHC complexes decomposition

## S1.1. Synthesis of new NHC-proligands 1a-l.

**Scheme S1.** Synthesis of NHC-proligands.



## S1.2. Explanatory notes to experimental studies of the reactions of Pd/NHC complexes with bases and additional experimental data.

**Clarification remarks on the procedure of $C_r$ determination by NMR in the studies of complexes 2a-j, 3a-c, 4a-c, 5a-d, 6 and 7 decomposition with strong bases**. Due to fast ligand exchange, starting complexes **2-7** in the presence of oxygen bases transform promptly into mixtures of Pd/NHC complexes via the substitution of halogen X, pyridine or amine coligands with base anions (Scheme 3, Scheme S2). To simplify quantitative determination of integral residual concentration ($C_r$) of Pd/NHC complexes by NMR, reaction mixtures after heating with bases were neutralized using appropriate pyridine·HX (in the case of **2, 5, 6** and **7**), HX solution (in the case of complexes **3**) or amine·HX salts (in the case of complexes **4**). According to NMR, various Pd/NHC complexes formed in the presence of bases were almost completely transformed into starting complexes (**2-7**) after neutralization. To corroborate the validity of the method, we performed model experiments that included treatment of complexes **2-7** with Bu$^t$OK at room temperature within 30 min – several hours, subsequent neutralization of the formed reaction mixtures, NMR analysis and isolation of residual Pd/NHC complexes. These model experiments confirmed predominantly recovering the starting complex (**2-7**) and afforded less than a 20% discrepancy between NMR and isolated yields. Moreover, discrepancies between NMR-determined initial concentrations of complexes **2-7** and their concentrations after base treatment within 10 min at room temperature and subsequent neutralization were less than 10% (the rate of Pd-NHC bond cleavage at room temperature was quite low). Therefore, we believe that the method used for quantitative NMR analysis of residual Pd/NHC concentrations can be accepted as reliable within ±20%.

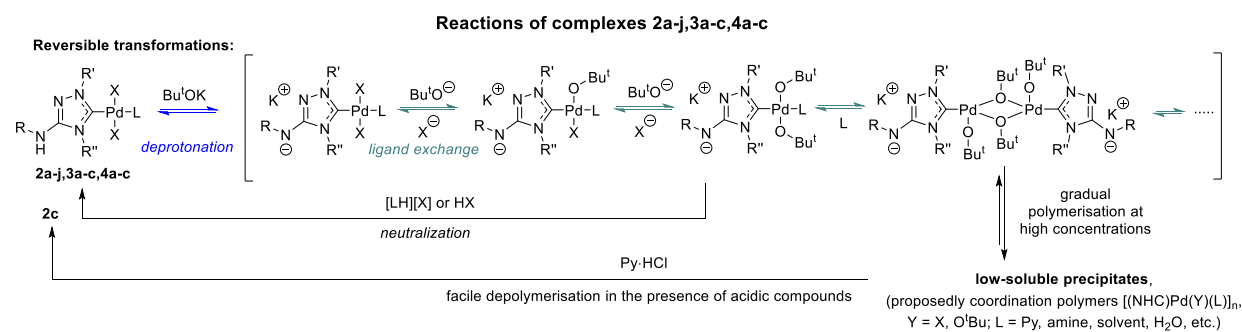**Table S1.** Stability of complexes **2b,5a** in the presence of various bases and in various solvents.[a]
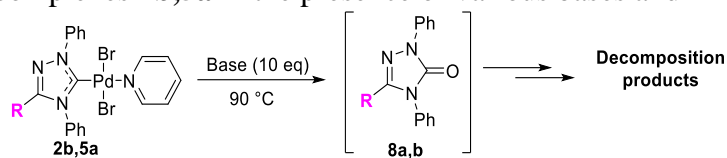


| Entry | Solvent | Base | $C_r^b$ of complex **2b** (R=PhNH) | | $C_r^b$ of complex **5a** (R=PhBnN) | |
|-------|---------|------|-----------|------------|-----------|------------|
| | | | 1 hours | 12 hours | 1 hours | 12 hours |
| 1. | DMSO | Bu$^t$OK | 90 | 52 | 36 | 0 |
| 2. | DMSO | Bu$^t$ONa | 92 | 85 | 45 | 0 |
| 3. | DMSO | KOH | 70 | 38 | 41 | 0 |
| 4. | DMSO | NaOH | 77 | 44 | 46 | 0 |
| 5. | DMSO | K$_2$CO$_3$ | 93 | 87 | 56 | 0 |
| 6. | dioxane | Bu$^t$OK | 60 | 36 | 26 | 0 |
| 7. | Py | Bu$^t$OK | 80 | 20 | 34 | 0 |
| 8. | PhMe | Bu$^t$OK | 81 | 55 | 53 | 0 |
| 9. | DMF | Bu$^t$OK | 4$^c$ | 0 | 15$^c$ | 0 |
| 10. | Pr$^i$OH | Bu$^t$OK | 0$^c$ | 0 | 0$^c$ | 0 |

[a] *Reaction conditions*: complex **2b,5a** (0.01 mmol), base (0.1 mmol), solvent (0.5 mL), heating at 90 °C within 1 or 12 h
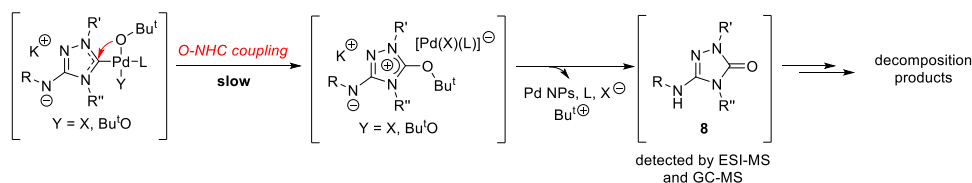
[b] Approximate values determined by NMR; see Section S1 for details.

[c] Nitron **1a** (from compound **2b**) and compound **1l** (from compound **5a**) were detected as the main decomposition products by HPLC and NMR.
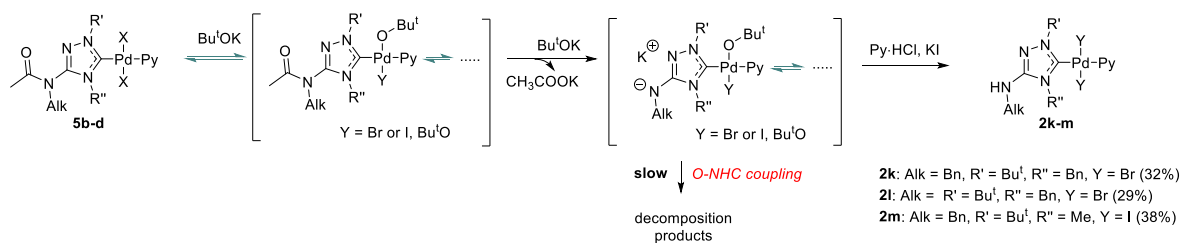
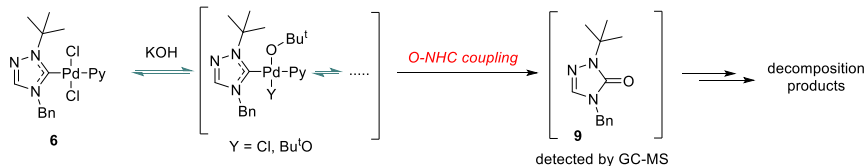**Scheme S2.** Transformations of complexes **2-7** in the presence of Bu$^t$OK in solutions.
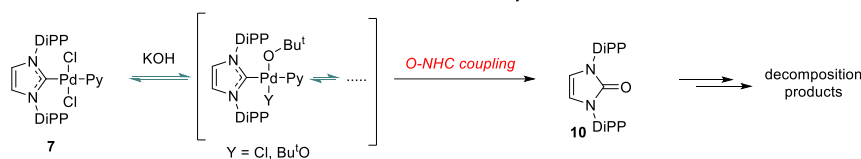
**Reactions of complexes 2a-j,3a-c,4a-c**

Reversible transformations:



Irreversible transformations:



**Reactions of complexes 5b-d**



**2k**: Alk = Bn, R' = Bu$^t$, R" = Bn, Y = Br (32%)
**2l**: Alk = R' = Bu$^t$, R" = Bn, Y = Br (29%)
**2m**: Alk = Bn, R' = Bu$^t$, R" = Me, Y = I (38%)

**Reactions of complex 6**



**Reactions of complex 7**
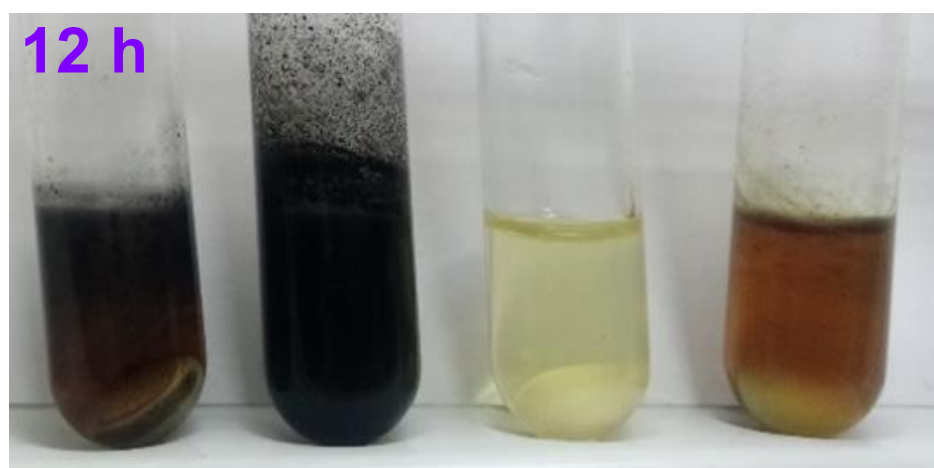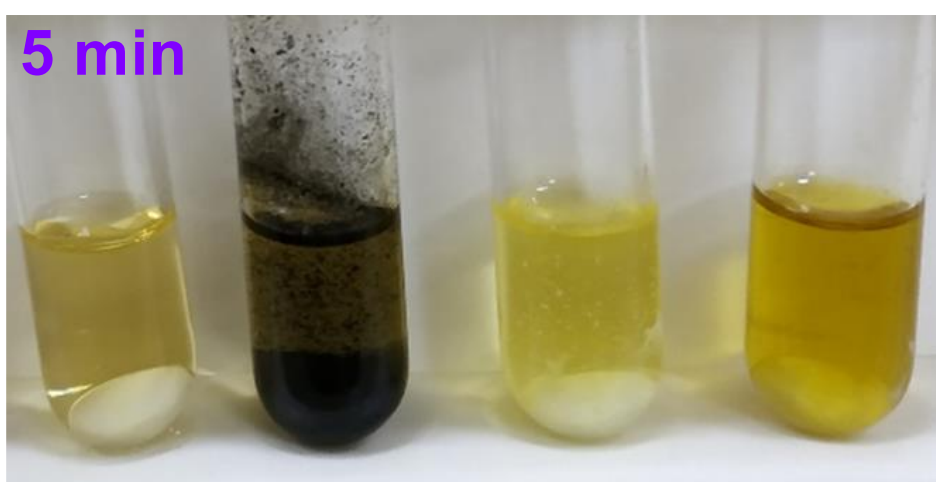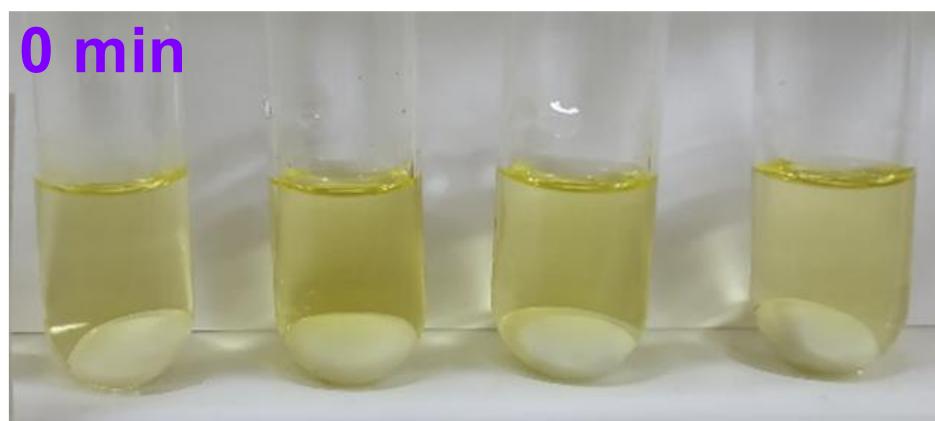
**Figure S1.** Photos of reaction mixtures after heating complexes **2a, c, 6** and **7** with Bu$^t$OK in DMSO at 90 °C.

### S1.3. Kinetic curves for the decomposition of complex 2a and triazolone 8a under the action of Bu$^t$ONa.

  Special kinetic experiments with the use of complex **2a** and an authentic sample of triazolone **8a** were performed to corroborate the instability of 3-RNH-substituted-1,2,4-triazol-5-ones, the anticipated products of the O-NHC coupling reaction, under the conditions of strong base-induced decomposition of Pd/NHC complexes (Figures S2 and S3).

  It was revealed that the yield of triazolone **8a** from complex **2a** has an extreme dependance on time. The yield of **8a** increases up to ~ 4-5% after 5-7 h and then decreases to trace values due to the further course of the reaction (Figure S2). In addition, it was observed that triazolone **8a** decomposes quite fast in the presence of Bu$^t$OK, and decomposition is accelerated significantly in the presence of Pd compounds (see, for example, kinetic curves in Figure S3).

  The experiments presented in Figures S2 and S3 corroborate the instability of triazolones, the products of O-NHC coupling, in conditions of strong base-induced decomposition of Pd/NHC complexes. Kinetic curves for the decomposition of complex **2a** (Figures S2) and for the decomposition of triazolone **8a** in the presence of PdCl$_2$Py$_2$ (Figure S3) demonstrate that the rates of both processes are comparable. These data explain the low yields of triazolones from complexes **2-5** in the studied reactions with strong bases.
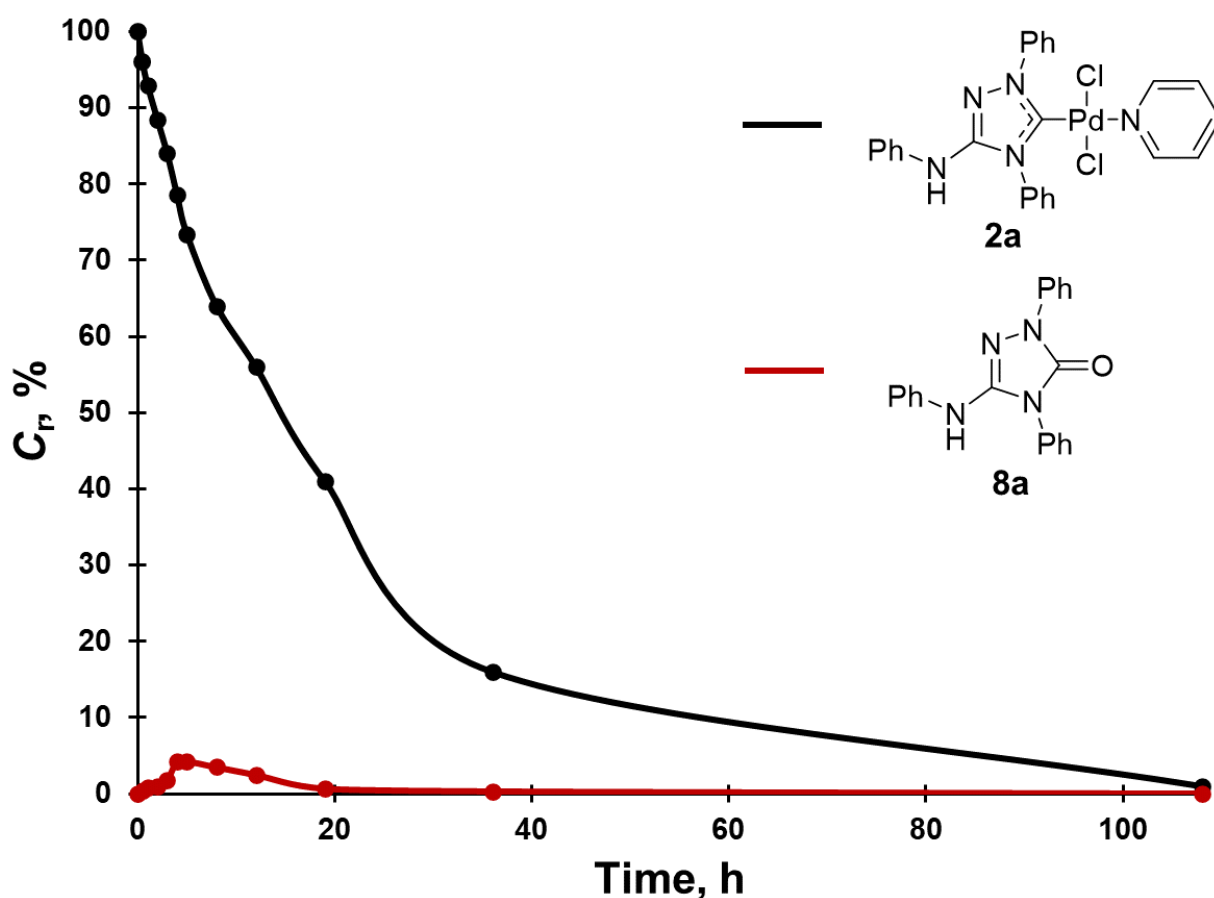


**Figure S2.** Kinetic curves for the decomposition of complex **2a** and the formation of azolone **8a** in the presence of Bu$^t$OK. $C_r$ is the observed residual concentration of the corresponding compound (relative to its initial concentration). *Reaction conditions*: complex **2a** (5.69 mg, 0.01 mmol), Bu$^t$OK (11.2 mg, 0.1 mmol), DMSO (0.5 mL), heating at 90 °C within 0.5-108 h, neutralization by pyridine hydrochloride (11.5 mg, 0.1 mmol) in CH$_3$CN (0.1 mL) and analysis by HPLC and GC-MS.
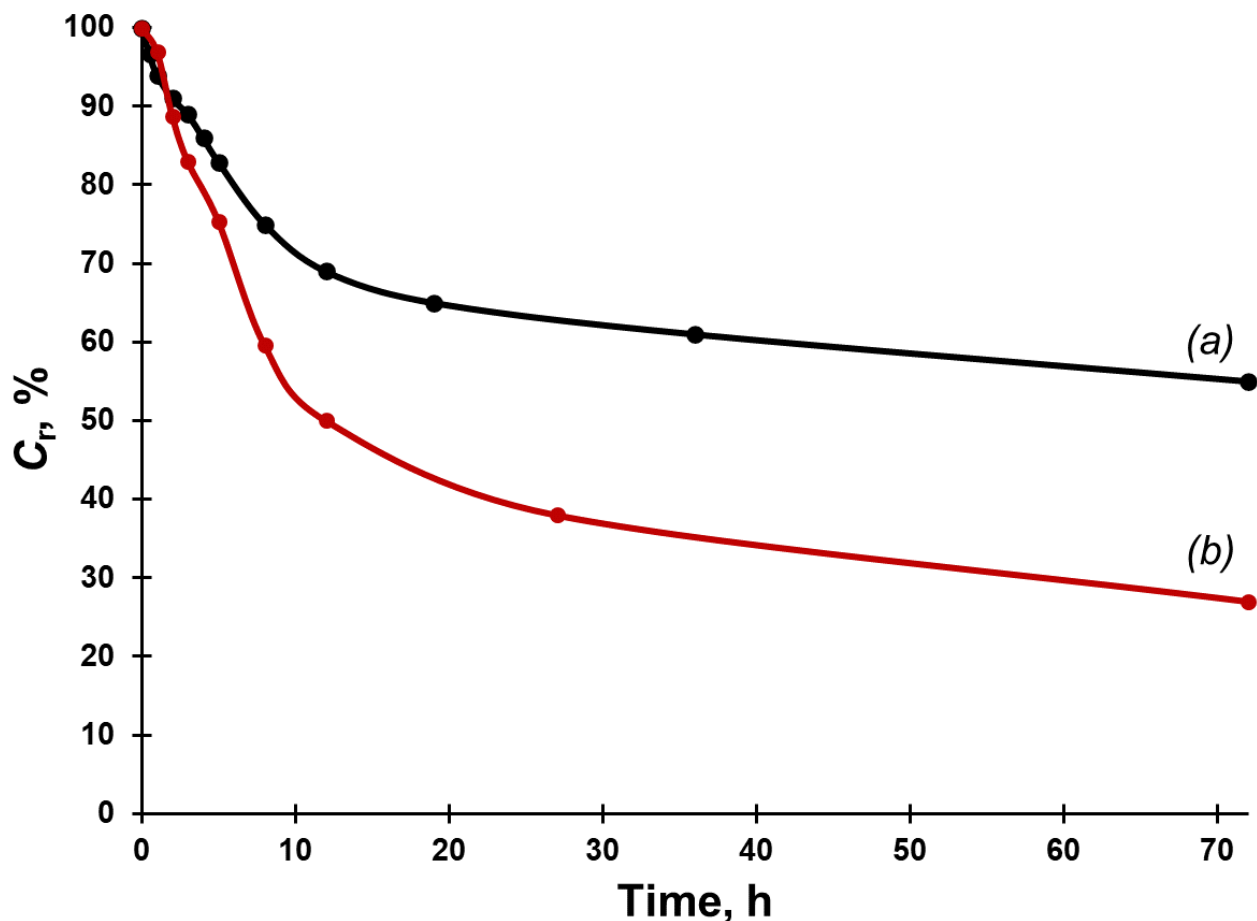
**Figure S3.** Kinetic curves for the decomposition of azolone **8a** upon heating with Bu$^t$OK in DMSO in the absence *(a)* and presence *(b)* of PdCl$_2$Py$_2$. $C_r$ is the observed residual concentration of **8a** (relative to its initial concentration). *Reaction conditions (a)*: azolone **8a** (3.3 mg, 0.01 mmol), Bu$^t$OK (11.2 mg, 0.1 mmol), naphthalene (internal standard, 0.64 mg, 0.005 mmol), DMSO (0.5 mL), heating at 90 °C within 1-72 h, neutralization by CH$_3$COOH (6 mg, 0.1 mmol) in CH$_3$CN (0.1 mL) and analysis by GC-MS. *Reaction conditions (b)*: azolone **8a** (3.3 mg, 0.01 mmol), PdCl$_2$Py$_2$ (3.3 mg, 0.01 mmol), other reagents and conditions were the same as in the *conditions (a)*.

**S1.4. ESI-MS studies of reaction mixtures formed in the reactions of Pd/NHC complexes with strong bases.**
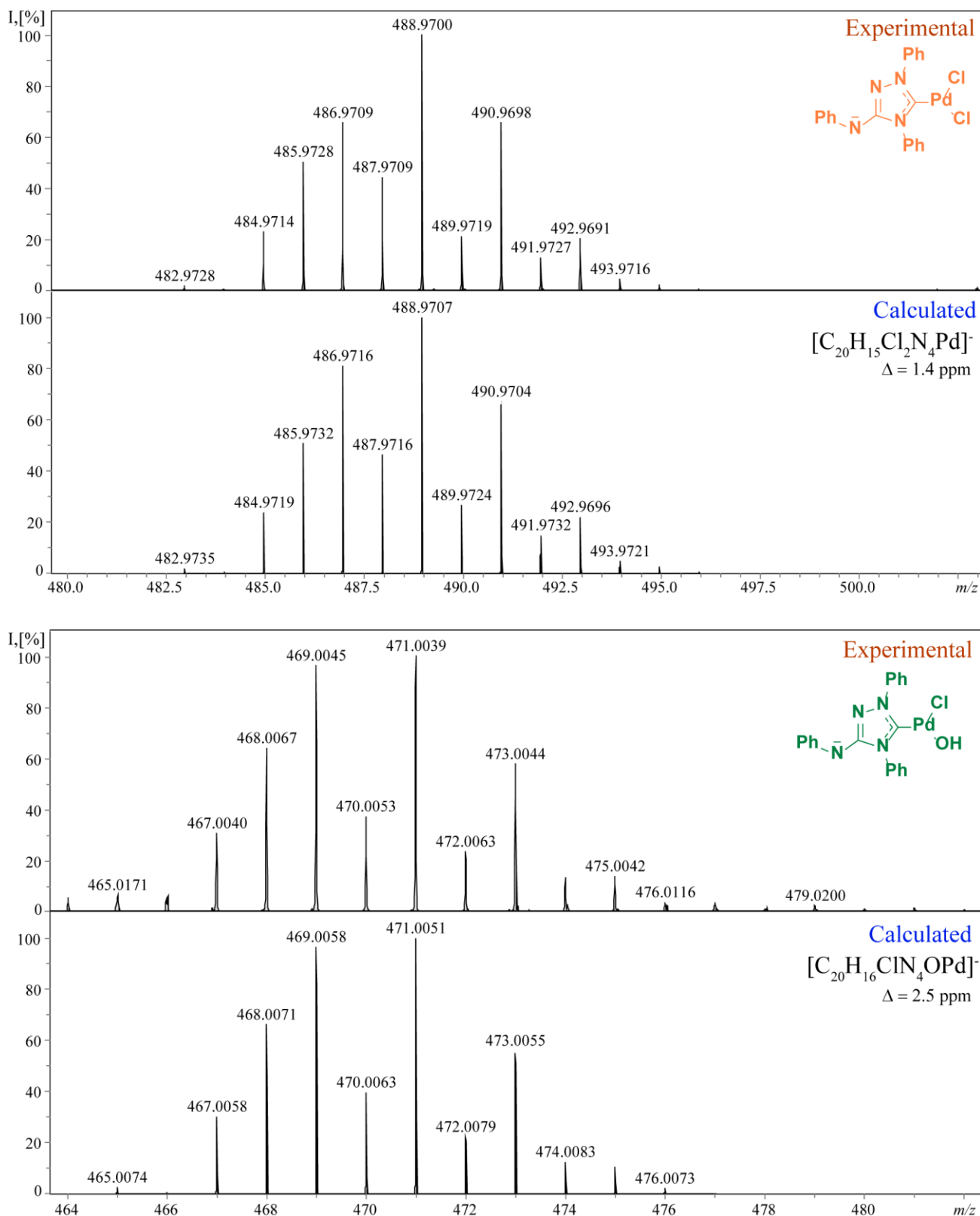


**Figure S4.** ESI-(-)MS spectra of various ionic forms of Pd(NHC)X$_2$ complexes formed in the reaction of compound **2a** with KOH in THF at 25 °C within 5 minutes.
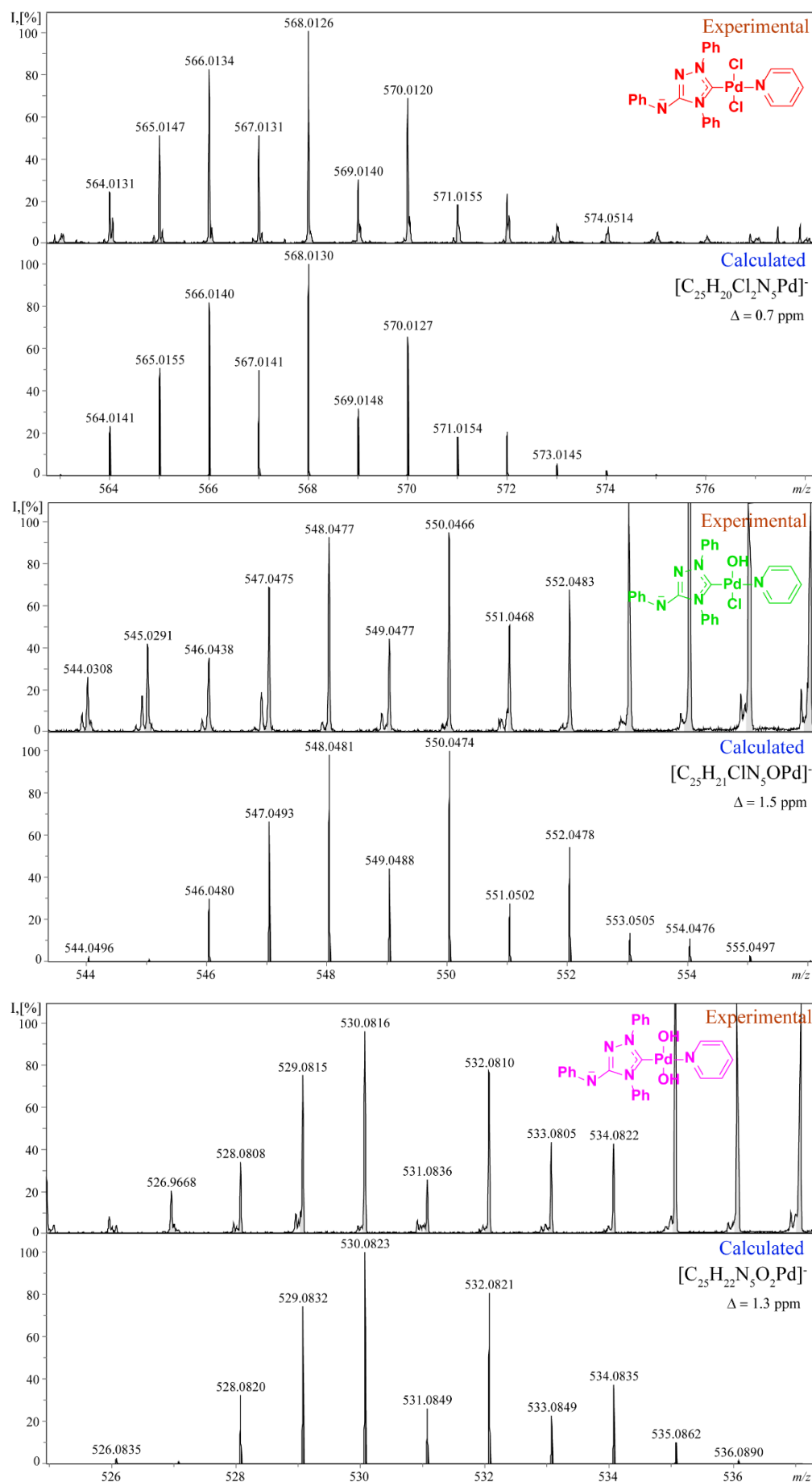
**Figure S5.** ESI-(-)MS spectra of various ionic forms of Pd(NHC)X₂Py complexes formed in the reaction of compound **2a** with KOH in THF at 25 °C within 5 minutes (a general comment for all ESI-MS spectra analyzed in the present study: only plausible identification of the ions may be suggested in the cases of signal overlap or low intensity).
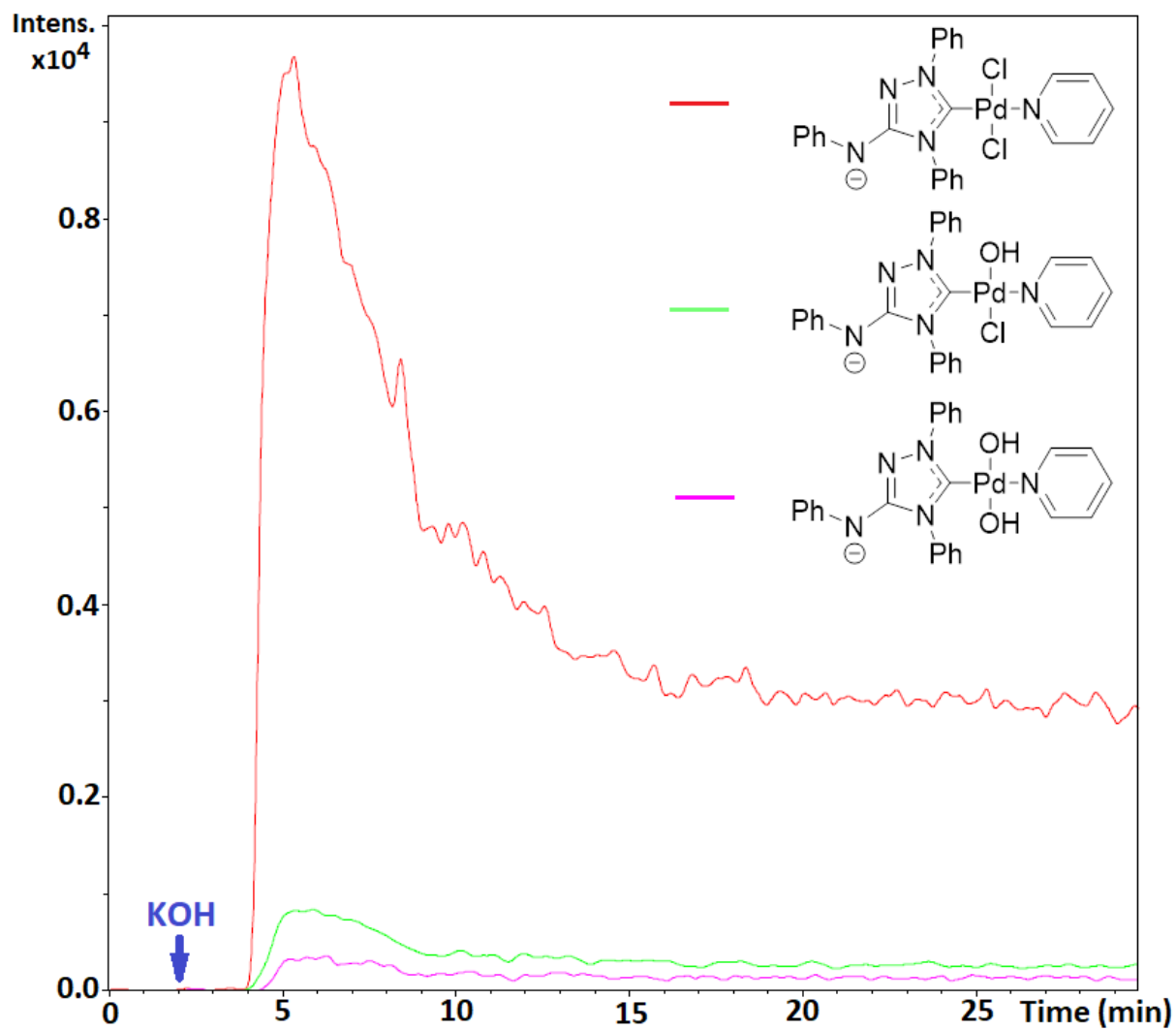
**Figure S6.** Real-time formation of various ionic forms of Pd(NHC)X₂Py complexes in the reaction of compound **2a** with KOH in THF at 25 °C. The KOH solution was added after 2 minutes.
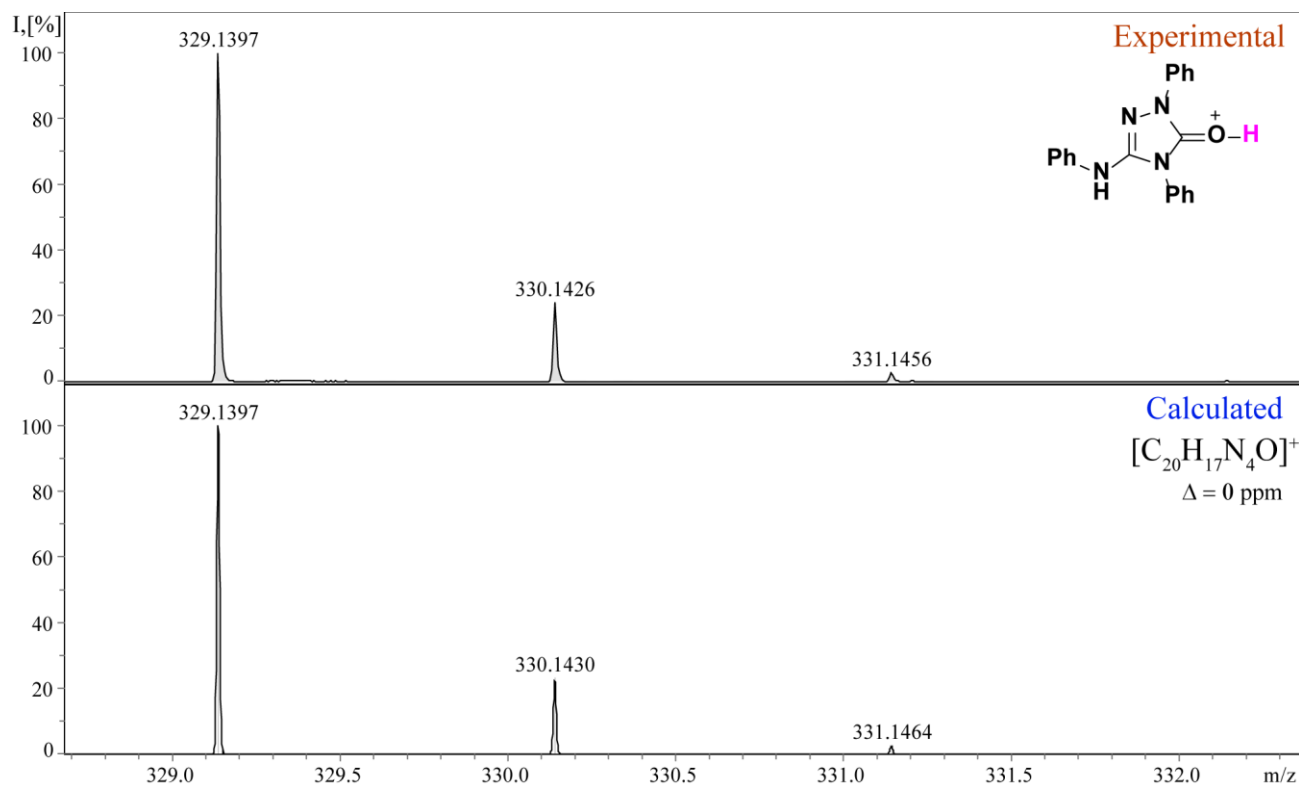
**Figure S7.** ESI-(+)MS spectrum of azolone **8a** detected in the reaction mixture after heating compound **3a** with Bu$^t$OK in DMSO at 90 °C within 60 minutes.
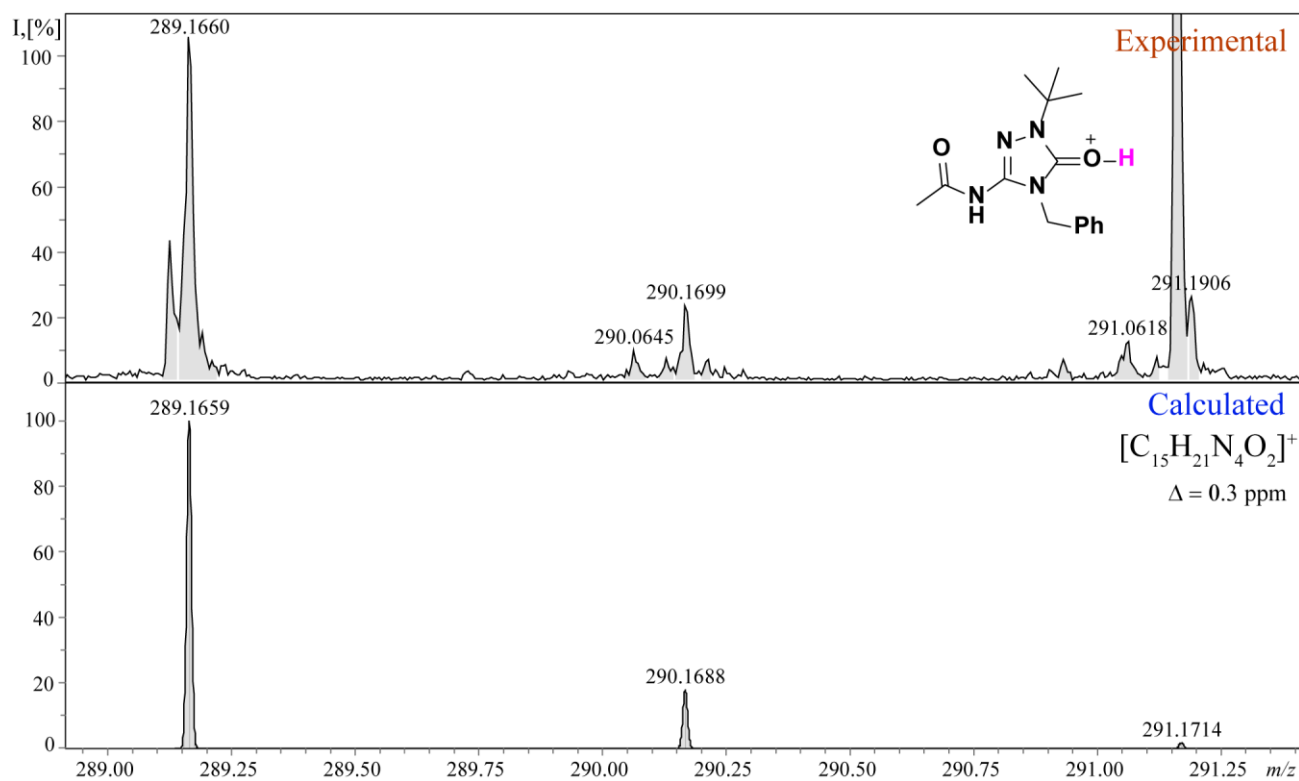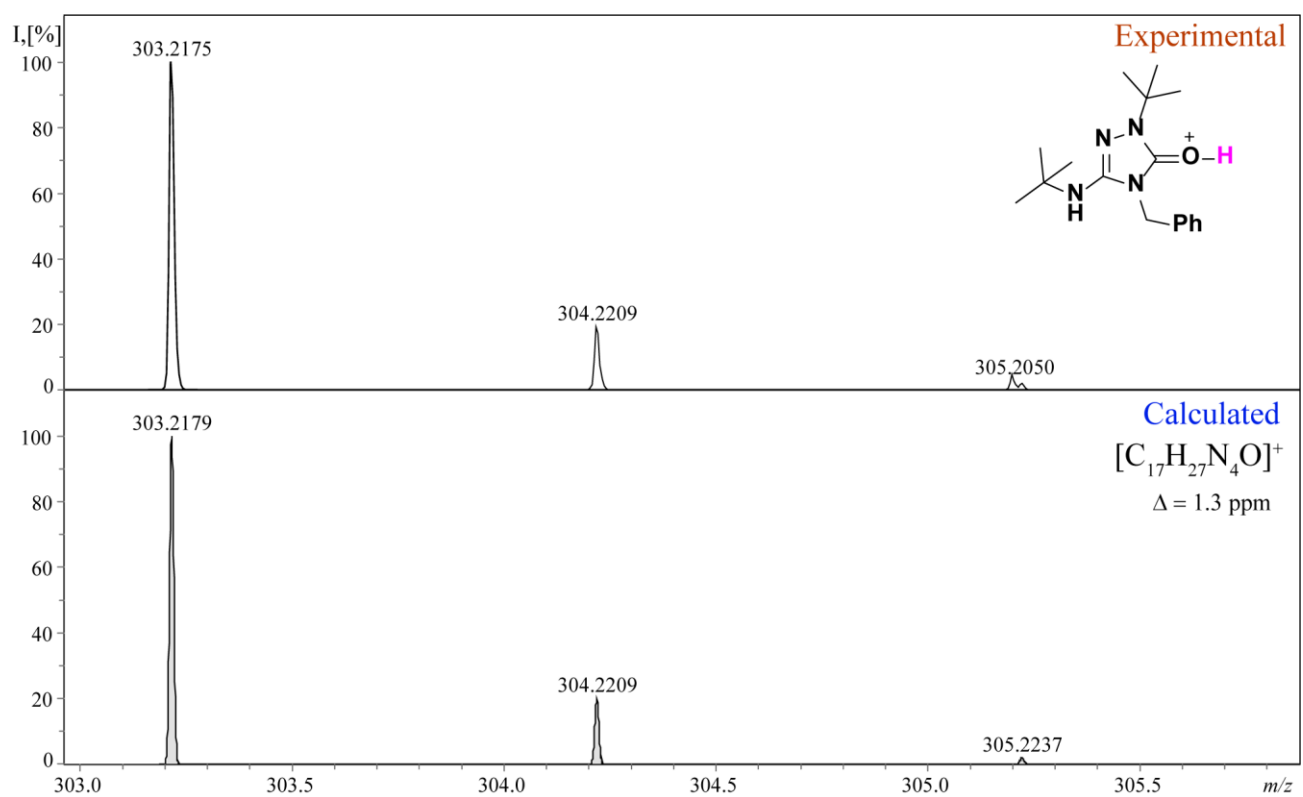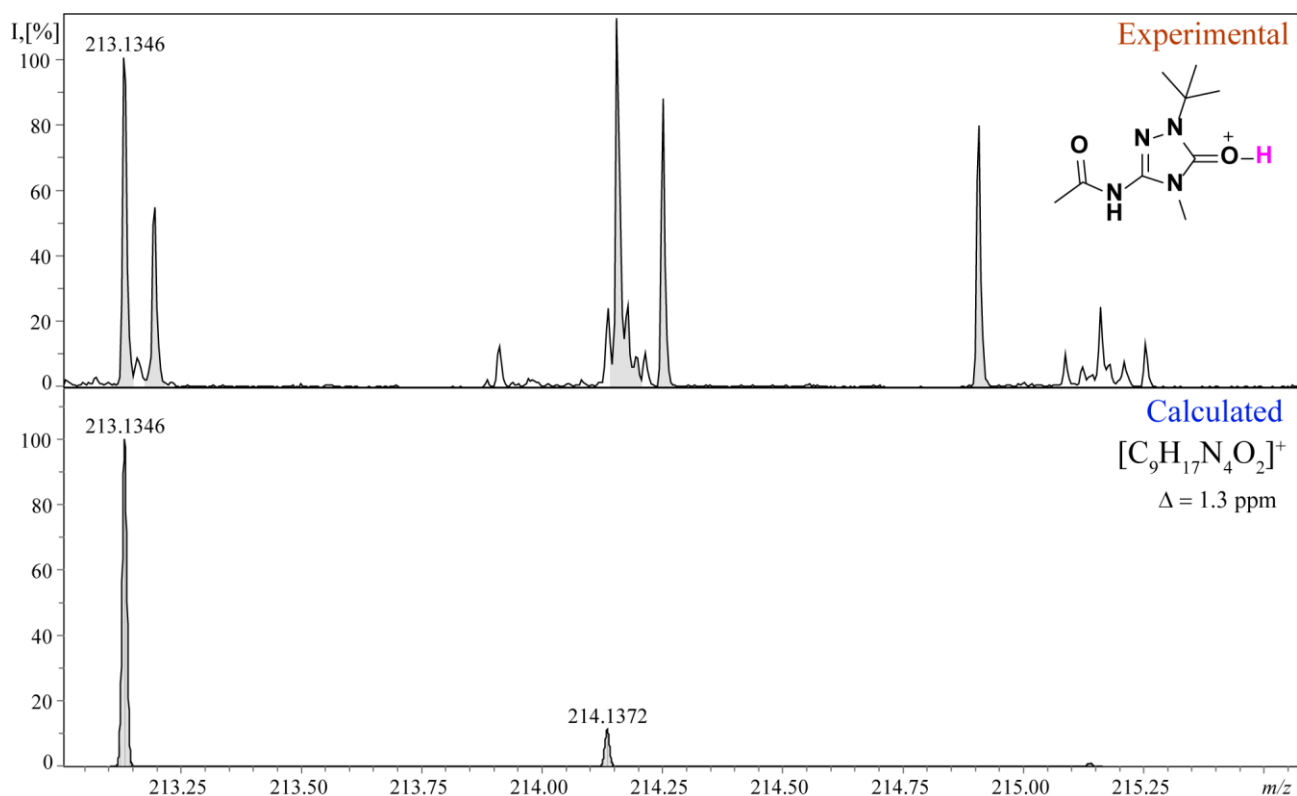


**Figure S8.** ESI-(+)MS spectrum azolone detected in the reaction mixture after heating compound **2c** with Bu$^t$OK in DMSO at 90 °C within 60 minutes.
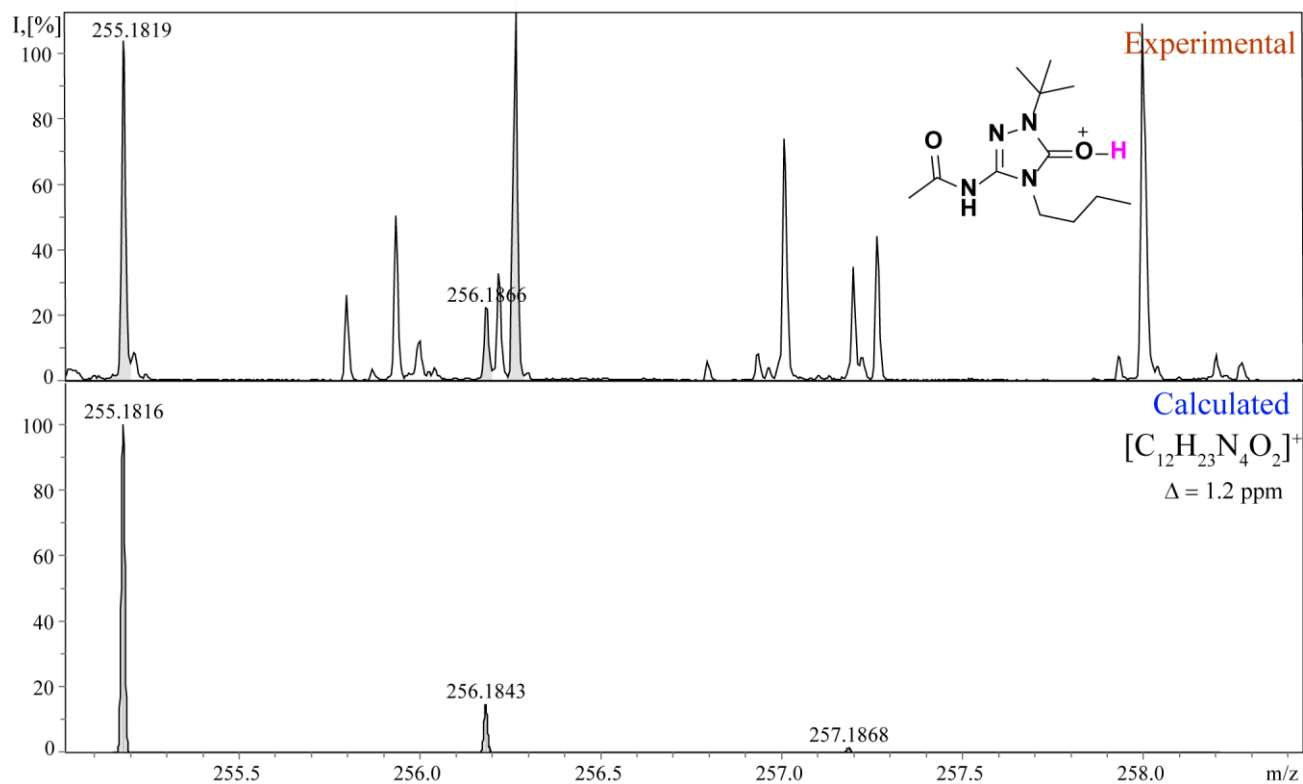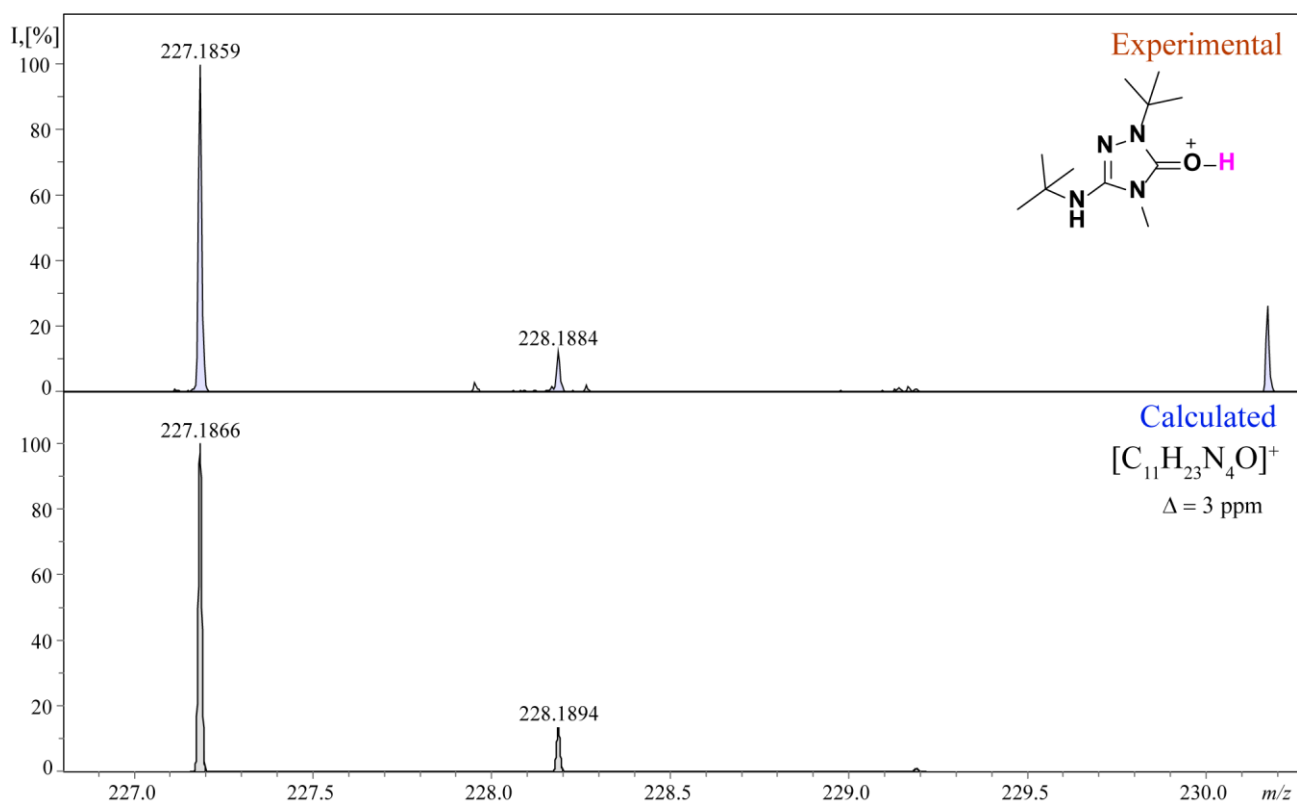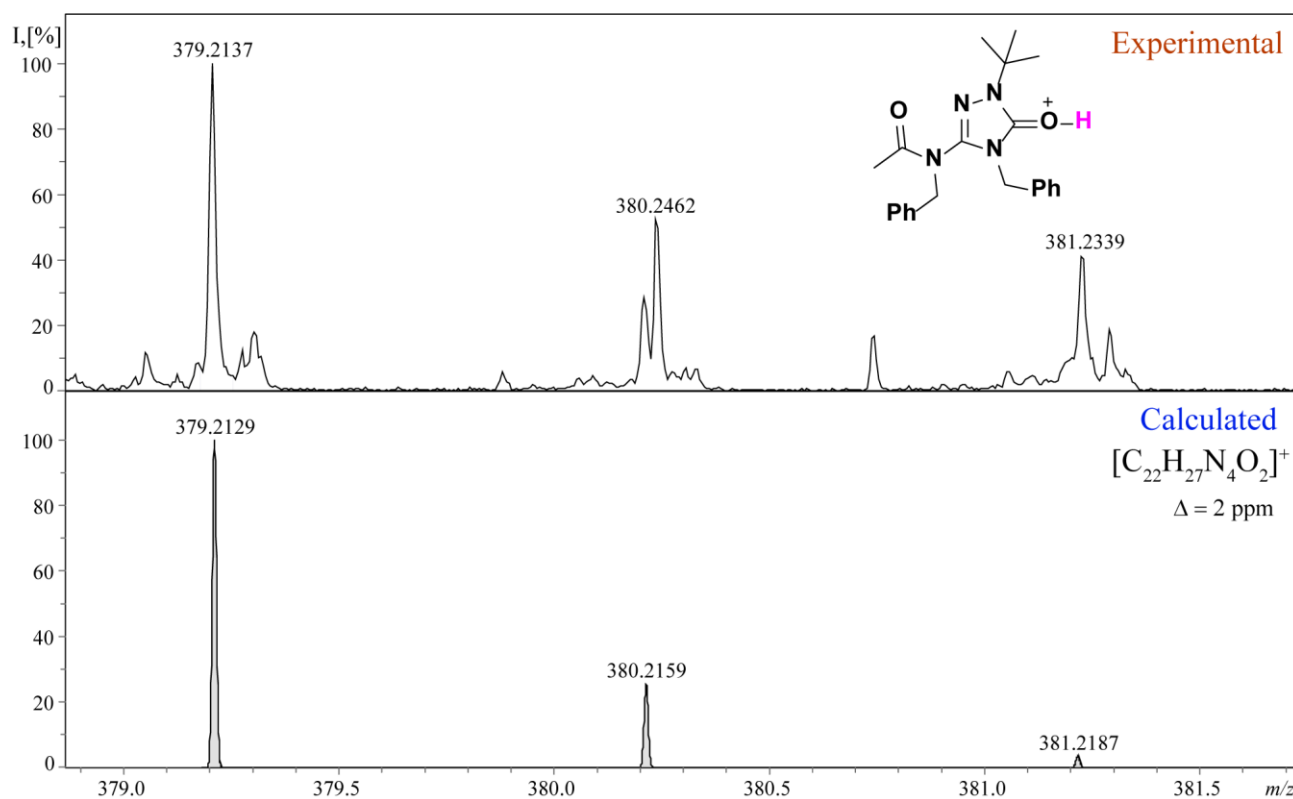
**Figure S9.** ESI-(+)MS spectrum of azolone detected in the reaction mixture after heating compound **2g** with Bu$^t$OK in DMSO at 90 °C within 60 minutes.



**Figure S10.** ESI-(+)MS spectrum of azolone detected in the reaction mixture after heating compound **2h** with Bu$^t$OK in DMSO at 90 °C within 60 minutes.
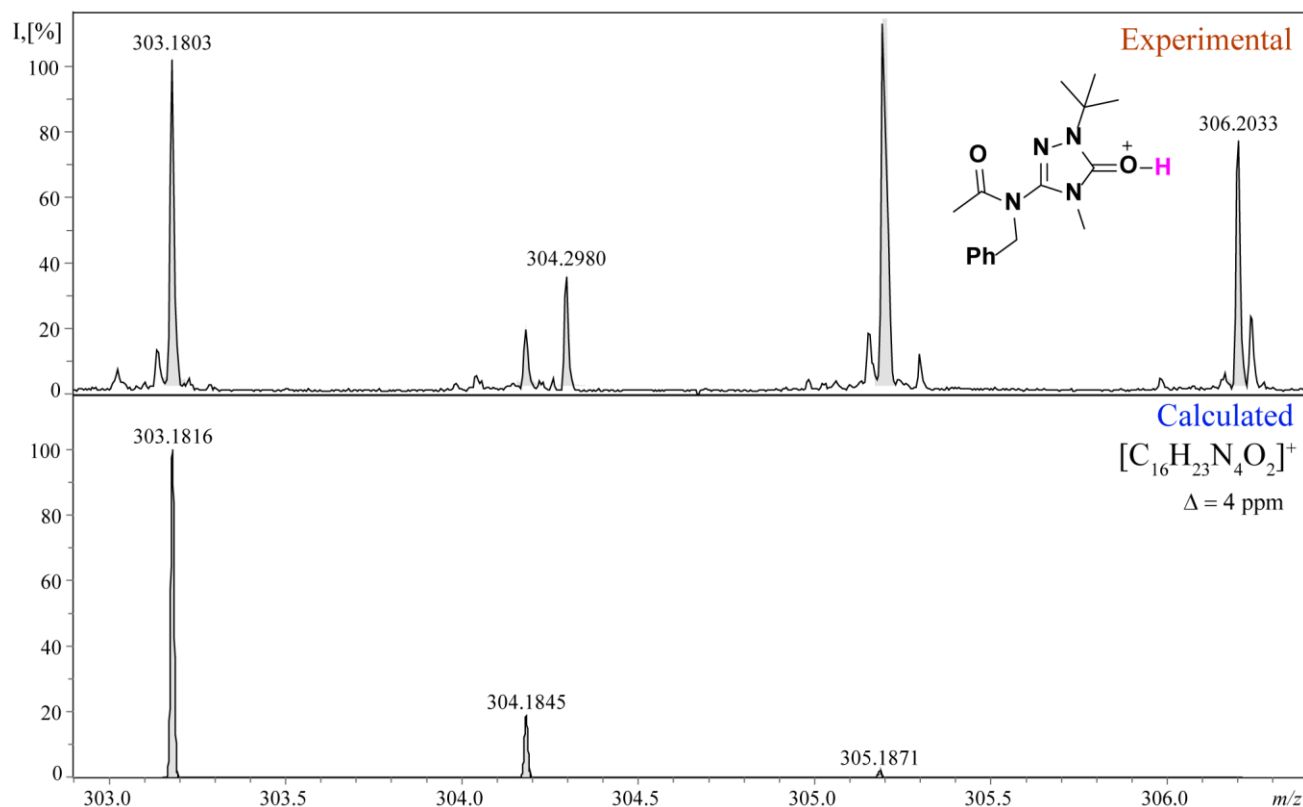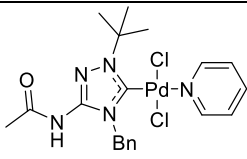
**Figure S11.** ESI-(+)MS spectrum of azolone detected in the reaction mixture after heating compound **2i** with Bu$^t$OK in DMSO at 90 °C within 60 minutes.



**Figure S12.** ESI-(+)MS spectrum of azolone detected in the reaction mixture after heating compound **4a** with Bu$^t$OK in DMSO at 90 °C within 60 minutes.

**Figure S13.** ESI-(+)MS spectrum of azolone detected in the reaction mixture after heating compound **5b** with Bu$^t$OK in DMSO at 90 °C within 60 minutes.
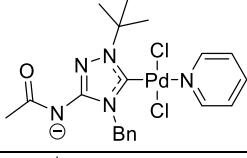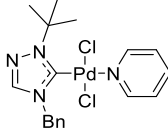


**Figure S14.** ESI-(+)MS spectrum of azolone detected in the reaction mixture after heating compound **5d** with Bu$^t$OK in DMSO at 90 °C within 60 minutes.
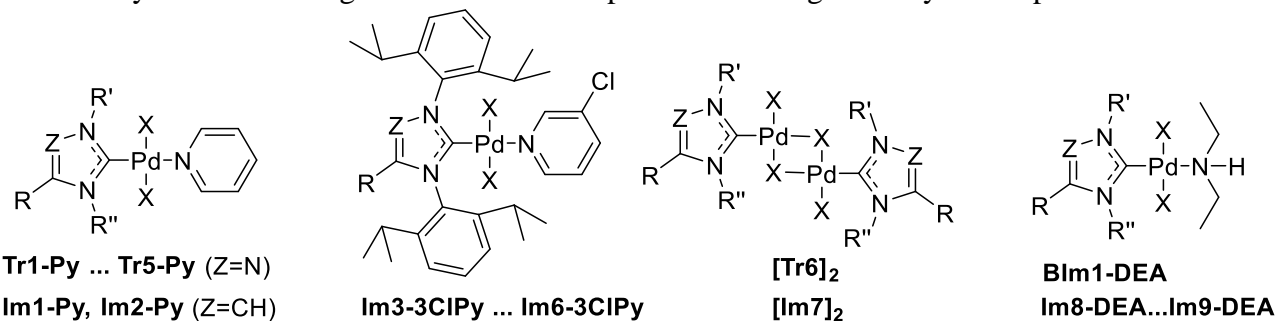
# S2. DFT calculations (additional data)

**Table S2**. Energies (kcal/mol) of Pd-L bond dissociation in complexes **2c**, **2c-an** and **6** at 298 K in vacuum, (U)PBE1PBE-D3BJ/def2-TZVP level.

| Complex | Dissociating L | $\Delta E$ | $\Delta H^{298}$ | $\Delta G^{298}$ |
|---|---|---|---|---|
| **2c** | **NHC** | **70.9** | **69.0** | **55.9** |
| | Py | 36.2 | 34.4 | 21.6 |
| | Cl$^-$ | 125.5 | 125.4 | 119.2 |
| **2c-an** | **NHC$^-$** | **81.9** | **79.9** | **66.7** |
| | Py | 28.2 | 26.6 | 13.7 |
| | Cl$^-$ | 65.7 | 65.6 | 59.4 |
| **6** | **NHC** | **74.1** | **72.1** | **57.2** |
| | Py | 36.5 | 34.7 | 21.8 |
| | Cl$^-$ | 131.3 | 131.1 | 124.4 |

**Figure S15.** Total energy (a) and free energy (b) profiles (in kcal mol$^{-1}$) of the O−NHC coupling calculated at the PBE1PBE-D3BJ/def2-TZVP level in DMSO (SMD).

# S3. Single crystal X-ray data

**Table S3.** Key Pd-L bond lengths in Pd/NHC complexes according to X-ray data reported in the literature



**Tr1-Py ... Tr5-Py** (Z=N)

**Im1-Py, Im2-Py** (Z=CH)

**Im3-3ClPy ... Im6-3ClPy**

**[Tr6]₂**

**[Im7]₂**

**BIm1-DEA**

**Im8-DEA...Im9-DEA**

| Comp. | R | Z | R' | R'' | X | $d$(Pd-NHC), Å | $d$(Pd-N), Å | Lit. |
|---|---|---|---|---|---|---|---|---|
| Tr1-Py | H | N | Bn | Bn | Cl | 1.974 | 2.098 | 1 |
| Tr2-Py | H | N | Me | Bu | Cl | 1.969 | 2.102 | 2 |
| Tr3-Py | H | N | Pr$^i$ | Et | Br | 1.958 | 2.094 | 3 |
| Tr4-Py | H | N | Pr$^i$ | Bn | Br | 1.951 | 2.092 | 4 |
| Tr5-Py | H | N | CH₂CONHBu$^t$ | Bn | Br | 1.945 | 2.099 | 4 |
| Im1-Py | H | CH | Bu$^t$ | 2MeO-Bn | Br | 1.953 | 2.100 | 5 |
| Im2-Py | H | CH | Bu$^t$ | Bn | Cl | 1.956 | 2.110 | 6 |
| Im3-3ClPy | NMe₂ | CH | DiPP | DiPP | Cl | 1.974 | 2.104 | 7 |
| Im4-3ClPy | NMe₂ | C-NMe₂ | DiPP | DiPP | Cl | 1.978 | 2.125 | 7 |
| Im5-3ClPy | N(Pr$^i$)₂ | CH | DiPP | DiPP | Cl | 1.972 | 2.105 | 8 |
| Im6-3ClPy | NMe₂ | C-Cl | DiPP | DiPP | Cl | 1.963 | 2.092 | 8 |
| [Tr6]₂ | H | N | Bu$^t$ | Bu | Br | 1.950 | — | 9 |
| [Im7]₂ | H | CH | Bu | Bu | Br | 1.977 | — | 9 |
| BIm1-DEA | benzene | | Me | Me | I | 1.944 | 2.124 | 10 |
| Im8-DEA | H | CH | Me | Me | I | 1.953 | 2.125 | 10 |
| Im9-DEA | H | CH | DiPP | DiPP | Cl | 1.988 | 2.128 | 11 |
| **2a** | PhNH | N | Ph | Ph | Cl | 1.949 | 2.105 | — |
| **2c** | AcNH | N | Bu$^t$ | Bn | Cl | 1.967 | 2.102 | — |
| **2i** | AcNH | N | Bu$^t$ | Me | I | 1.959 | 2.087 | — |
| **2j** | Bu$^t$NH | N | Bu$^t$ | Me | I | 1.972 | 2.090 | — |
| **3a** | Bu$^t$NH | N | Bu$^t$ | Me | I | 1.967 | — | — |
| **4a** | Bu$^t$NH | N | Bu$^t$ | Me | I | 1.983 | 2.138 | — |

# Literature

(1)      Astakhov, A. V.; Khazipov, O. V.; Chernenko, A. Y.; Pasyukov, D. V.; Kashin, A. S.; Gordeev, E. G.; Khrustalev, V. N.; Chernyshev, V. M.; Ananikov, V. P. A New Mode of Operation of Pd-NHC Systems Studied in a Catalytic Mizoroki–Heck Reaction. *Organometallics* **2017**, *36*, 1981-1992.

(2)      Chernenko, A. Y.; Astakhov, A. V.; Pasyukov, D. V.; Dorovatovskii, P. V.; Zubavichus, Y. V.; Khrustalev, V. N.; Chernyshev, V. M. Pd-PEPPSI complexes based on 1,2,4-triazol-3-ylidene ligands as efficient catalysts in the Suzuki—Miyaura reaction. *Russian Chemical Bulletin* **2018**, *67*, 79-84.

(3)      Kumar, A.; Gangwar, M. K.; Prakasham, A. P.; Mhatre, D.; Kalita, A. C.; Ghosh, P. Accessing a Biologically Relevant Benzofuran Skeleton by a One-Pot Tandem Heck Alkynylation/Cyclization Reaction Using Well-Defined Palladium N-Heterocyclic Carbene Complexes. *Inorganic Chemistry* **2016**, *55*, 2882-2893.

(4)      Dash, C.; Shaikh, M. M.; Ghosh, P. Fluoride-Free Hiyama and Copper- and Amine-Free Sonogashira Coupling in Air in a Mixed Aqueous Medium by a Series of PEPPSI-Themed Precatalysts. *European Journal of Inorganic Chemistry* **2009**, *2009*, 1608-1618.

(5)      Ray, L.; Shaikh, M. M.; Ghosh, P. Air-stable, convenient to handle Pd based PEPPSI (pyridine enhanced precatalyst preparation, stabilization and initiation) themed precatalysts of N/O-functionalized N-heterocyclic carbenes and its utility in Suzuki–Miyaura cross-coupling reaction. *Dalton Transactions* **2007**, 4546-4555.

(6)      Ray, S.; Mohan, R.; Singh, J. K.; Samantaray, M. K.; Shaikh, M. M.; Panda, D.; Ghosh, P. Anticancer and Antimicrobial Metallopharmaceutical Agents Based on Palladium, Gold, and Silver N-Heterocyclic Carbene Complexes. *Journal of the American Chemical Society* **2007**, *129*, 15042-15053.

(7)      Zhang, Y.; César, V.; Storch, G.; Lugan, N.; Lavigne, G. Skeleton Decoration of NHCs by Amino Groups and its Sequential Booster Effect on the Palladium-Catalyzed Buchwald–Hartwig Amination. *Angewandte Chemie International Edition* **2014**, *53*, 6482-6486.

(8)      Zhang, Y.; Lavigne, G.; Lugan, N.; César, V. Buttressing Effect as a Key Design Principle towards Highly Efficient Palladium/N-Heterocyclic Carbene Buchwald–Hartwig Amination Catalysts. *Chemistry – A European Journal* **2017**, *23*, 13792-13801.

(9)      Chernenko, A. Y.; Pasyukov, D. V.; Astakhov, A. V.; Tafeenko, V. A.; Chernyshev, V. M. Reactions of Pd-PEPPSI complexes with protic acids. *Russian Chemical Bulletin* **2018**, *67*, 1196-1201.

(10)     Khazipov, O. V.; Shevchenko, M. A.; Pasyukov, D. V.; Chernenko, A. Y.; Astakhov, A. V.; Tafeenko, V. A.; Chernyshev, V. M.; Ananikov, V. P. Preventing Pd–NHC bond cleavage and switching from nano-scale to molecular catalytic systems: amines and temperature as catalyst activators. *Catalysis Science & Technology* **2020**, *10*, 1228-1247.

(11)     Khazipov, O. V.; Shevchenko, M. A.; Chernenko, A. Y.; Astakhov, A. V.; Pasyukov, D. V.; Eremin, D. B.; Zubavichus, Y. V.; Khrustalev, V. N.; Chernyshev, V. M.; Ananikov, V. P. Fast and Slow Release of Catalytically Active Species in Metal/NHC Systems Induced by Aliphatic Amines. *Organometallics* **2018**, *37*, 1483-1492.

**X-ray crystallographic data and refinement details.**

X-ray diffraction data for **2a** and **2c** were collected at the 'Belok' beamline of the Kurchatov Synchrotron Radiation Source. In total, 360 (**2a**) and 720 (**2c**, using two different orientations for the crystal) frames were collected with an oscillation range of 1.0° in the $\varphi$ scanning mode. The semiempirical correction for absorption was applied using the *Scala* program [1]. The data were indexed and integrated using the utility *iMOSFLM* from the *CCP4* software suite [2, 3]. For details, see Table S4. The structures were solved by intrinsic phasing modification of direct methods [4] and refined by a full-matrix least-squares technique on $F^2$ with anisotropic displacement parameters for all nonhydrogen atoms. The *tert*-butyl substituent in **2c** is disordered over two sites with equal occupancies. The hydrogen atoms of the amino groups in **2c** were objectively localized in the difference-Fourier map and refined isotropically with fixed displacement parameters [$U_{iso}(H) = 1.2U_{eq}(N)$]. The other hydrogen atoms were placed in calculated positions and refined within the riding model with fixed isotropic displacement parameters [$U_{iso}(H) = 1.5U_{eq}(C)$ for the methyl groups and $1.2U_{eq}(C)$ for the other groups]. All calculations were carried out using the *SHELXL* program [5]. Although some properties of crystals make measurements difficult under standard conditions, the determined chemical structure of compound **2a** is beyond doubts.

X-ray diffraction data for **2i**, **2j**, **3a** and **4a** were collected on a Bruker Quest D8 diffractometer equipped with a Photon-III area detector (shutterless φ- and ω-scanning mode) using graphite-monochromatized Mo K$_\alpha$ radiation. The data collection was performed at 100 K for **2i**, **2j** and **3a** and at 150 K for **4a** due to crystal decay of the latter below 130 K. The intensity data of collected reflections were integrated by the *SAINT* program [6] and were semiempirically corrected for absorption and decay basing on measurements of equivalent reflections by the multiscan method implemented in the *SADABS* program [7]. The structures were solved by direct methods using the *SHELXT* program suit [4] and refined by the full-matrix least-squares method on $F^2$ using *SHELXL* [5]. All nonhydrogen atoms were refined with individual anisotropic displacement parameters. Positions of all amino H-atoms were found from electron density-difference maps (e-maps); these atoms were refined with individual isotropic displacement parameters. The position of H4 in **4a** was restrained at a distance of 0.85(4) Å from N4. All other hydrogen atoms were also found from the e-maps (with the exception of the disordered CH$_2$Cl$_2$ molecule in **3a**) but were placed in ideal calculated positions (C-H distance = 0.950 Å for aromatic, 0.980 Å for methyl, and 0.990 Å for methylene hydrogen atoms) and refined as riding atoms with relative isotropic displacement parameters ($U_{iso}(H)=1.5 U_{eq}(C)$ for methyl, $1.2 U_{eq}(C)$ for other hydrogen atoms). A rotating group model was applied for methyl groups. Crystal channels in **3a** contained a disordered noncoordinating hexane molecule and a disordered unidentified solvent molecule both located at the same place and having partial occupancies; these molecules were removed by the *SQUEEZE* method [8] implemented in the *PLATON* program [9].

Crystal data, data collection and structure refinement details are summarized in Table S4. The *Mercury* program [10] was used for molecular graphics in the manuscript, and the *SHELXTL* program suite [6] was used for molecular graphics herein. Crystallographic data for **2a, 2c, 2i, 2j, 3a** and **4a** have been deposited with the Cambridge Crystallographic Data Center; the CCDC numbers are 2074482, 2074483, 2074560-2074563, respectively. The supplementary crystallographic data can be obtained free of charge from the Cambridge Crystallographic Data Centre *via* https://www.ccdc.cam.ac.uk/structures/.

**References**

[1] Evans, P. Scaling and assessment of data quality. *Acta Crystallogr.* **2006**, *D62*, 72-82.

[2] Battye, T.G.G.; Kontogiannis, L.; Johnson, O.; Powell, H.R.; Leslie, A.G.W. iMOSFLM: a new graphical interface for diffraction-image processing with MOSFLM. *Acta Crystallogr.* **2011**, *D67*, 271-281.

[3]     Winn, M.D.; Ballard, C.C.; Cowtan, K.D.; Dodson, E.J.; Emsley, P.; Evans, P.R.; Keegan, R.M.; Krissinel, E.B.; Leslie, A.G.W.; McCoy, A.; McNicholas, S.J.; Murshudov, G.N.; Pannu, N.S.; Potterton, E.A.; Powell, H.R.; Read, R.J.; Vagin, A.; Wilson, K.S. Overview of the CCP4 suite and current developments. *Acta Crystallogr.* **2011**, *D67*, 235-242.

[4]     Sheldrick, G.M. SHELXT - Integrated space-group and crystal-structure determination. *Acta Crystallogr.* **2015**, *A71*, 3-8.

[5]     Sheldrick, G.M. Crystal structure refinement with SHELXL. *Acta Crystallogr.* **2015**, *C71*, 3-8.

[6]     Bruker. APEX-III. *Bruker AXS Inc.*, Madison, Wisconsin, USA, **2019**.

[7]     Krause, L.; Herbst-Irmer, R.; Sheldrick, G.M.; Stalke, D. Comparison of silver and molybdenum microfocus X-ray sources for single-crystal structure determination. *J. Appl. Crystallogr.* **2015**, *48*, 3-10.

[8]     Spek, A.L. PLATON SQUEEZE: a tool for the calculation of the disordered solvent contribution to the calculated structure factors. *Acta Crystallogr.*, **2015**, *C71*, 9-18.

[9]     Spek, A. L. Structure validation in chemical crystallography. *Acta Crystallogr.*, **2009**, *D65*, 148-155.

[10]     Macrae, C.F.; Sovago, I.; Cottrell, S.J.; Galek, P.T.A.; McCabe, P.; Pidcock, E.; Platings, M.; Shields, G.P.; Stevens, J.S.; Towler, M.; Wood, P.A. Mercury 4.0: from visualization to analysis, design and prediction. *J. Appl. Crystallogr.*, **2020**, *53*, 226-235.

**Table S4**. Crystal data, data collection and structure refinement details.

| Compound | 2a | 2c | 2i | 2j | 3a | 4a |
|---|---|---|---|---|---|---|
| Empirical formula | $C_{25}H_{21}Cl_2N_5Pd$ | $C_{20}H_{25}Cl_2N_5OPd$ | $C_{14}H_{21}I_2N_5OPd$ | $C_{16}H_{27}I_2N_5Pd$ | $C_{22}H_{44}I_4N_8Pd_2 \cdot CH_2Cl_2$ | $C_{15}H_{33}I_2N_5Pd$ |
| Formula weight | 568.77 | 528.75 | 635.56 | 649.62 | 1225.98 | 643.66 |
| Temperature (K) | 200(2) | 100(2) | 100(2) | 100(2) | 100(2) | 150(2) K |
| Wavelength (Å) | 0.96600 | 0.80246 | 0.71073 | 0.71073 | 0.71073 | 0.71073 Å |
| Crystal system | Triclinic | Monoclinic | Monoclinic | Monoclinic | Orthorhombic | Monoclinic |
| Space group | P $\bar{1}$ | C2/c | P2$_1$/c | P2$_1$/c | Pbca | P2$_1$/c |
| Unit cell dimensions | | | | | | |
| a (Å) | 10.187(2) | 15.332(3) | 15.1906(5) | 20.4176(3) | 15.1329(14) | 20.0160(5) |
| b (Å) | 15.370(3) | 9.4559(19) | 15.3783(5) | 11.1135(2) | 22.941(2) | 11.7895(3) |
| c (Å) | 15.567(3) | 31.070(6) | 8.6698(3) | 10.0749(2) | 24.370(2) | 9.9197(3) |
| α (°) | 81.04(3) | 90 | 90 | 90 | c | 90 |
| β (°) | 84.72(3) | 91.70(3) | 92.3454(6) | 103.2749(5) | 90 | 94.5118(10) |
| γ (°) | 82.80(3) | 90 | 90 | 90 | 90 | 90 |
| Volume (Å$^3$) | 2382.1(8) | 4502.5(15) | 2023.62(12) | 2225.02(7) | 8460.4(14) | 2333.58(11) |
| Z | 4 | 8 | 4 | 4 | 8 | 4 |
| Calcd density (g/cm$^3$) | 1.586 | 1.560 | 2.086 | 1.939 | 1.925 | 1.832 |
| μ (mm$^{-1}$) | 2.340 | 1.486 | 3.978 | 3.617 | 3.919 | 3.447 |
| F(000) | 1144 | 2144 | 1200 | 1240 | 4624 | 1240 |
| Crystal size (mm) | 0.18×0.15×0.12 | 0.30×0.25×0.25 | 0.57×0.48×0.10 | 0.47×0.22×0.09 | 0.51×0.16×0.13 | 0.58×0.47×0.31 |
| θ range (°) | 2.379 to 36.372 | 3.387 to 30.870 | 2.684 to 31.535 | 2.100 to 33.179 | 2.322 to 29.500 | 2.006 to 25.997 |
| Index ranges | -10<=h<=10 -18<=k<=18 -19<=l<=19 | -19<=h<=19 -12<=k<=12 -39<=l<=39 | -22<=h<=22 -22<=k<=22 -12<=l<=12 | -31<=h<=31 -17<=k<=17 -15<=l<=15 | -20<=h<=20 -31<=k<=31 -33<=l<=33 | -24<=h<=24 -14<=k<=14 -12<=l<=12 |
| Reflections | | | | | | |
| collected | 58909 | 30928 | 94365 | 105746 | 118510 | 46494 |
| independent [$R_{int}$] | 7824 [0.0781] | 4851 [0.0715] | 6741 [0.0205] | 8492 [0.0229] | 11772 [0.0699] | 4581 [0.0256] |
| observed [with I>2σ(I)] | 6585 | 4779 | 6716 | 8254 | 8524 | 4437 |
| Completeness to $\theta_{full}$ / $\theta_{max}$ | 0.869 / 0.847 | 0.983 / 0.983 | 0.997 / 0.998 | 0.998 / 0.998 | 0.999 / 0.999 | 0.999 / 0.999 |
| Transmission $T_{min}$ / $T_{max}$ | 0.753 / 0.654 | 0.670 / 0.630 | 0.0341 / 0.0077 | 0.2694 / 0.1583 | 0.0333 / 0.0086 | 0.0638 / 0.0210 |
| Data / restraints / parameters | 7824 / 0 / 602 | 4851 / 6 / 267 | 6741 / 0 / 217 | 8492 / 0 / 228 | 11772 / 11 / 387 | 4581 / 1 / 226 |
| Goodness-of-fit on $F^2$ | 1.067 | 1.051 | 1.229 | 1.210 | 1.030 | 1.049 |
| R1 / wR2 indices [I>2σ(I)] | 0.0418 / 0.1098 | 0.0699 / 0.1659 | 0.0337 / 0.0832 | 0.0173 / 0.0395 | 0.0375, 0.0777 | 0.0331, 0.0707 |
| R1 / wR2 indices [all data] | 0.0532 / 0.1260 | 0.0704 / 0.1662 | 0.0338 / 0.0833 | 0.0182 / 0.0400 | 0.0633, 0.0923 | 0.0340, 0.0713 |
| Δρ$_{max}$ / Δρ$_{min}$ (e•Å$^{-3}$) | 0.676 / -0.907 | 1.170 / -2.170 | 2.395 / -1.446 | 0.711 / -1.154 | 0.999 / -0.798 | 2.487 / -2.185 |
| Extinction coefficient | 0.0047(3) | 0.0031(3) | - | - | - | 0.00112(9) |
| CCDC deposition number | 2074482 | 2074483 | 2074560 | 2074561 | 2074562 | 2074563 |

**The structure of 2a.**



(**1**)

(**2**)
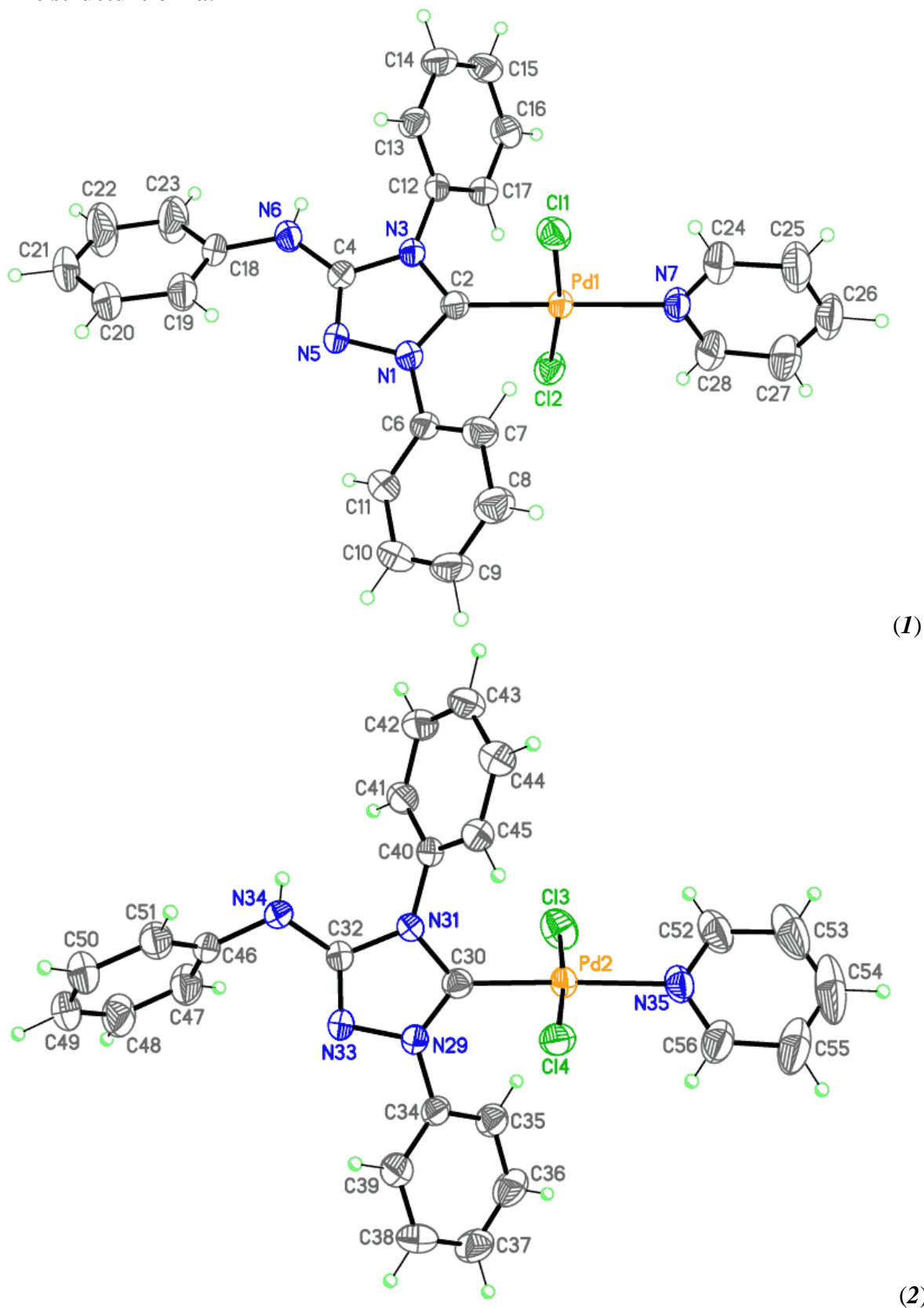
**Figure S16.** The structures of two crystallographically nonequivalent molecules (**1** and **2**) of **2a**. Displacement ellipsoids are drawn at the 50% probability level.

**Table S5**. Selected bond distances for **2a** (Å).

| | | | | | |
|---|---|---|---|---|---|
| Pd(1)-Cl(1) | 2.3011(12) | C(6)-C(11) | 1.381(5) | C(18)-C(19) | 1.383(6) |
| Pd(1)-Cl(2) | 2.3231(12) | C(7)-C(8) | 1.393(6) | C(18)-C(23) | 1.394(6) |
| Pd(1)-C(2) | 1.950(4) | C(8)-C(9) | 1.373(6) | C(19)-C(20) | 1.382(6) |
| Pd(1)-N(7) | 2.146(3) | C(9)-C(10) | 1.380(7) | C(20)-C(21) | 1.376(7) |
| N(1)-C(2) | 1.324(5) | C(10)-C(11) | 1.388(6) | C(21)-C(22) | 1.377(8) |
| N(1)-N(5) | 1.394(4) | C(12)-C(17) | 1.377(5) | C(22)-C(23) | 1.370(7) |
| N(1)-C(6) | 1.429(5) | C(12)-C(13) | 1.387(5) | N(7)-C(28) | 1.330(5) |
| C(2)-N(3) | 1.359(5) | C(13)-C(14) | 1.387(6) | N(7)-C(24) | 1.330(6) |
| N(3)-C(4) | 1.390(4) | C(14)-C(15) | 1.367(6) | C(24)-C(25) | 1.381(6) |
| N(3)-C(12) | 1.437(4) | C(15)-C(16) | 1.386(6) | C(25)-C(26) | 1.373(7) |
| C(4)-N(5) | 1.304(5) | C(16)-C(17) | 1.382(5) | C(26)-C(27) | 1.352(7) |
| C(4)-N(6) | 1.356(5) | N(6)-C(18) | 1.408(5) | C(27)-C(28) | 1.382(6) |
| C(6)-C(7) | 1.377(6) | N(6)-H(4) | 0.84(4) | | |
| Pd(2)-Cl(3) | 2.2931(13) | C(34)-C(39) | 1.388(5) | C(46)-C(51) | 1.376(6) |
| Pd(2)-Cl(4) | 2.3251(12) | C(35)-C(36) | 1.392(6) | C(46)-C(47) | 1.376(6) |
| Pd(2)-C(30) | 1.949(4) | C(36)-C(37) | 1.368(7) | C(47)-C(48) | 1.377(6) |
| Pd(2)-N(35) | 2.104(3) | C(37)-C(38) | 1.366(7) | C(48)-C(49) | 1.392(7) |
| N(29)-C(30) | 1.326(5) | C(38)-C(39) | 1.378(6) | C(49)-C(50) | 1.370(7) |
| N(29)-N(33) | 1.391(4) | C(40)-C(45) | 1.376(6) | C(50)-C(51) | 1.384(6) |
| N(29)-C(34) | 1.429(5) | C(40)-C(41) | 1.378(5) | N(35)-C(52) | 1.333(6) |
| C(30)-N(31) | 1.360(5) | C(41)-C(42) | 1.389(6) | N(35)-C(56) | 1.339(6) |
| N(31)-C(32) | 1.390(4) | C(42)-C(43) | 1.373(6) | C(52)-C(53) | 1.380(7) |
| N(31)-C(40) | 1.440(4) | C(43)-C(44) | 1.392(6) | C(53)-C(54) | 1.360(10) |
| C(32)-N(33) | 1.297(5) | C(44)-C(45) | 1.386(5) | C(54)-C(55) | 1.368(10) |
| C(32)-N(34) | 1.361(5) | N(34)-C(46) | 1.429(4) | C(55)-C(56) | 1.376(6) |
| C(34)-C(35) | 1.370(6) | N(34)-H(32) | 0.85(4) | | |

**Table S6**. Hydrogen bonds for **2a** (Å and °).

| D-H...A | d(D-H) | d(H...A) | d(D...A) | <(DHA) |
|---|---|---|---|---|
| N(6)-H(4)...Cl(2)#1 | 0.84(4) | 2.75(5) | 3.544(4) | 157(4) |
| N(34)-H(32)...Cl(4)#2 | 0.85(4) | 2.48(5) | 3.322(4) | 170(4) |

Symmetry transformations used to generate equivalent atoms: #1 -x+2,-y+1,-z+1   #2 -x+2,-y+2,-z

**The structure of 2c**
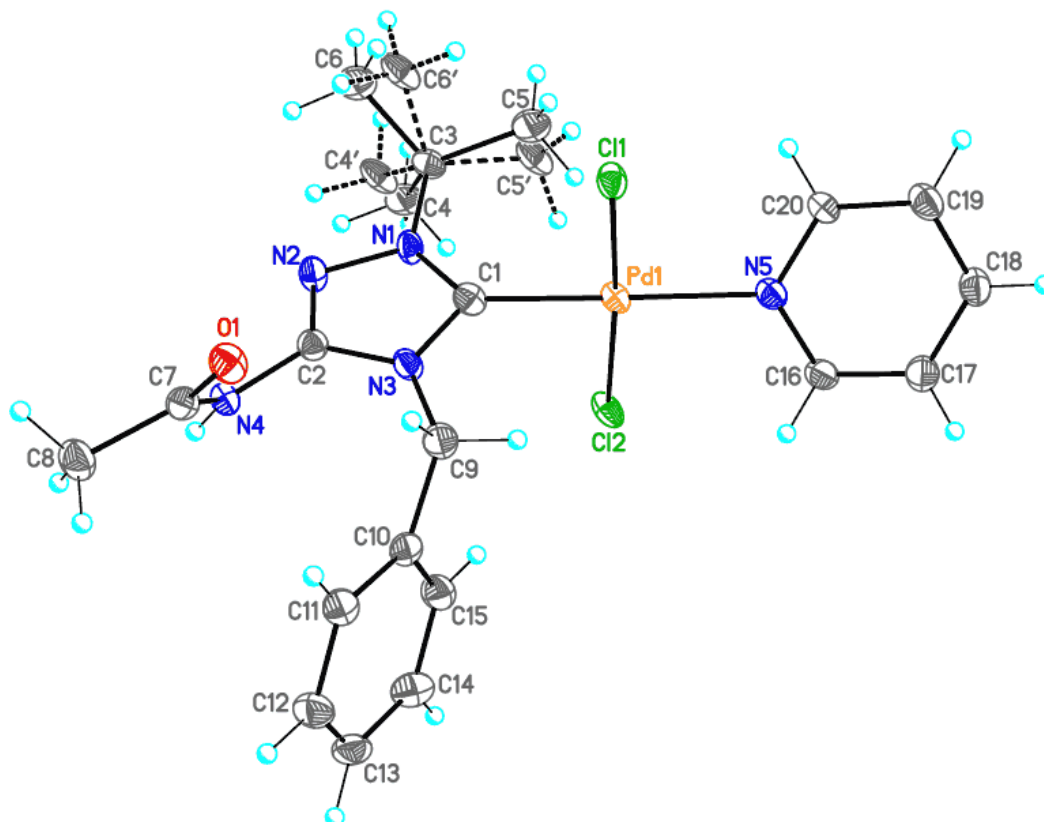


**Figure S17.** The structure of **2c**. The *tert*-Bu group is disordered over two sites with equal occupancies. Displacement ellipsoids are drawn at the 50% probability level.

**Table S7**. Selected bond distances for **2c** (Å).

| | | | | | |
|---|---|---|---|---|---|
| Pd(1)-Cl(1) | 2.3236(15) | N(4)-C(7) | 1.369(8) | C(9)-C(10) | 1.510(9) |
| Pd(1)-Cl(2) | 2.3211(16) | N(4)-C(2) | 1.398(7) | C(10)-C(15) | 1.387(9) |
| Pd(1)-C(1) | 1.968(6) | N(4)-H(4) | 0.8800 | C(10)-C(11) | 1.396(8) |
| Pd(1)-N(5) | 2.103(5) | N(5)-C(16) | 1.342(8) | C(11)-C(12) | 1.392(9) |
| O(1)-C(7) | 1.223(7) | N(5)-C(20) | 1.353(8) | C(12)-C(13) | 1.383(10) |
| N(1)-C(1) | 1.340(8) | C(3)-C(4') | 1.538(3) | C(13)-C(14) | 1.392(10) |
| N(1)-N(2) | 1.380(7) | C(3)-C(5) | 1.538(3) | C(14)-C(15) | 1.392(9) |
| N(1)-C(3) | 1.487(7) | C(3)-C(6') | 1.538(3) | C(16)-C(17) | 1.385(9) |
| N(2)-C(2) | 1.299(8) | C(3)-C(4) | 1.540(3) | C(17)-C(18) | 1.379(9) |
| N(3)-C(1) | 1.366(7) | C(3)-C(5') | 1.541(3) | C(18)-C(19) | 1.382(9) |
| N(3)-C(2) | 1.371(8) | C(3)-C(6) | 1.541(3) | C(19)-C(20) | 1.382(9) |
| N(3)-C(9) | 1.472(8) | C(7)-C(8) | 1.503(8) | | |

**Table S8**. Hydrogen bonds for **2c** (Å and °).

| D-H...A | d(D-H) | d(H...A) | d(D...A) | <(DHA) |
|---|---|---|---|---|
| N(4)-H(4)...Cl(1)#1 | 0.88 | 2.53 | 3.334(5) | 152.7 |

Symmetry transformations used to generate equivalent atoms: #1 x+1/2,y-1/2,z

**The structure of 2i**
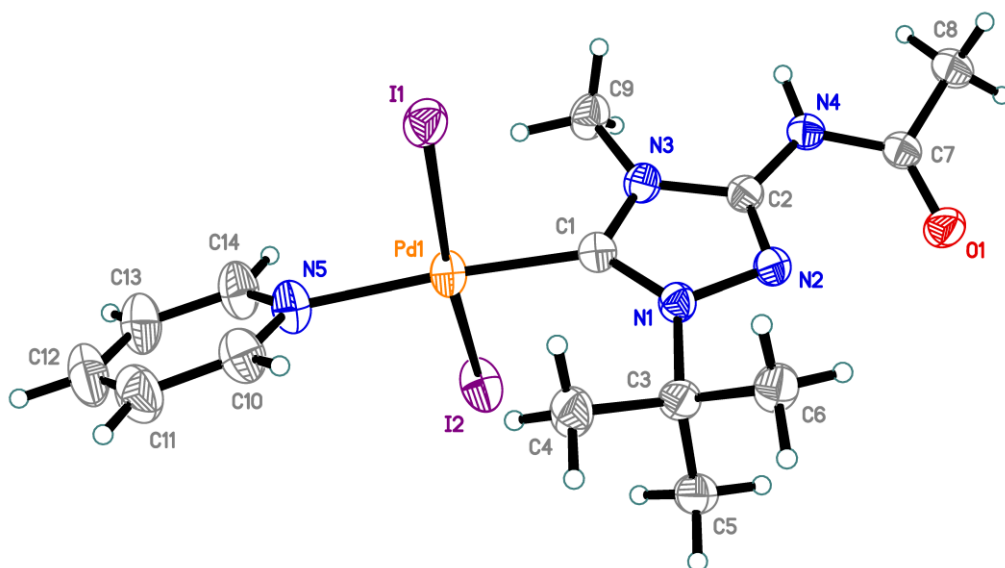


**Figure S18.** The structure **2i**. Displacement ellipsoids are drawn at the 50% probability level.
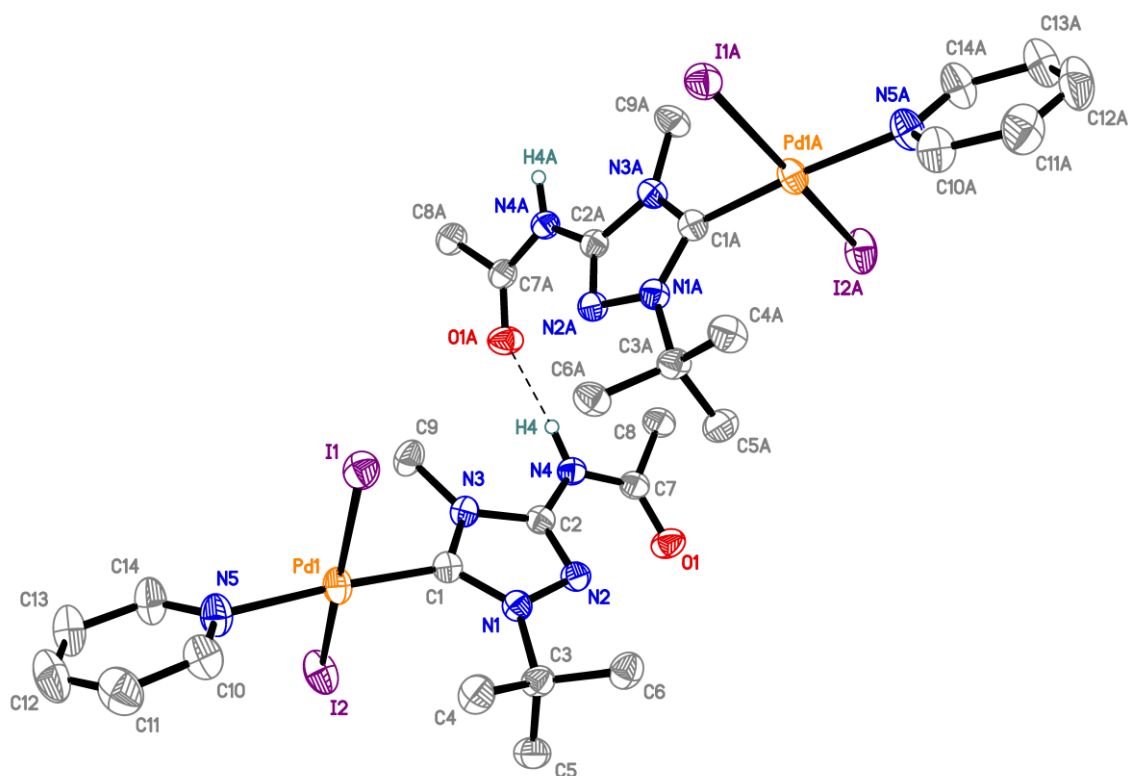


**Figure S19.** The hydrogen bonding in **2i**. Displacement ellipsoids are drawn at the 50% probability level. All but amino hydrogen atoms are omitted. Symmetry transformation: (A) x ,-y+3/2, z-1/2.

**Table S9**. Selected bond distances for **2i** (Å).

| | | | | | |
|---|---|---|---|---|---|
| I(1)-Pd(1) | 2.6180(3) | N(3)-C(1) | 1.362(4) | C(3)-C(6) | 1.525(5) |
| I(2)-Pd(1) | 2.6032(3) | N(3)-C(2) | 1.372(4) | C(3)-C(5) | 1.528(5) |
| Pd(1)-C(1) | 1.959(3) | N(3)-C(9) | 1.462(4) | C(3)-C(4) | 1.528(4) |
| Pd(1)-N(5) | 2.087(3) | N(4)-C(7) | 1.364(4) | C(7)-C(8) | 1.501(4) |
| O(1)-C(7) | 1.213(4) | N(4)-C(2) | 1.374(4) | C(10)-C(11) | 1.383(6) |
| N(1)-C(1) | 1.337(4) | N(4)-H(4) | 0.87(5) | C(11)-C(12) | 1.371(7) |
| N(1)-N(2) | 1.392(3) | N(5)-C(10) | 1.340(4) | C(12)-C(13) | 1.382(7) |
| N(1)-C(3) | 1.499(4) | N(5)-C(14) | 1.343(5) | C(13)-C(14) | 1.390(5) |
| N(2)-C(2) | 1.307(4) | | | | |

**Table S10**. Hydrogen bonds for **2i** (Å and °).

| D-H...A | d(D-H) | d(H...A) | d(D...A) | <(DHA) |
|---|---|---|---|---|
| N(4)-H(4)...O(1)#1 | 0.87(5) | 1.92(5) | 2.761(3) | 163(4) |

Symmetry transformations used to generate equivalent atoms: #1 x,-y+3/2,z-1/2

**The structure of 2j**
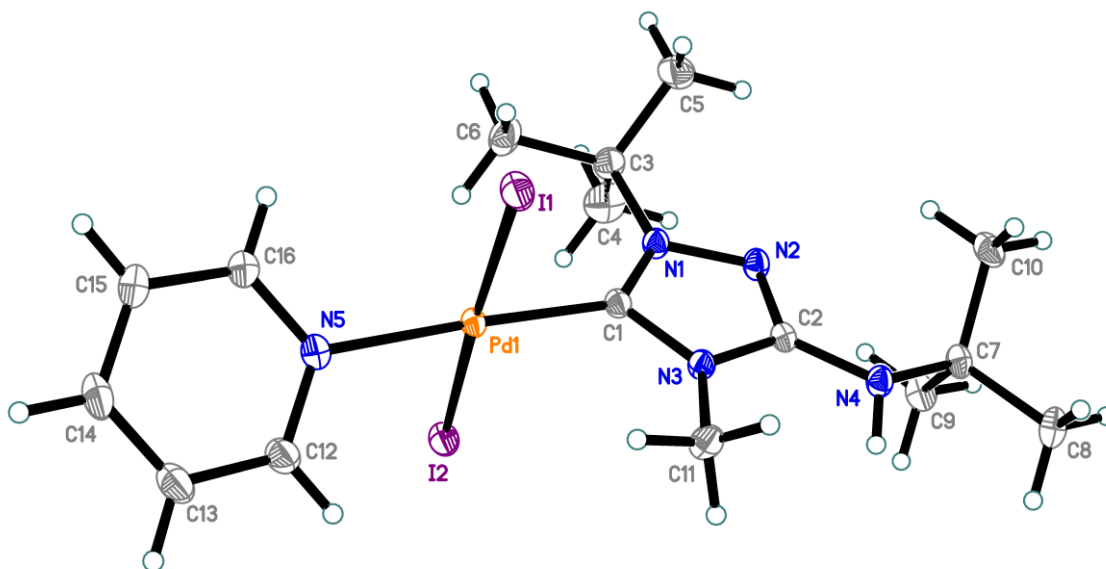


**Figure S20.** The structure **2j**. Displacement ellipsoids are drawn at the 50% probability level.
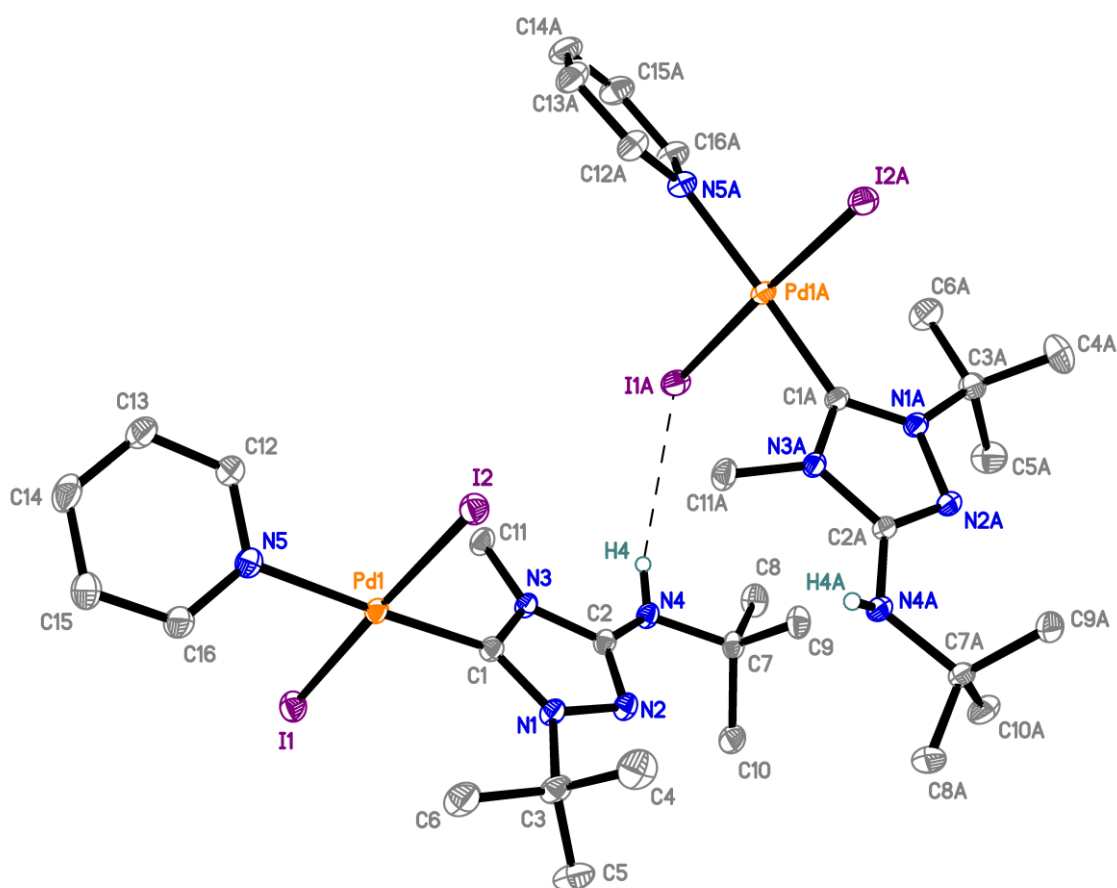
**Figure S21.** The hydrogen bonding in **2j**. Displacement ellipsoids are drawn at the 50% probability level. All but amino hydrogen atoms are omitted. Symmetry transformation: (A) x, -y+3/2, z-1/2.

**Table S11**. Selected bond distances for **2j** (Å).

| | | | | | |
|---|---|---|---|---|---|
| I(1)-Pd(1) | 2.60963(13) | N(3)-C(2) | 1.3772(15) | C(3)-C(5) | 1.529(2) |
| I(2)-Pd(1) | 2.60763(12) | N(3)-C(11) | 1.4597(16) | C(7)-C(9) | 1.5267(17) |
| Pd(1)-C(1) | 1.9716(11) | N(4)-C(2) | 1.3662(15) | C(7)-C(10) | 1.5267(18) |
| Pd(1)-N(5) | 2.0901(11) | N(4)-C(7) | 1.4881(15) | C(7)-C(8) | 1.5287(18) |
| N(1)-C(1) | 1.3318(15) | N(4)-H(4) | 0.829(18) | C(12)-C(13) | 1.3862(19) |
| N(1)-N(2) | 1.3950(14) | N(5)-C(12) | 1.3437(17) | C(13)-C(14) | 1.387(2) |
| N(1)-C(3) | 1.4895(16) | N(5)-C(16) | 1.3468(17) | C(14)-C(15) | 1.388(2) |
| N(2)-C(2) | 1.3097(15) | C(3)-C(6) | 1.5181(19) | C(15)-C(16) | 1.3868(19) |
| N(3)-C(1) | 1.3672(15) | C(3)-C(4) | 1.526(2) | | |

**Table S12**. Hydrogen bonds for **2j** (Å and °).

| D-H...A | d(D-H) | d(H...A) | d(D...A) | <(DHA) |
|---|---|---|---|---|
| N(4)-H(4)...I(1)#1 | 0.829(18) | 2.970(18) | 3.7332(11) | 154.1(15) |

Symmetry transformations used to generate equivalent atoms: #1 x,-y+3/2,z-1/2
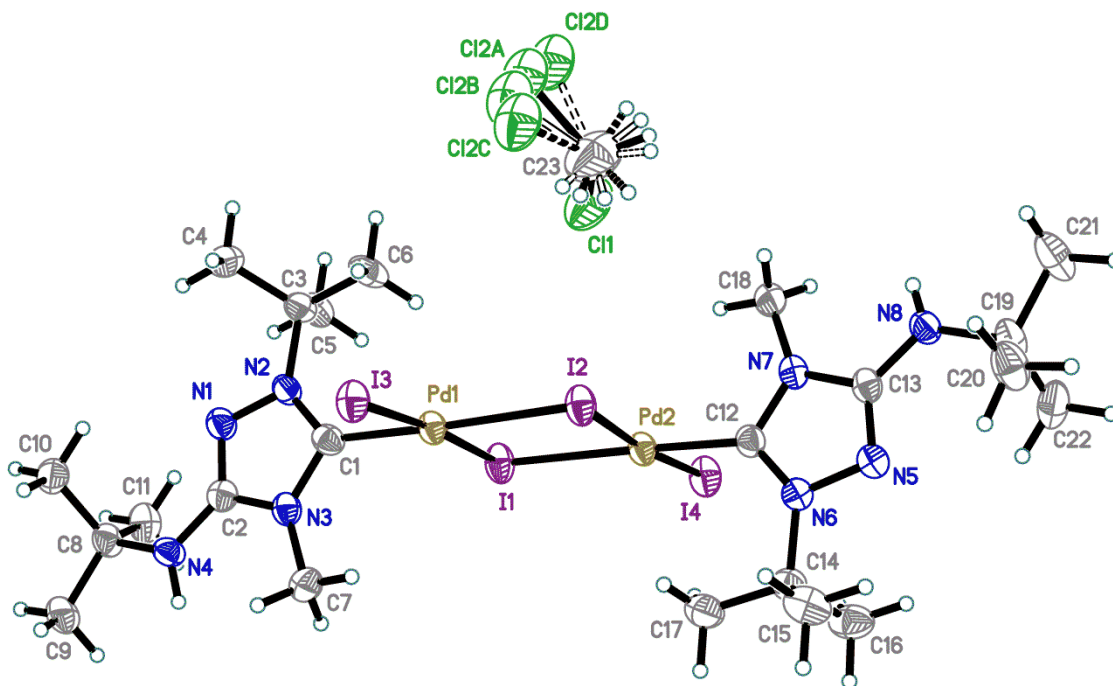
**The structure of 3a**



**Figure S22.** The structure of **3a**. Displacement ellipsoids are drawn at the 50% probability level. Atom Cl2 of a noncoordinating $CH_2Cl_2$ solvent molecule is disordered over four positions with a Cl2A/Cl2B/Cl2C/Cl2D occupancy ratio of 0.429(3):0.296(3):0.088(3):0.187(3).

**Table S13**. Selected bond distances for **3a** (Å).

| | | | | | |
|---|---|---|---|---|---|
| Pd(1)-I(1) | 2.6197(5) | N(3)-C(7) | 1.460(6) | C(12)-N(7) | 1.364(6) |
| Pd(1)-I(2) | 2.6614(5) | C(2)-N(4) | 1.356(6) | N(7)-C(13) | 1.373(6) |
| Pd(1)-I(3) | 2.5895(5) | C(3)-C(6) | 1.510(7) | N(7)-C(18) | 1.452(6) |
| Pd(1)-C(1) | 1.967(5) | C(3)-C(5) | 1.521(7) | C(13)-N(8) | 1.350(6) |
| Pd(2)-I(1) | 2.6676(5) | C(3)-C(4) | 1.528(7) | C(14)-C(17) | 1.508(8) |
| Pd(2)-I(2) | 2.6188(5) | N(4)-C(8) | 1.491(6) | C(14)-C(15) | 1.510(7) |
| Pd(2)-I(4) | 2.5879(5) | N(4)-H(4) | 0.88(7) | C(14)-C(16) | 1.524(7) |
| Pd(2)-C(12) | 1.967(5) | C(8)-C(9) | 1.515(7) | N(8)-C(19) | 1.477(7) |
| N(1)-C(2) | 1.303(6) | C(8)-C(10) | 1.521(7) | N(8)-H(8) | 0.76(5) |
| N(1)-N(2) | 1.398(5) | C(8)-C(11) | 1.530(7) | C(19)-C(22) | 1.518(8) |
| N(2)-C(1) | 1.327(6) | N(5)-C(13) | 1.307(6) | C(19)-C(20) | 1.523(7) |
| N(2)-C(3) | 1.494(6) | N(5)-N(6) | 1.400(6) | C(19)-C(21) | 1.527(8) |
| C(1)-N(3) | 1.365(6) | N(6)-C(12) | 1.321(6) | | |
| N(3)-C(2) | 1.382(6) | N(6)-C(14) | 1.499(6) | | |

**Table S14**. Hydrogen bonds for **3a** (Å and °).

| D-H...A | d(D-H) | d(H...A) | d(D...A) | <(DHA) |
|---|---|---|---|---|
| N(4)-H(4)...I(3)#1 | 0.88(7) | 3.08(7) | 3.926(4) | 162(5) |
| N(8)-H(8)...I(4)#2 | 0.76(5) | 3.28(5) | 4.000(5) | 160(5) |

Symmetry transformations used to generate equivalent atoms: #1 x+1/2,y,-z+1/2  #2 x-1/2,y,-z+1/2

**The structure of 4a**
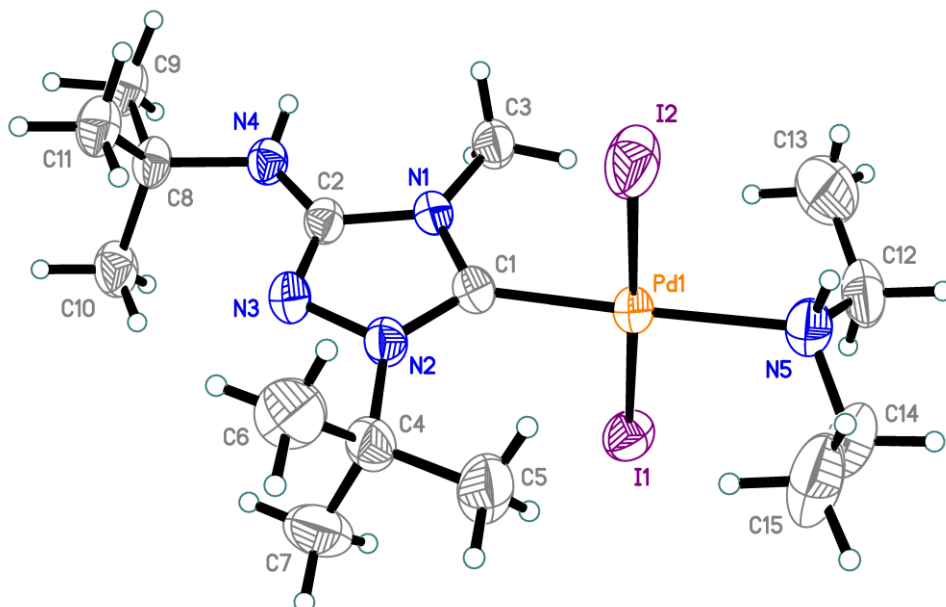


**Figure S23.** The structure of **4a**. Displacement ellipsoids are drawn at the 50% probability level.
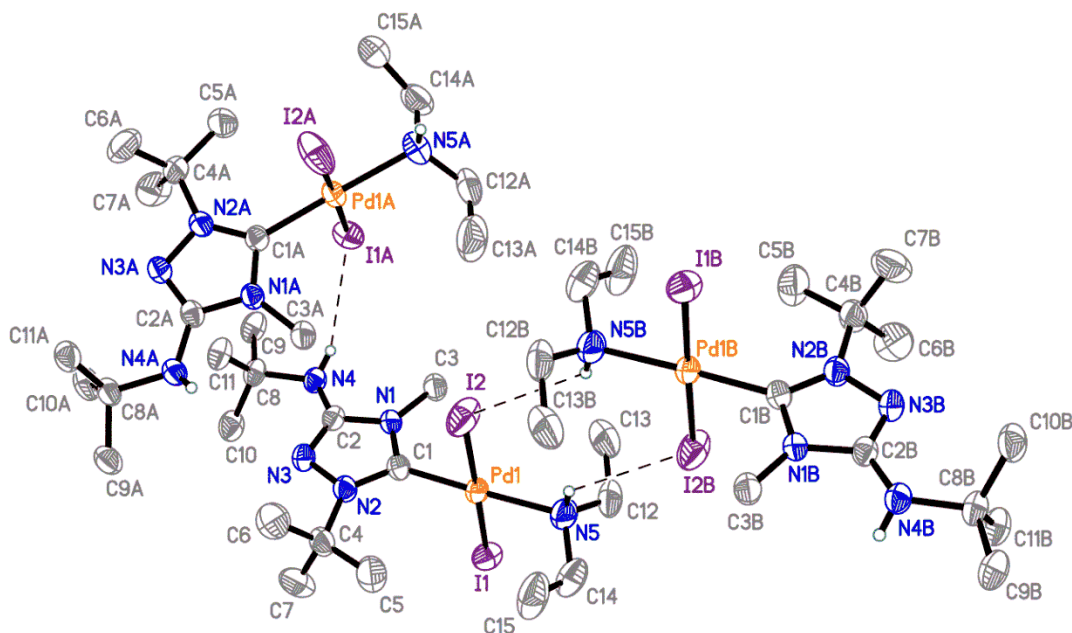


**Figure S24.** The hydrogen bonding in **4a**. Displacement ellipsoids are drawn at the 50% probability level. All but amino hydrogen atoms are omitted. Symmetry transformations: (A) x, -y+1/2, z+1/2; (B) -x, -y+1, -z+1.

**Table S15**. Selected bond distances for **4a** (Å).

| | | | | | |
|---|---|---|---|---|---|
| I(1)-Pd(1) | 2.6028(4) | N(2)-C(4) | 1.490(5) | C(8)-C(11) | 1.523(5) |
| I(2)-Pd(1) | 2.6068(4) | N(3)-C(2) | 1.299(5) | C(8)-C(9) | 1.524(6) |
| Pd(1)-C(1) | 1.983(4) | C(2)-N(4) | 1.364(5) | C(8)-C(10) | 1.527(6) |
| Pd(1)-N(5) | 2.139(4) | C(4)-C(5) | 1.516(6) | N(5)-C(12) | 1.481(7) |
| N(1)-C(1) | 1.362(5) | C(4)-C(6) | 1.517(7) | N(5)-C(14) | 1.483(7) |
| N(1)-C(2) | 1.382(4) | C(4)-C(7) | 1.526(7) | N(5)-H(5) | 0.91(6) |
| N(1)-C(3) | 1.457(5) | N(4)-C(8) | 1.489(5) | C(12)-C(13) | 1.468(9) |
| C(1)-N(2) | 1.331(5) | N(4)-H(4) | 0.80(3) | C(14)-C(15) | 1.480(8) |
| N(2)-N(3) | 1.393(4) | | | | |

**Table S16**. Hydrogen bonds for **4a** (Å and °).

| D-H...A | d(D-H) | d(H...A) | d(D...A) | <(DHA) |
|---|---|---|---|---|
| N(4)-H(4)...I(1)#1 | 0.80(3) | 2.97(3) | 3.697(3) | 152(4) |
| N(5)-H(5)...I(2) | 0.91(6) | 2.91(5) | 3.387(4) | 114(4) |
| N(5)-H(5)...I(2)#2 | 0.91(6) | 3.30(6) | 3.977(4) | 133(4) |

Symmetry transformations used to generate equivalent atoms: #1 x, -y+1/2, z+1/2   #2 -x, -y+1, -z+1

# S4. NMR spectra
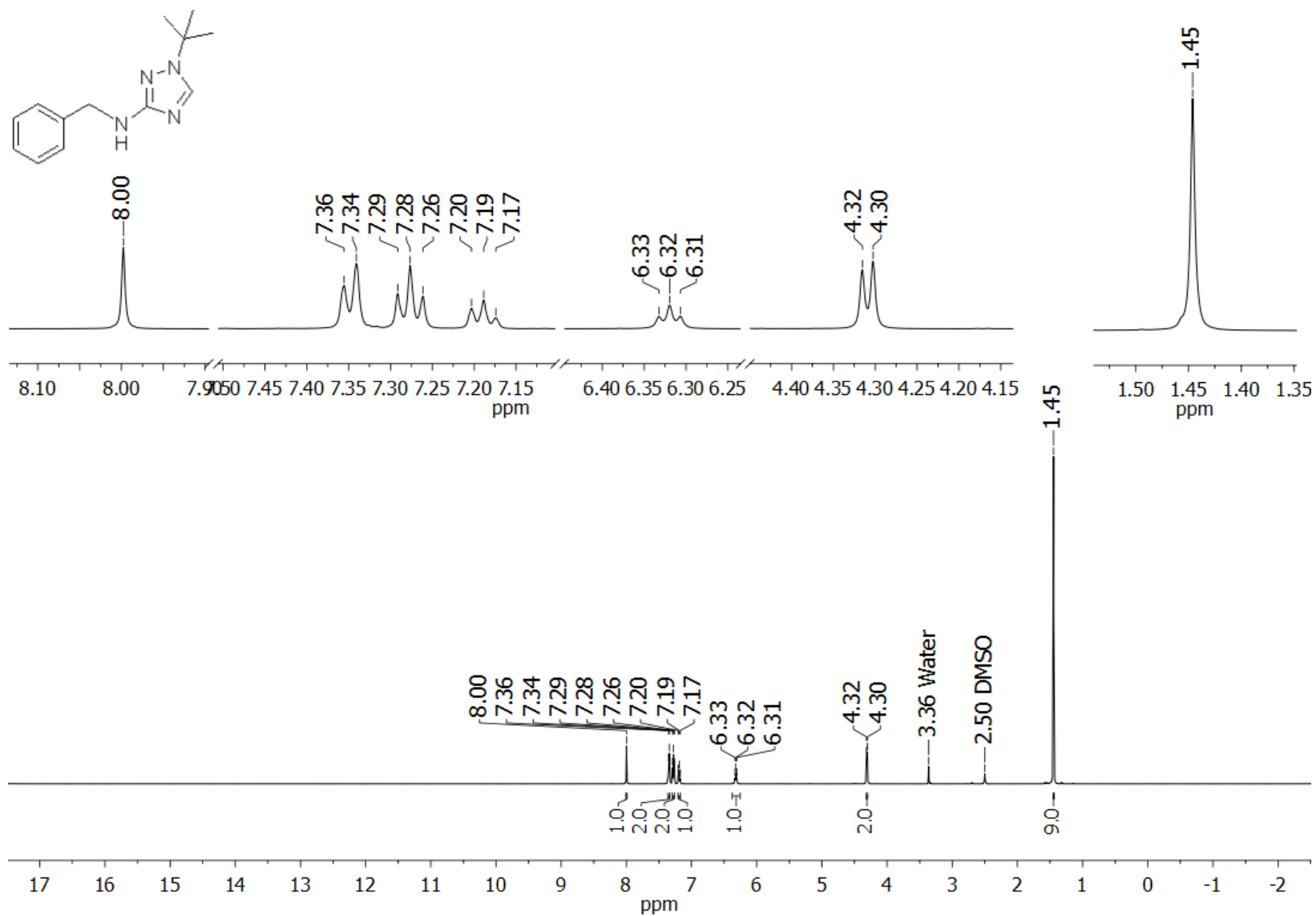
**Figure S25.** $^1$H NMR spectrum of compound **14b** (DMSO-$d_6$, 500 MHz)
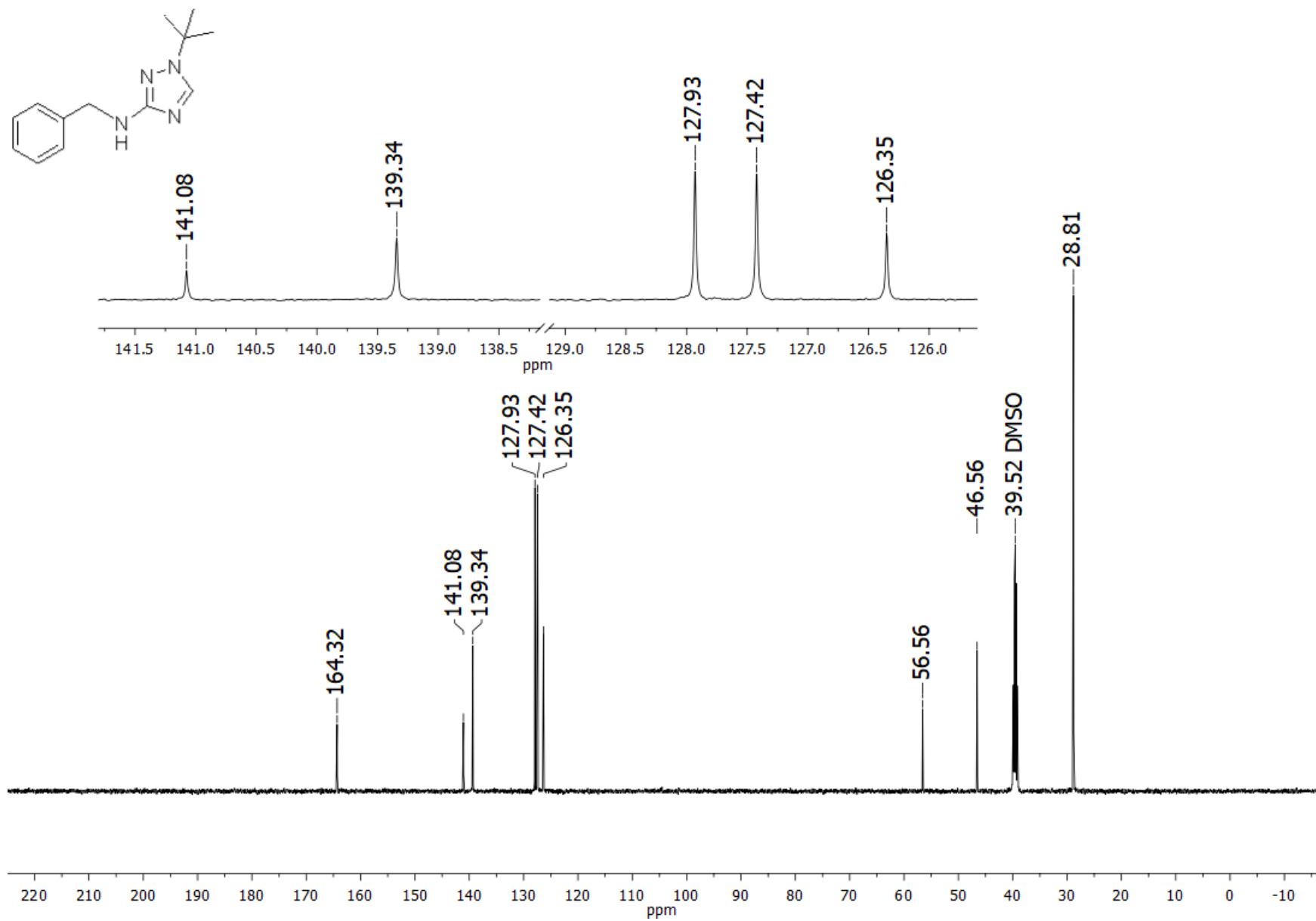
**Figure S26.** $^{13}$C NMR spectrum of compound **14b** (DMSO-$d_6$, 125 MHz)
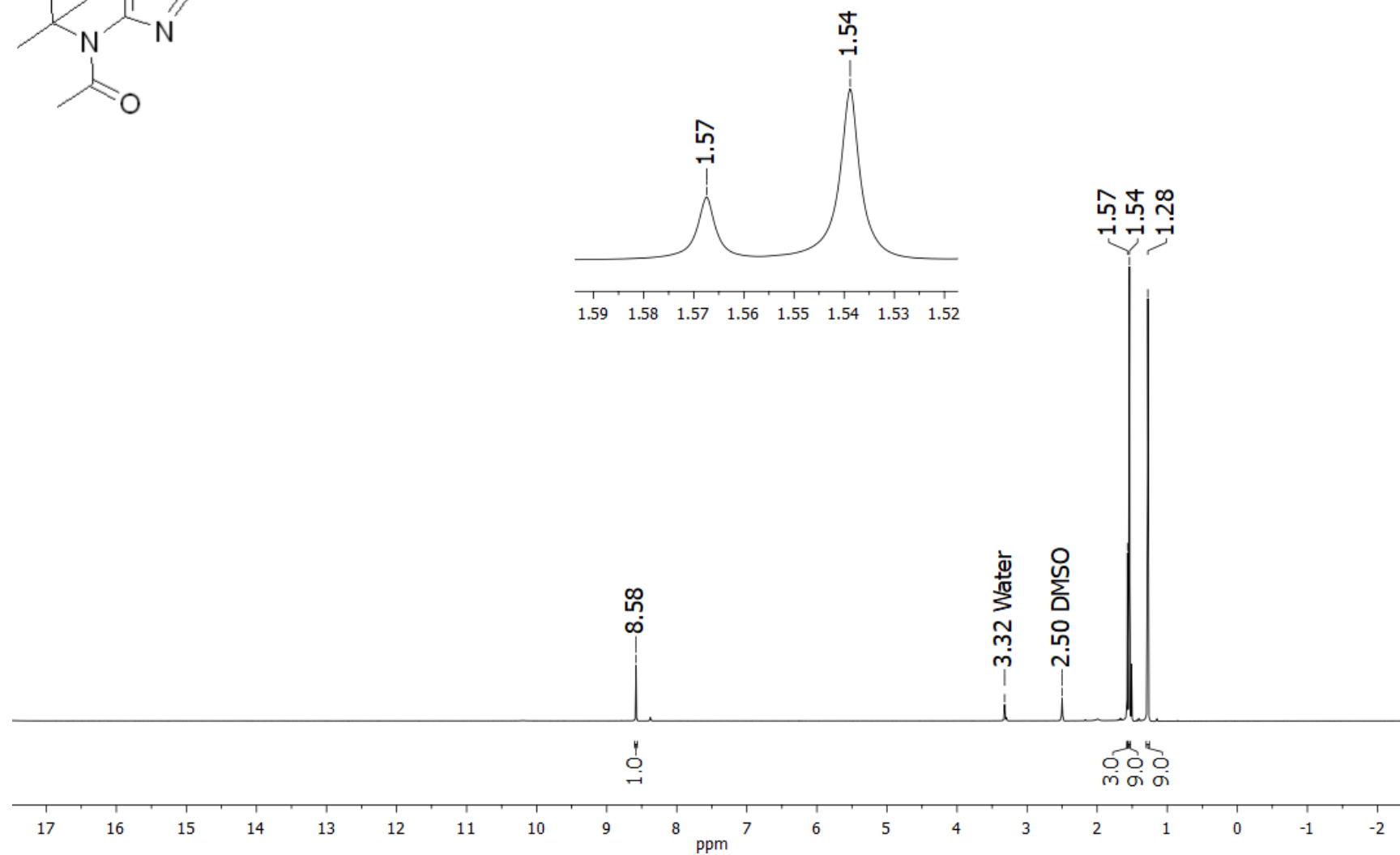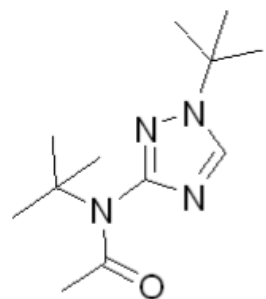
**Figure S27.** $^1$H NMR spectrum of compound **14e** (DMSO-$d_6$, 500 MHz)
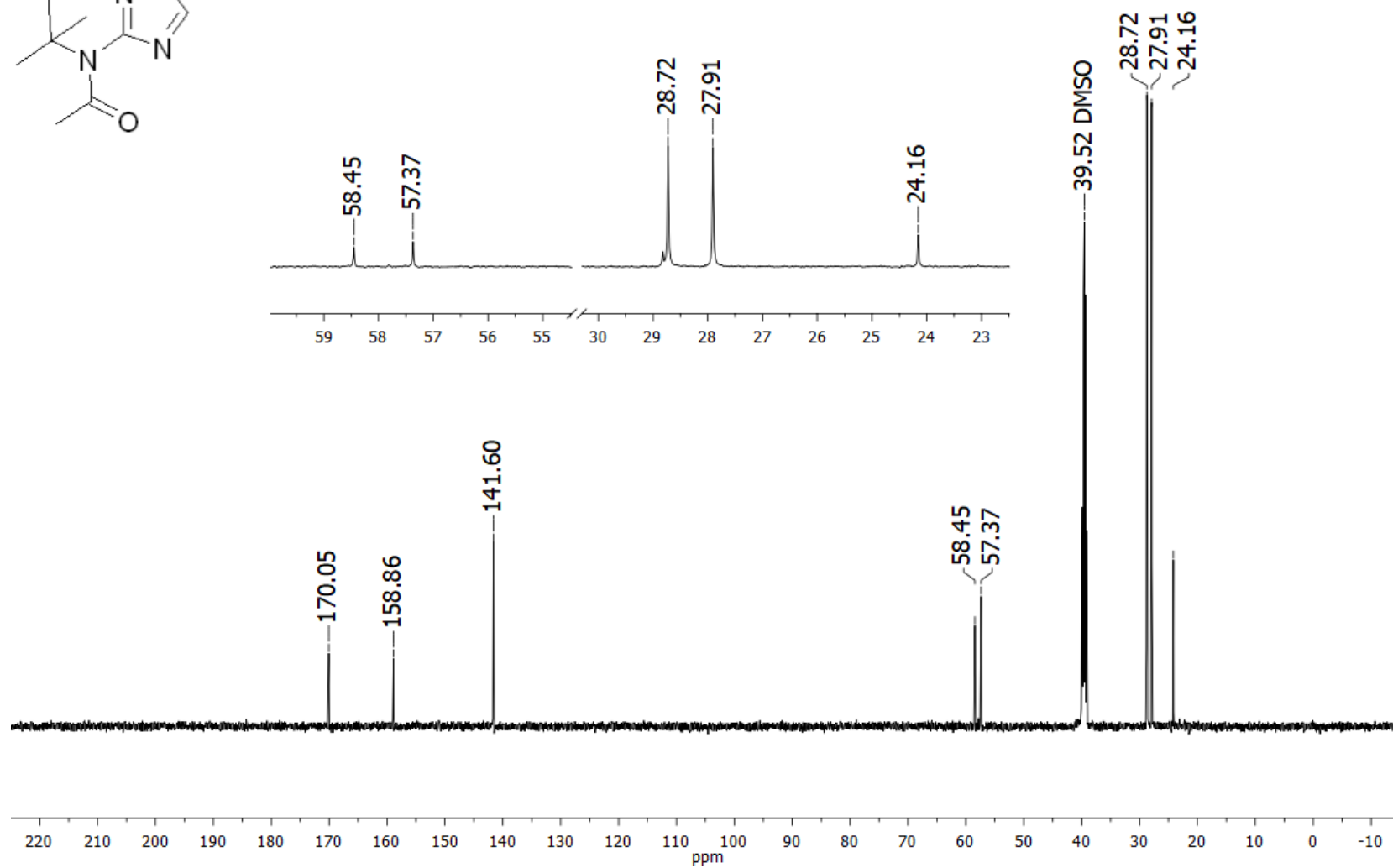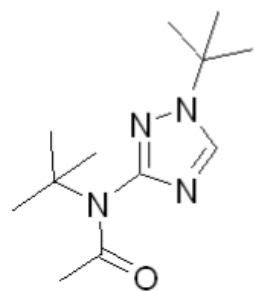
**Figure S28.** $^{13}$C NMR spectrum of compound **14e** (DMSO-$d_6$, 125 MHz)
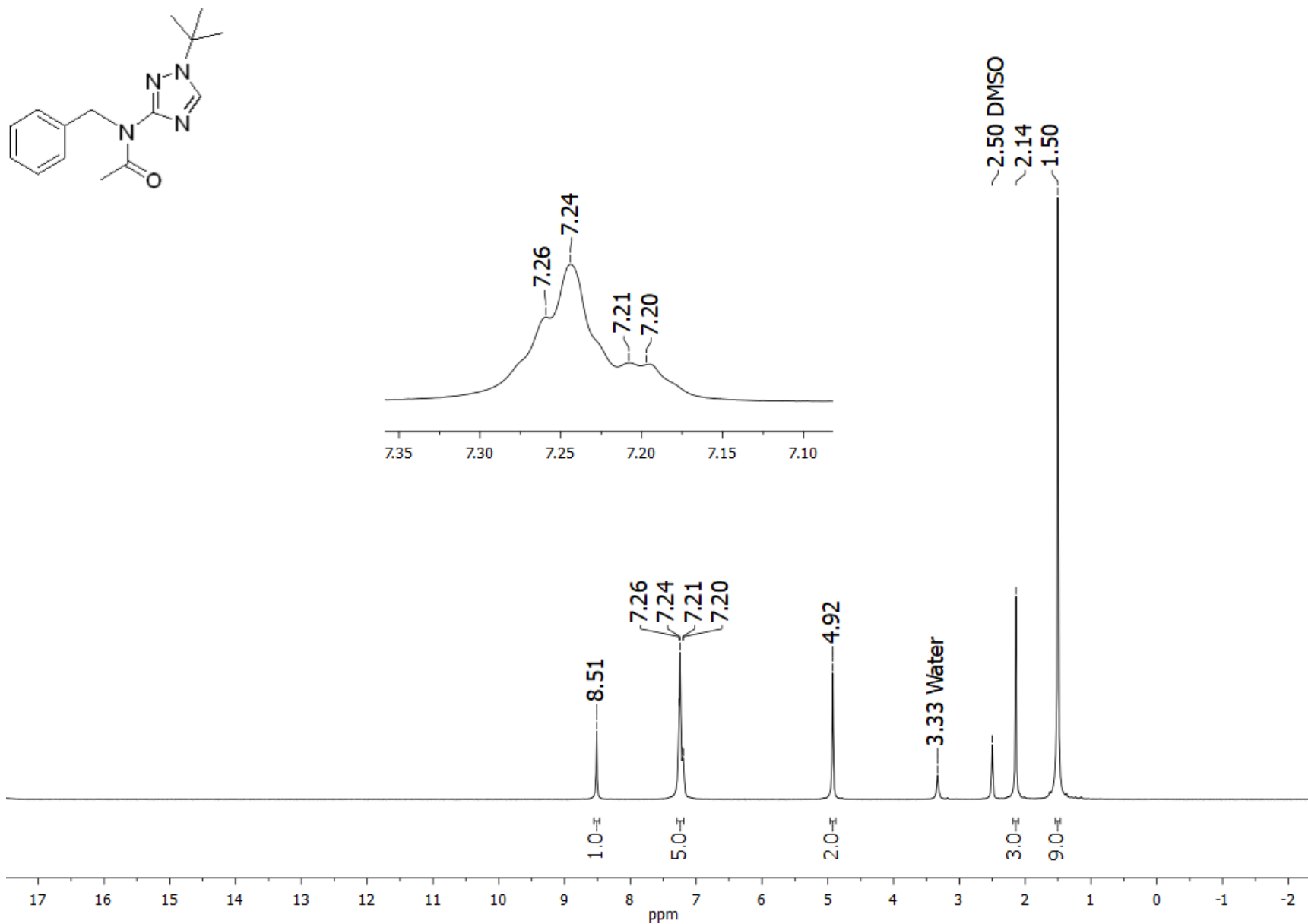
**Figure S29.** $^1$H NMR spectrum of compound **14f** (DMSO-$d_6$, 500 MHz)
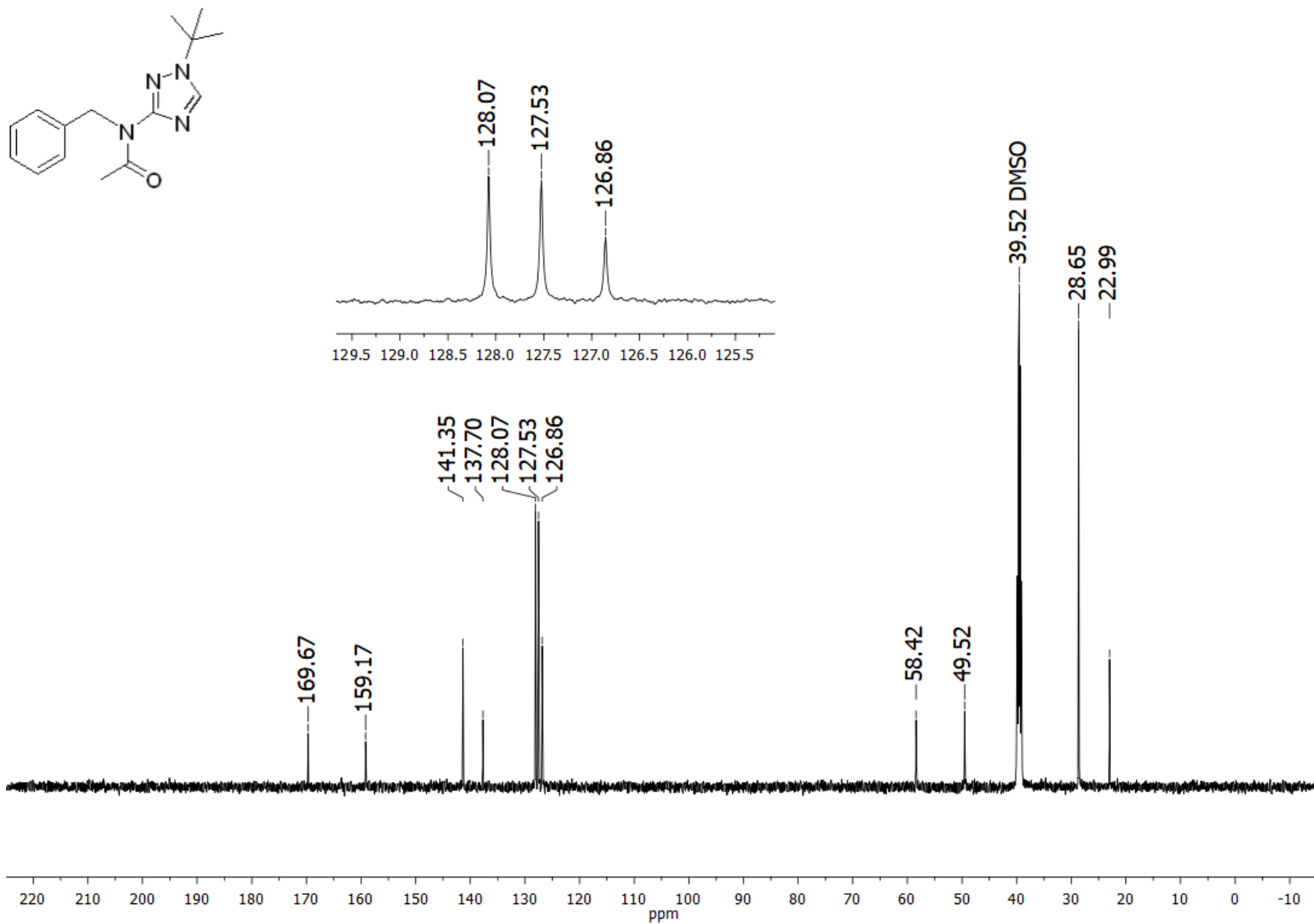
**Figure S30.** $^{13}$C NMR spectrum of compound **14f** (DMSO-$d_6$, 125 MHz)
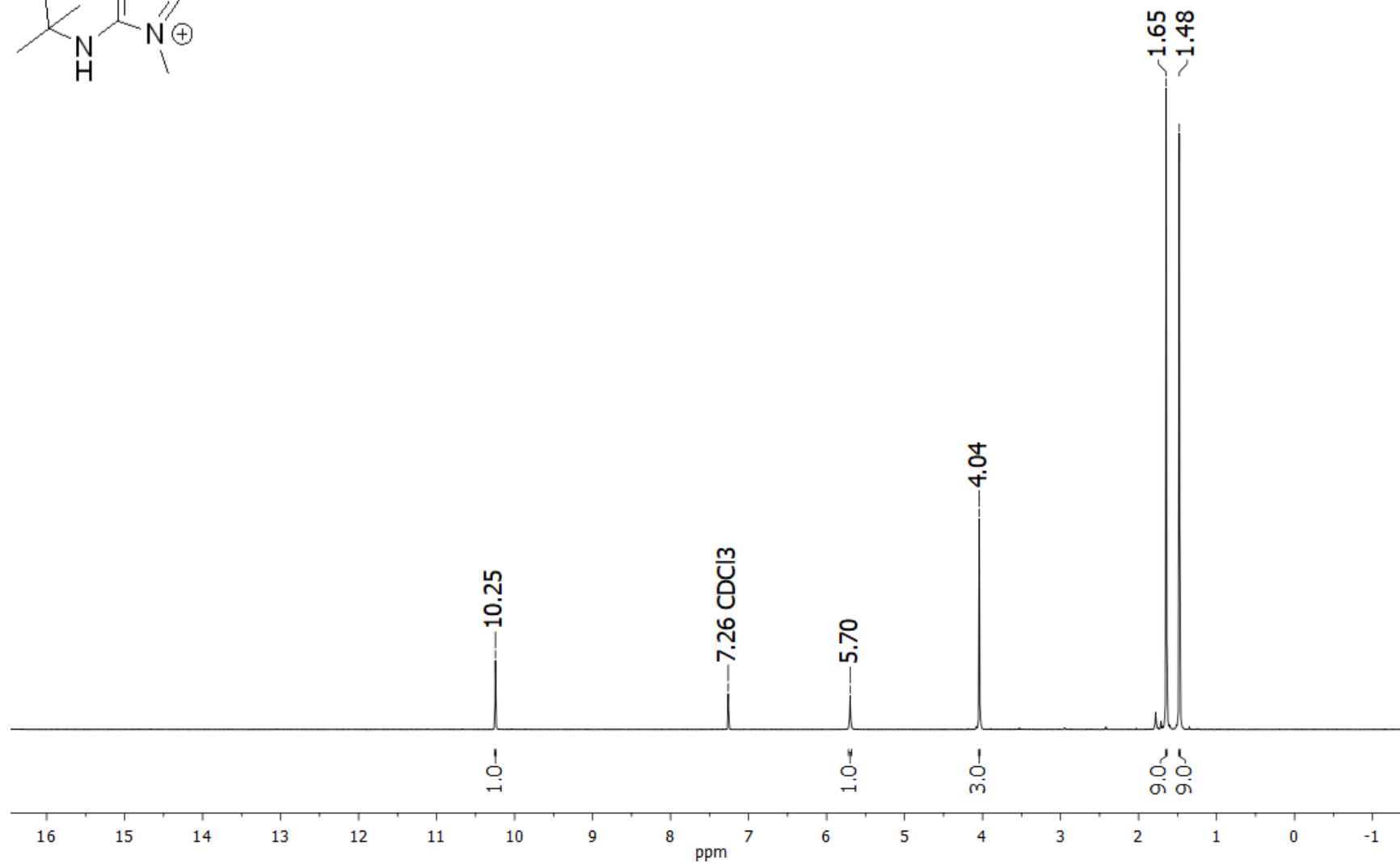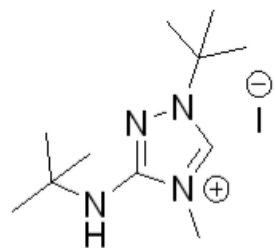
**Figure S31.** $^1$H NMR spectrum of compound **1c** (CDCl$_3$, 500 MHz)
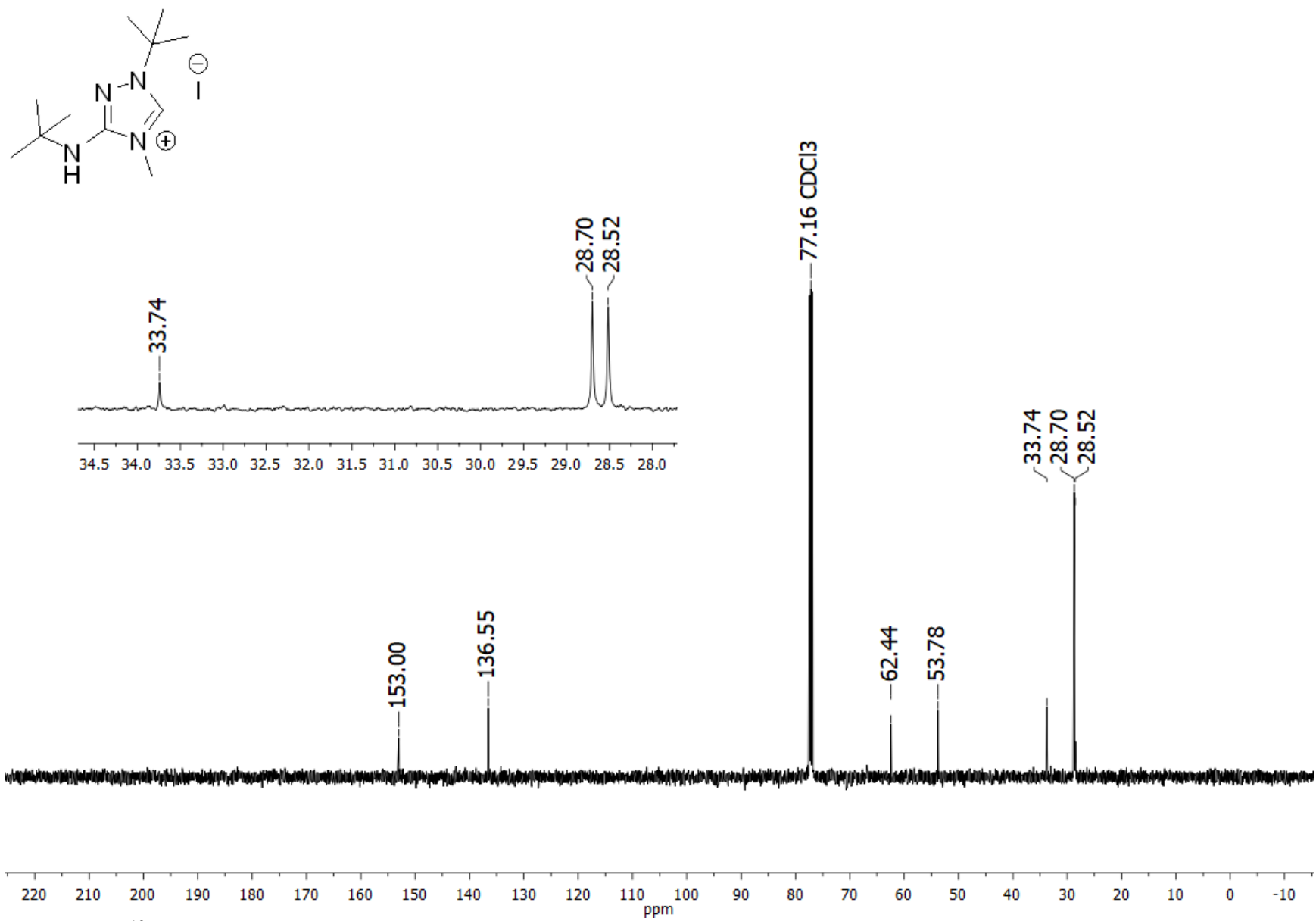
**Figure S32.** $^{13}C$ NMR spectrum of compound **1c** (CDCl$_3$, 125 MHz)
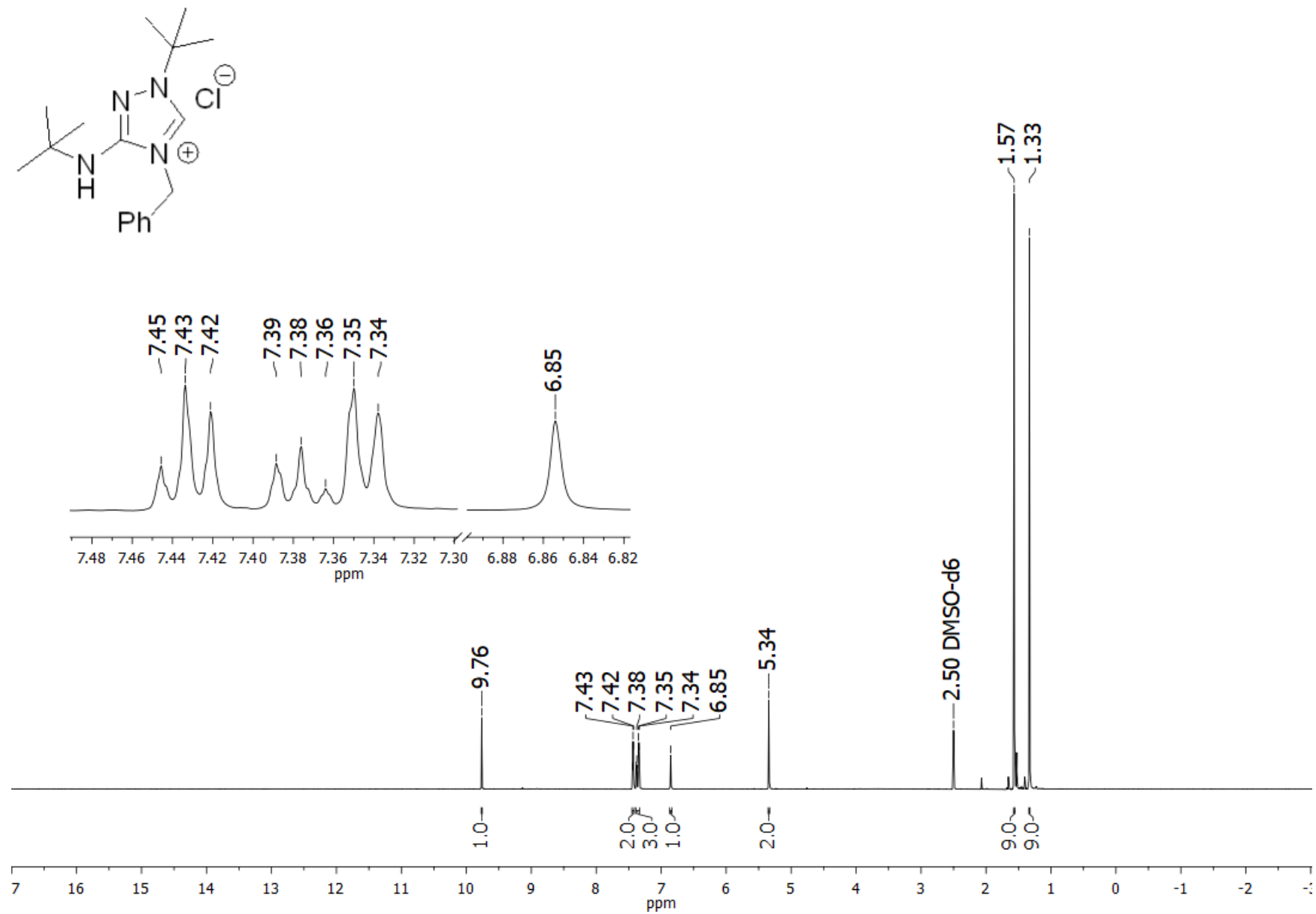
**Figure S33.** $^1$H NMR spectrum of compound **1d** (DMSO-$d_6$, 600 MHz)

43
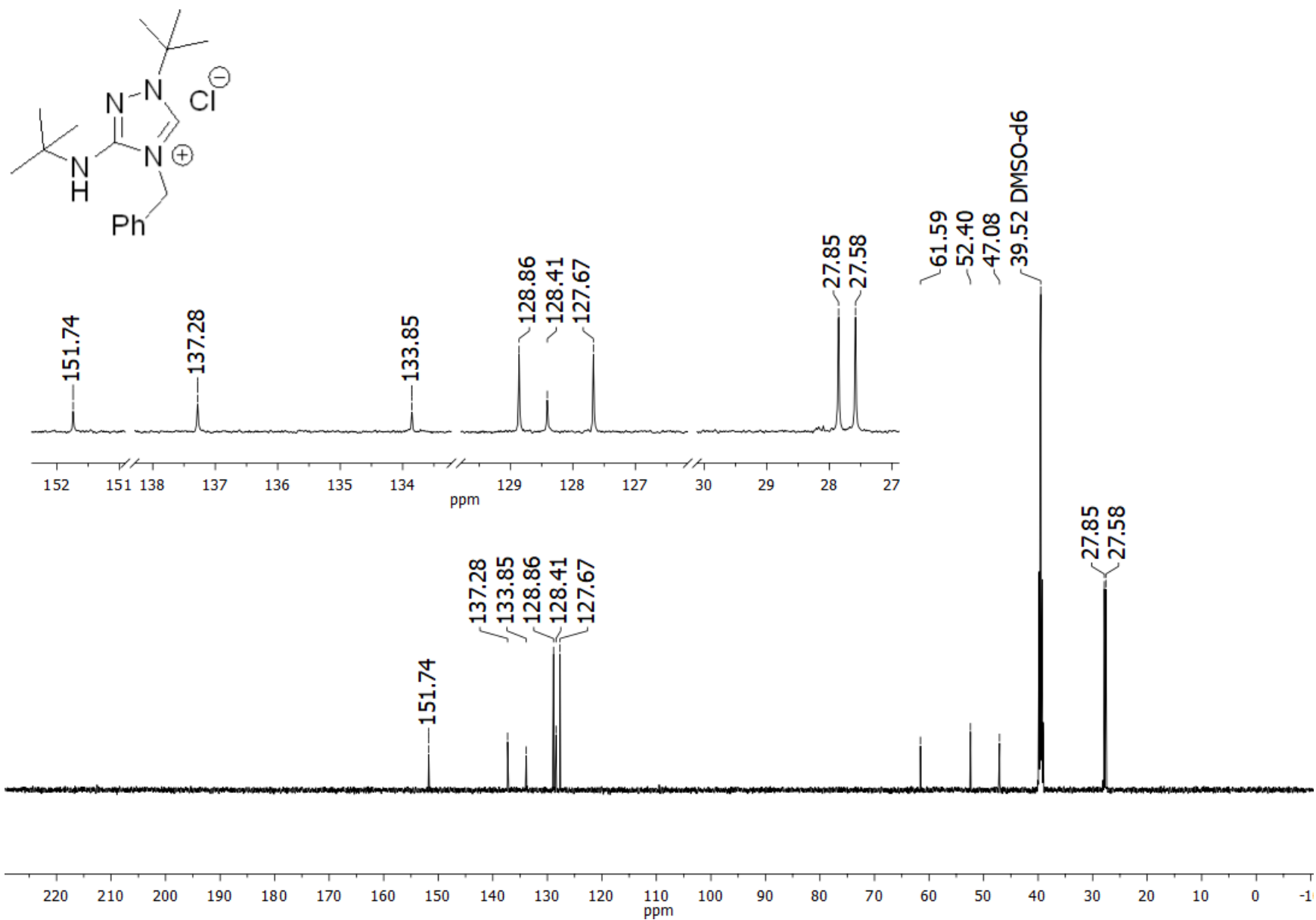
**Figure S34.** $^{13}$C NMR spectrum of compound **1d** (DMSO-$d_6$, 150 MHz)
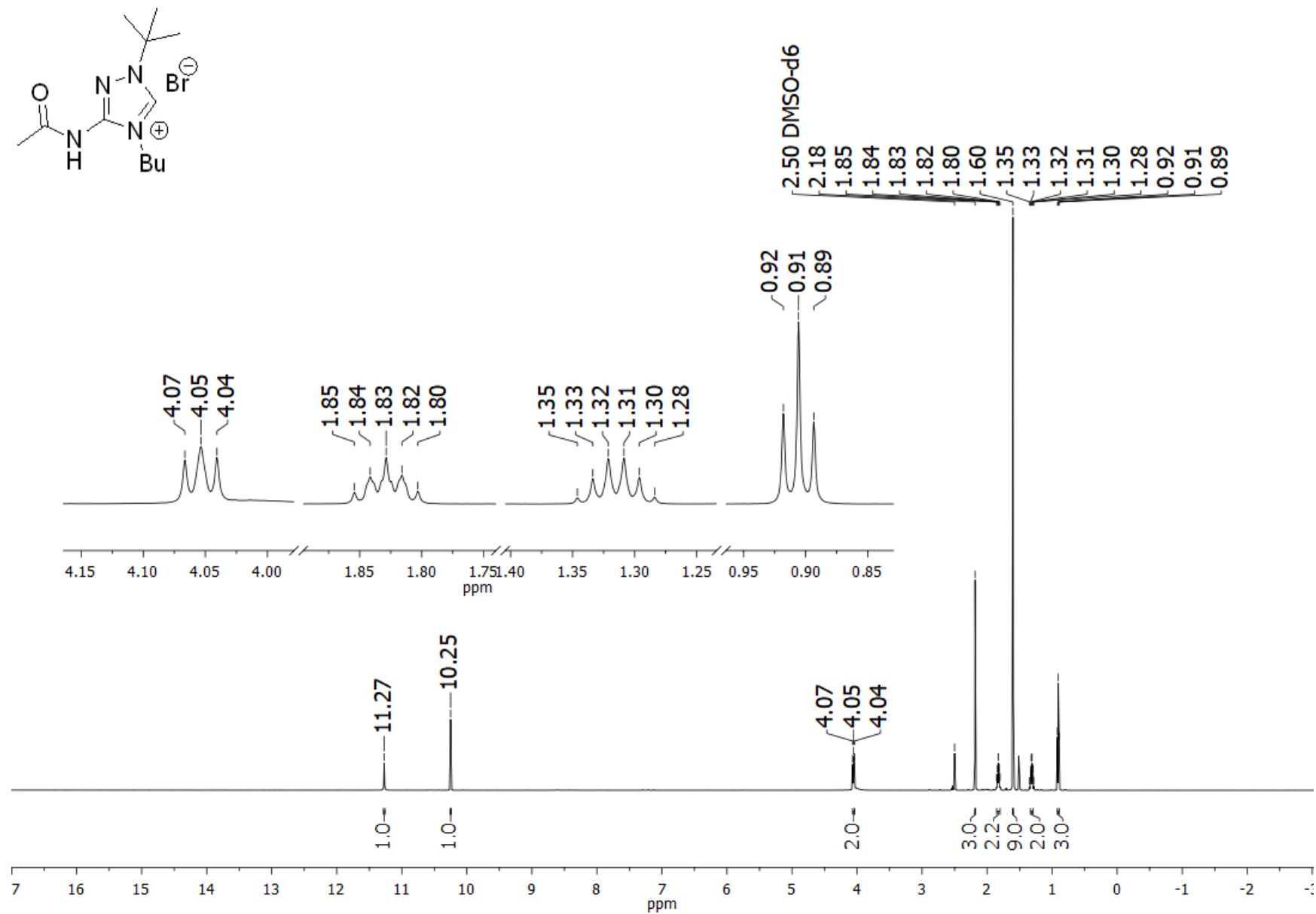
**Figure S35.** $^1$H NMR spectrum of compound **1f** (DMSO-$d_6$, 600 MHz)
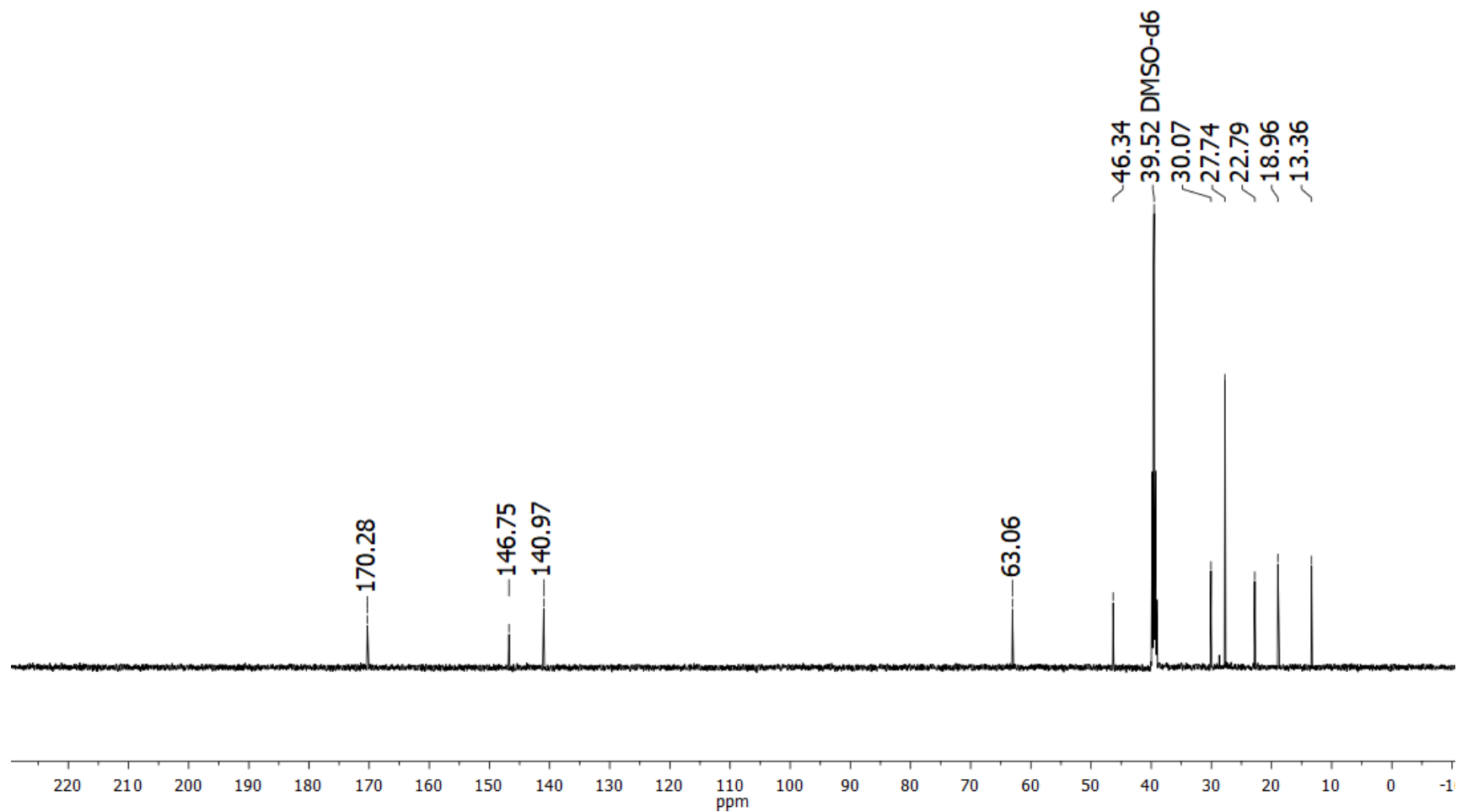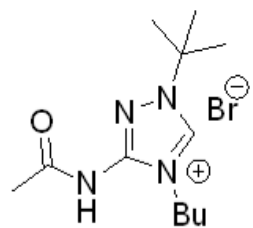
**Figure S36.** $^{13}$C NMR spectrum of compound **1f** (DMSO-$d_6$, 150 MHz)
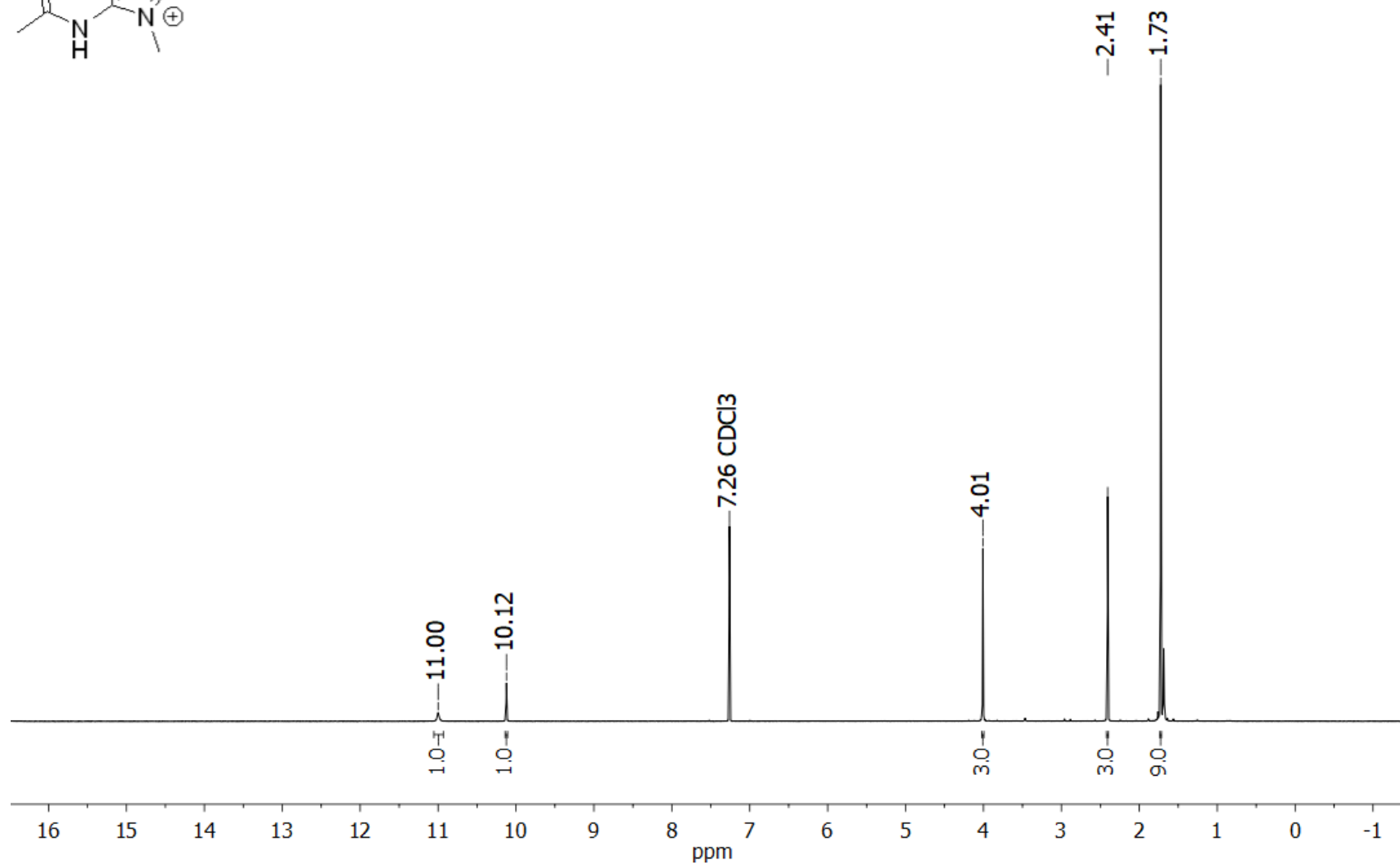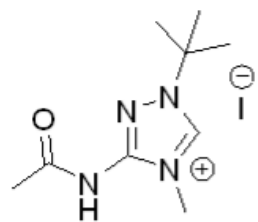
**Figure S37.** $^1$H NMR spectrum of compound **1g** (CDCl$_3$, 400 MHz)
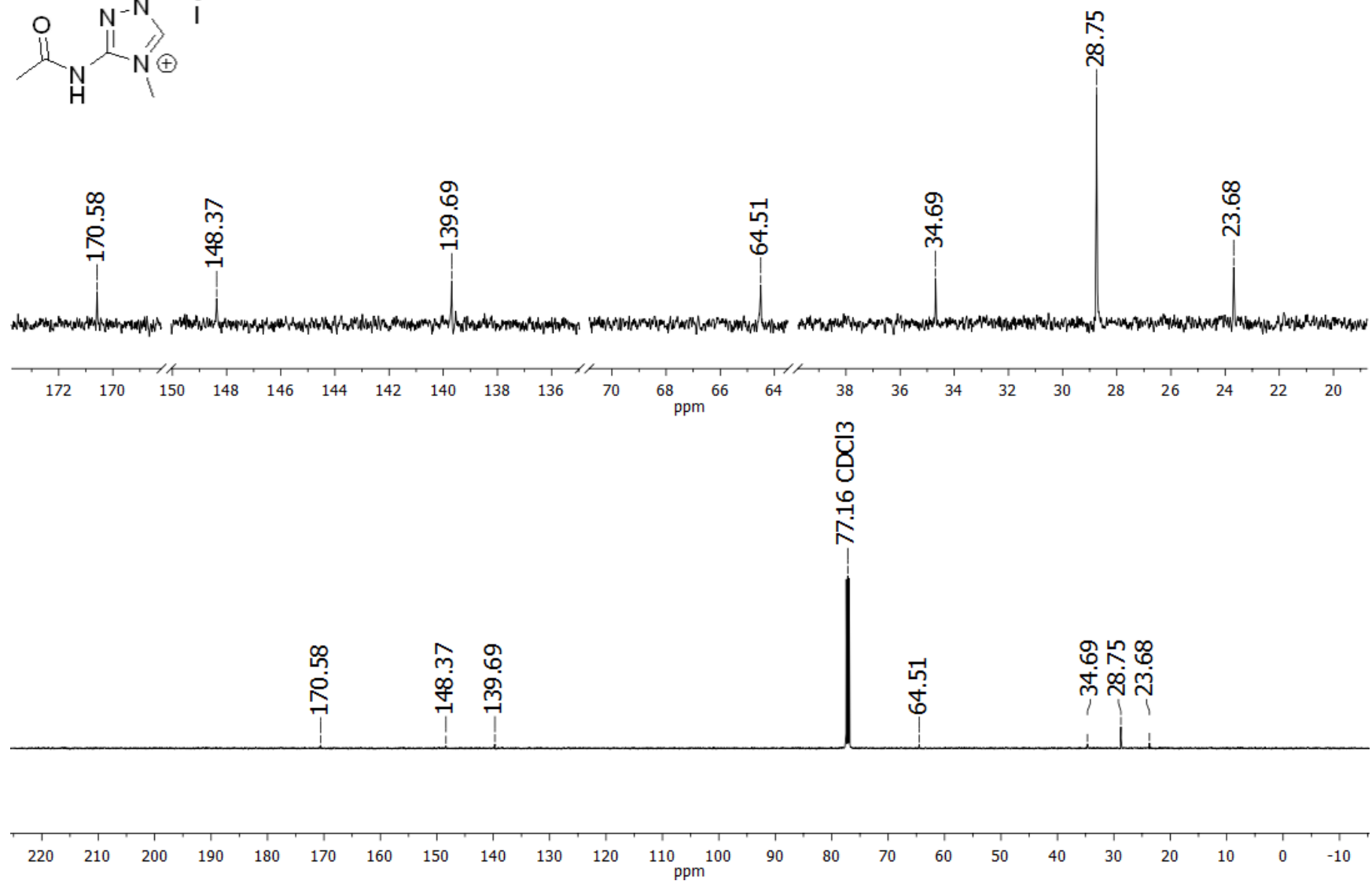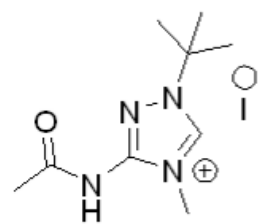
**Figure S38.** $^{13}C$ NMR spectrum of compound **1g** (CDCl$_3$, 125 MHz)
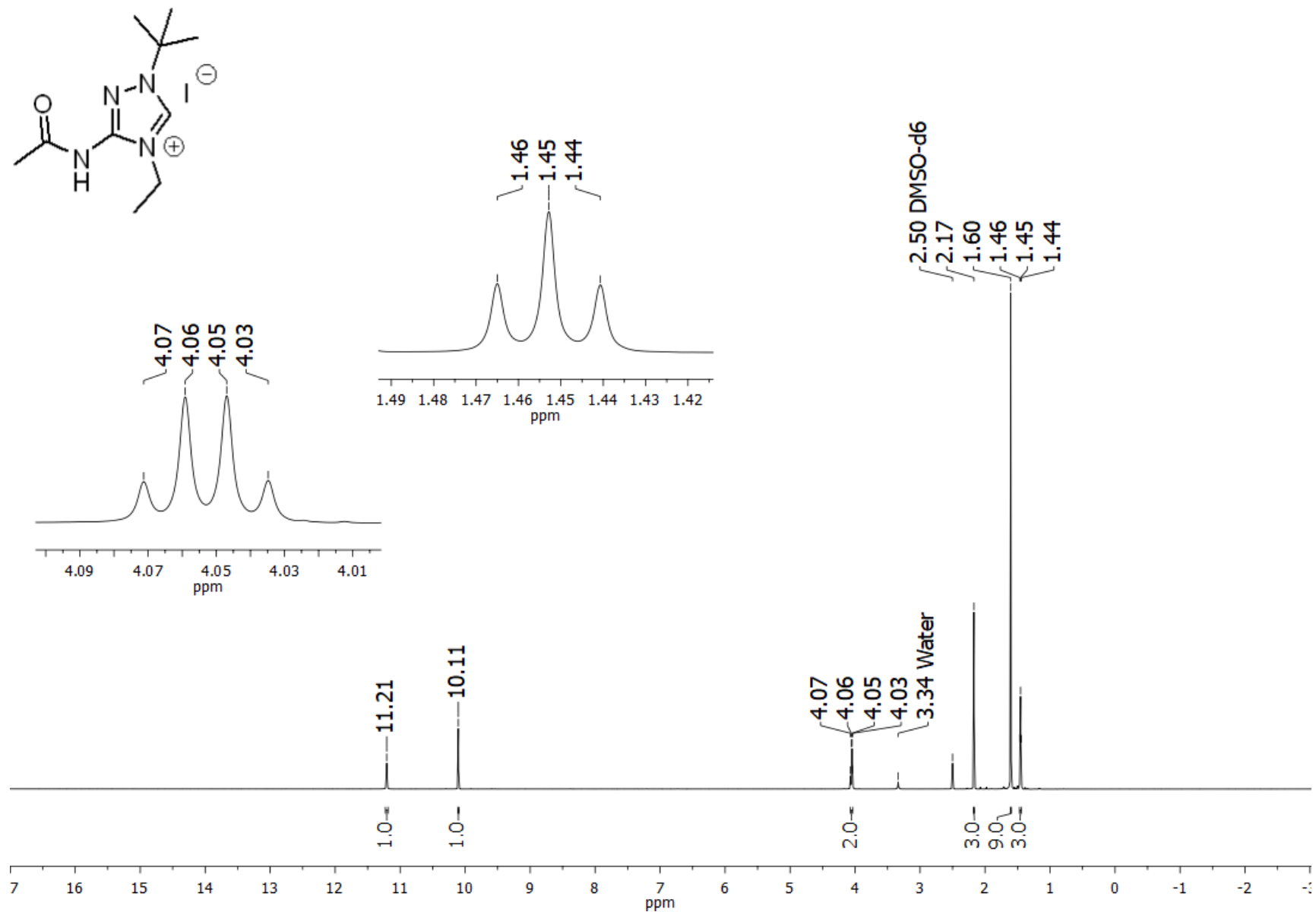
**Figure S39.** $^1$H NMR spectrum of compound **1h** (DMSO-$d_6$, 600 MHz)
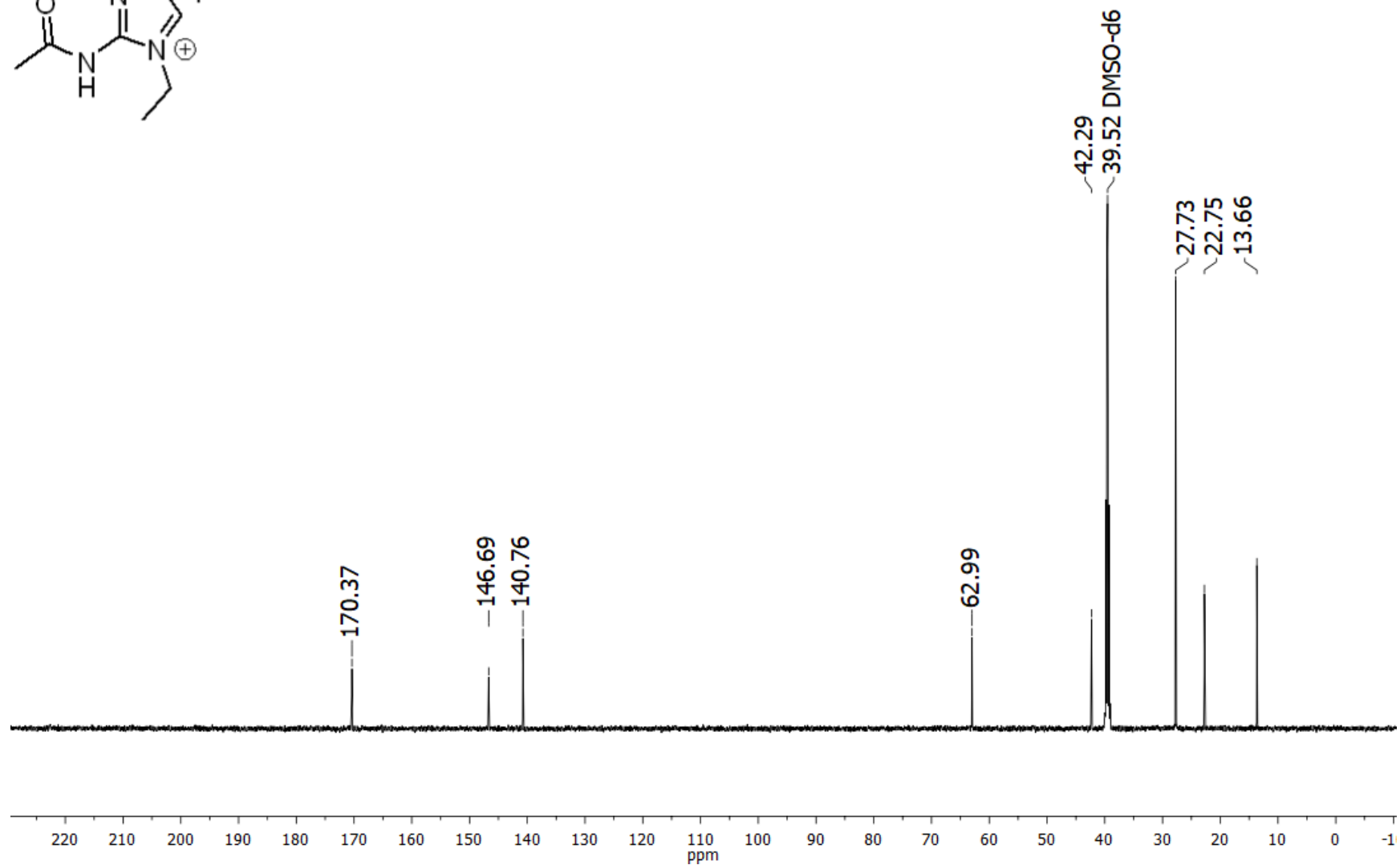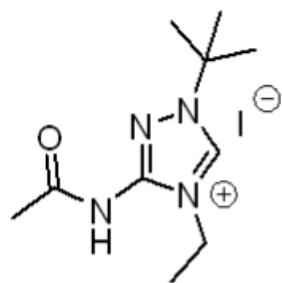
**Figure S40.** $^{13}C$ NMR spectrum of compound **1h** (DMSO-$d_6$, 150 MHz)
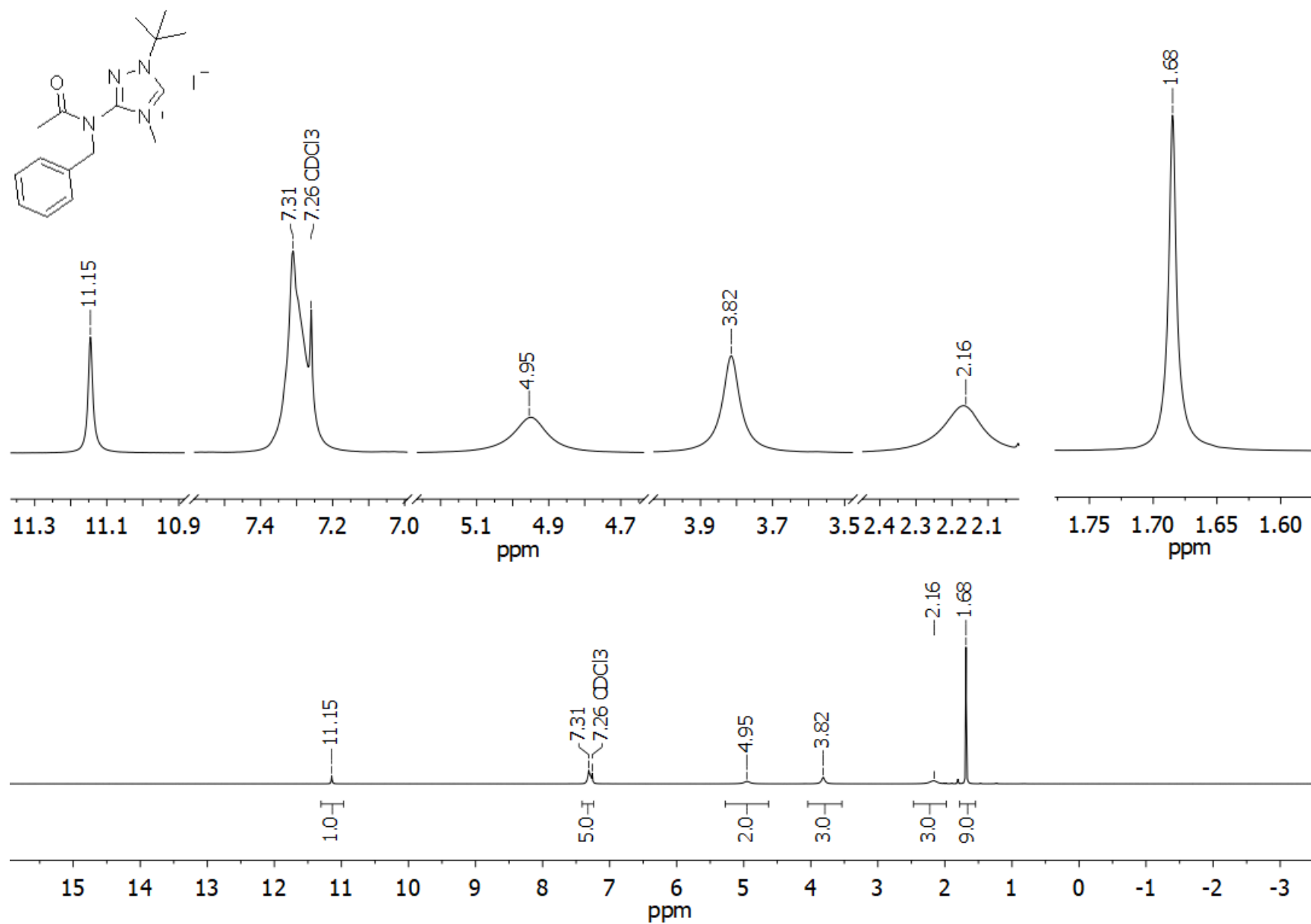
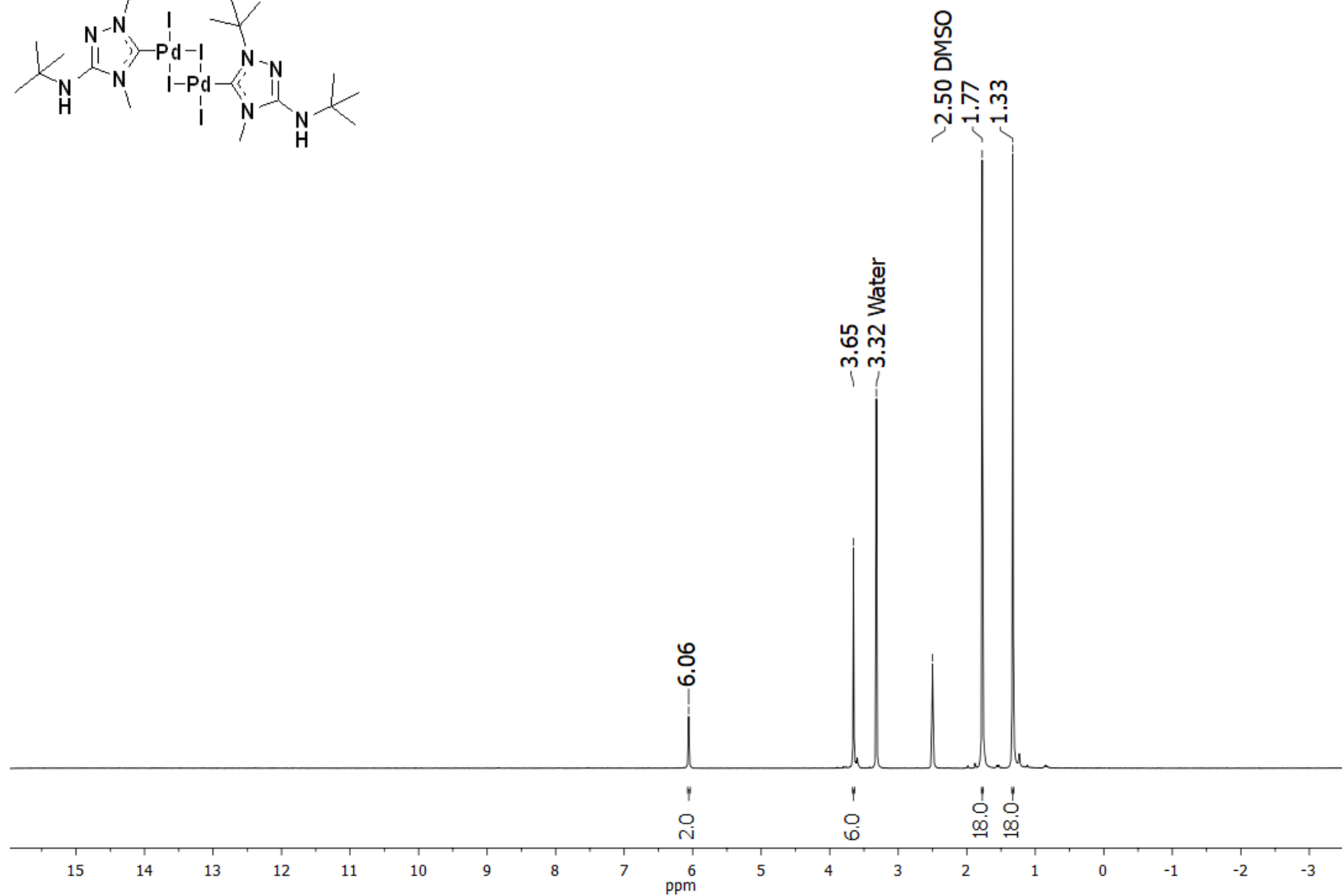**Figure S41.** $^1$H NMR spectrum of compound **1i** (CDCl$_3$, 300 MHz). Some signals are broadened due to hindered rotation of benzyl and acetamido groups.
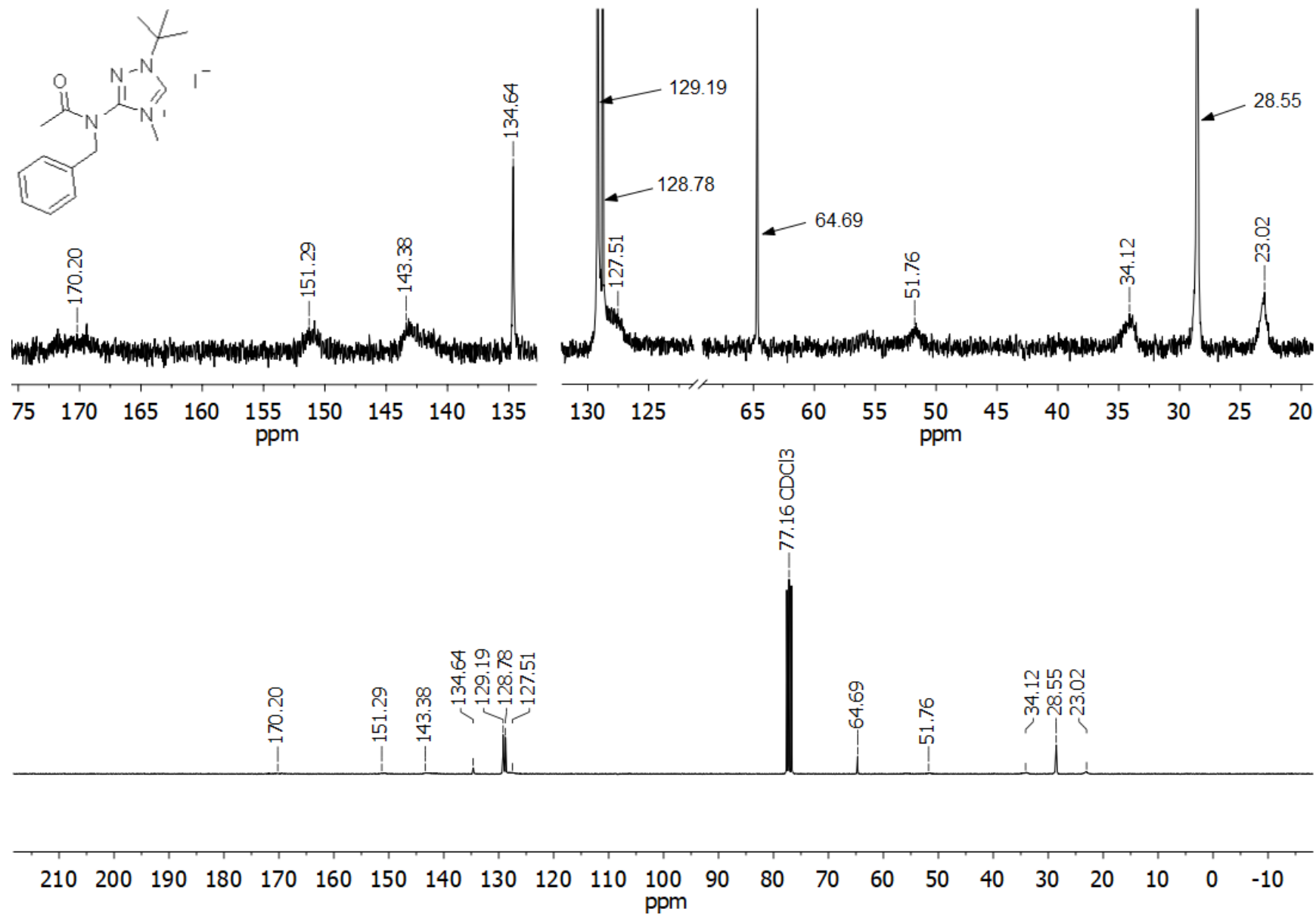
**Figure S42.** $^{13}$C NMR spectrum of compound **1i** (CDCl₃, 75 MHz). Some signals are broadened due to hindered rotation of benzyl and acetamido groups.
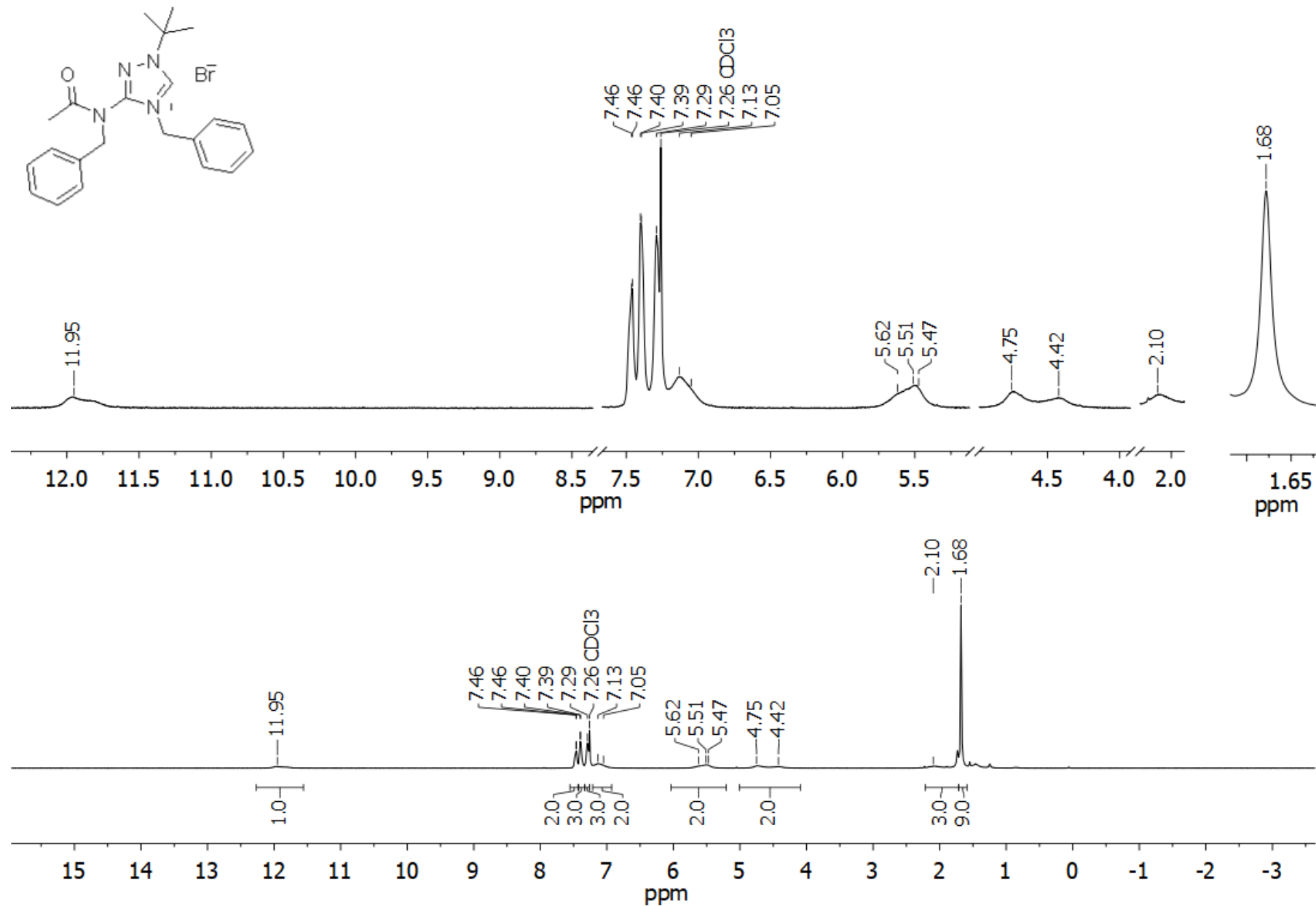
**Figure S43.** $^1$H NMR spectrum of compound **1j** (CDCl$_3$, 300 MHz). Some signals are broadened due to hindered rotation of substituents.
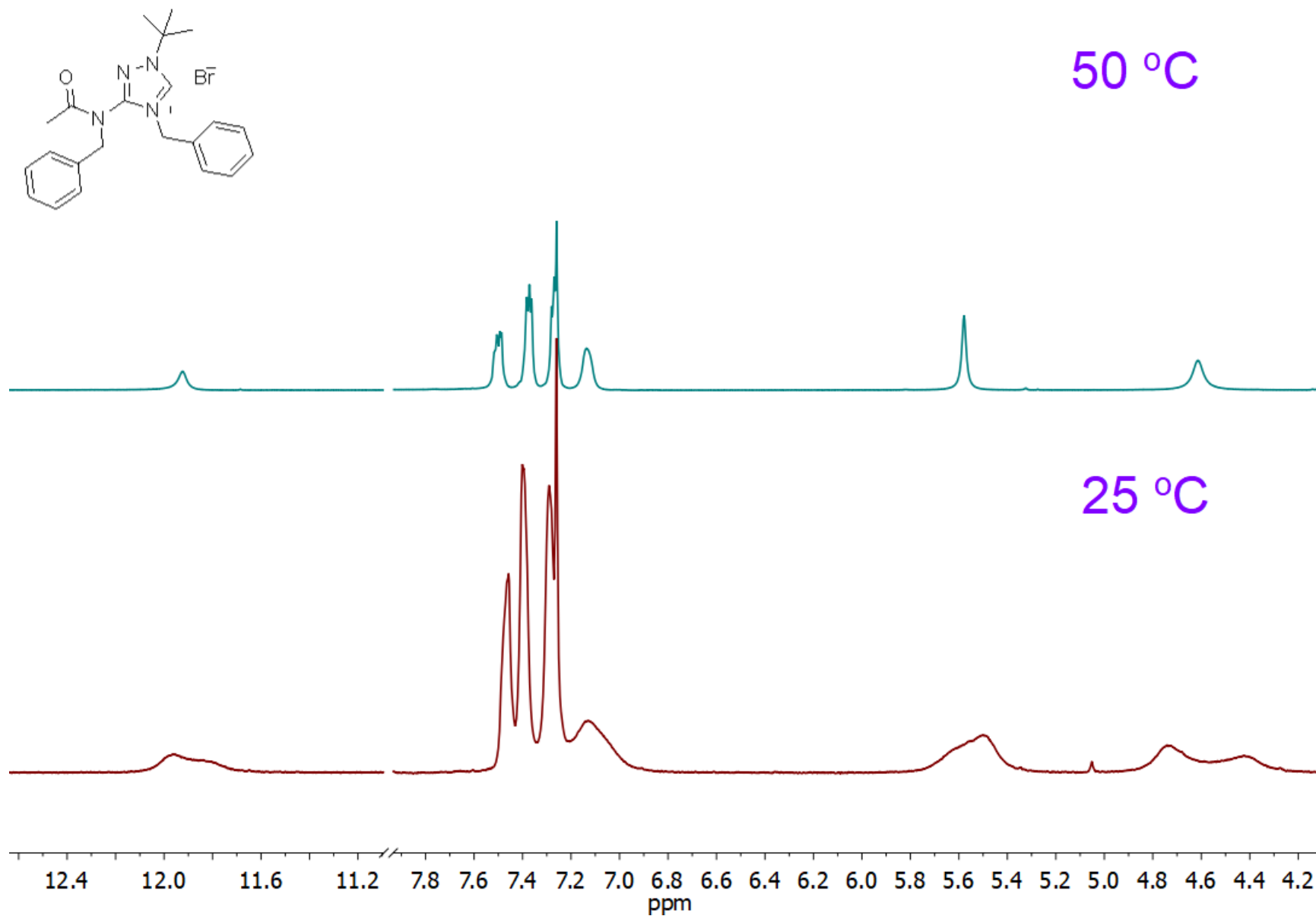
**Figure S44.** Comparison of $^1$H NMR spectra of compound **1j** at 25 and 50 °C (CDCl$_3$, 300 MHz).
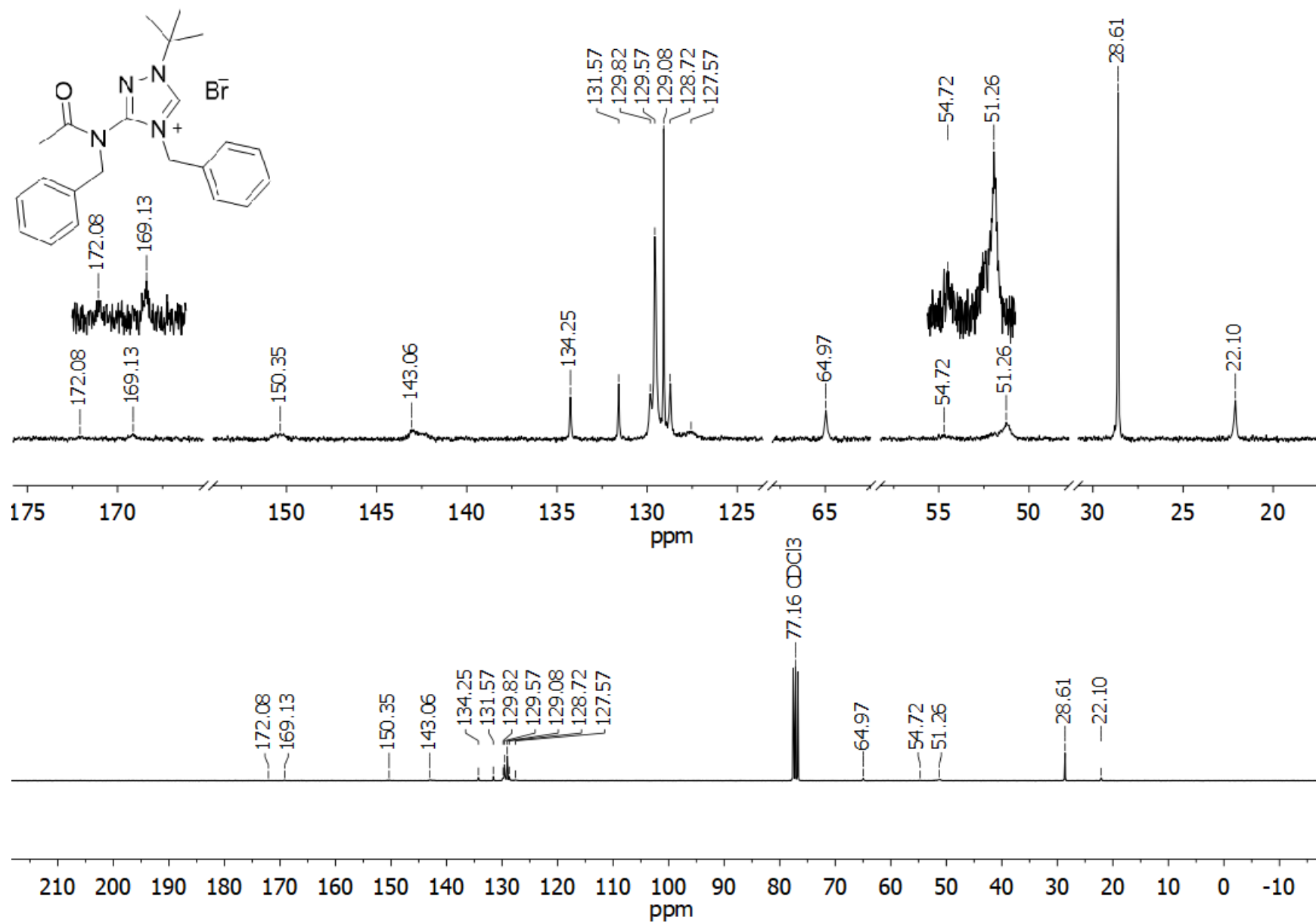
**Figure S45.** $^{13}C$ NMR spectrum of compound **1j** (CDCl₃, 75 MHz).
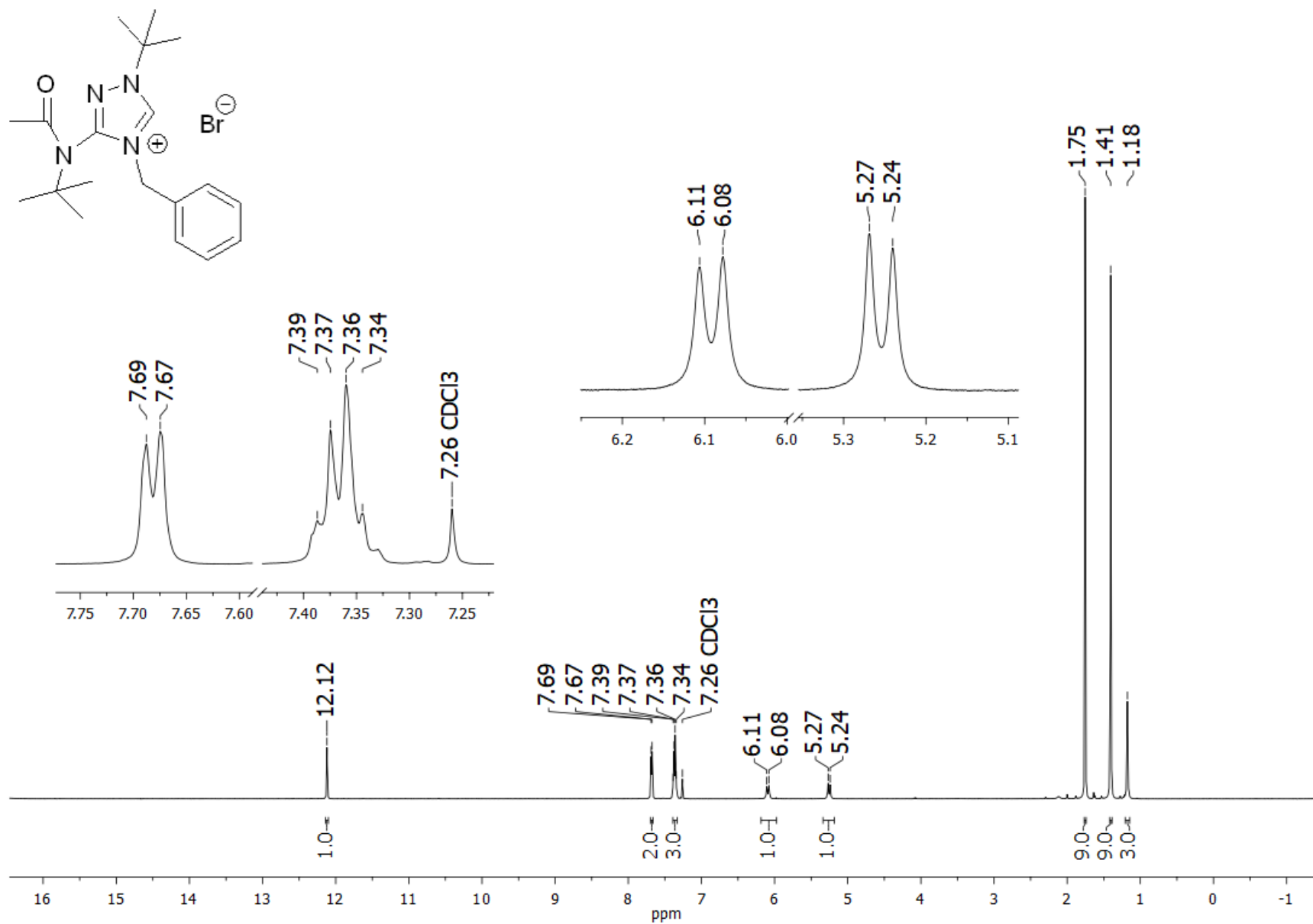
**Figure S46.** $^1$H NMR spectrum of compound **1k** (CDCl$_3$, 500 MHz).
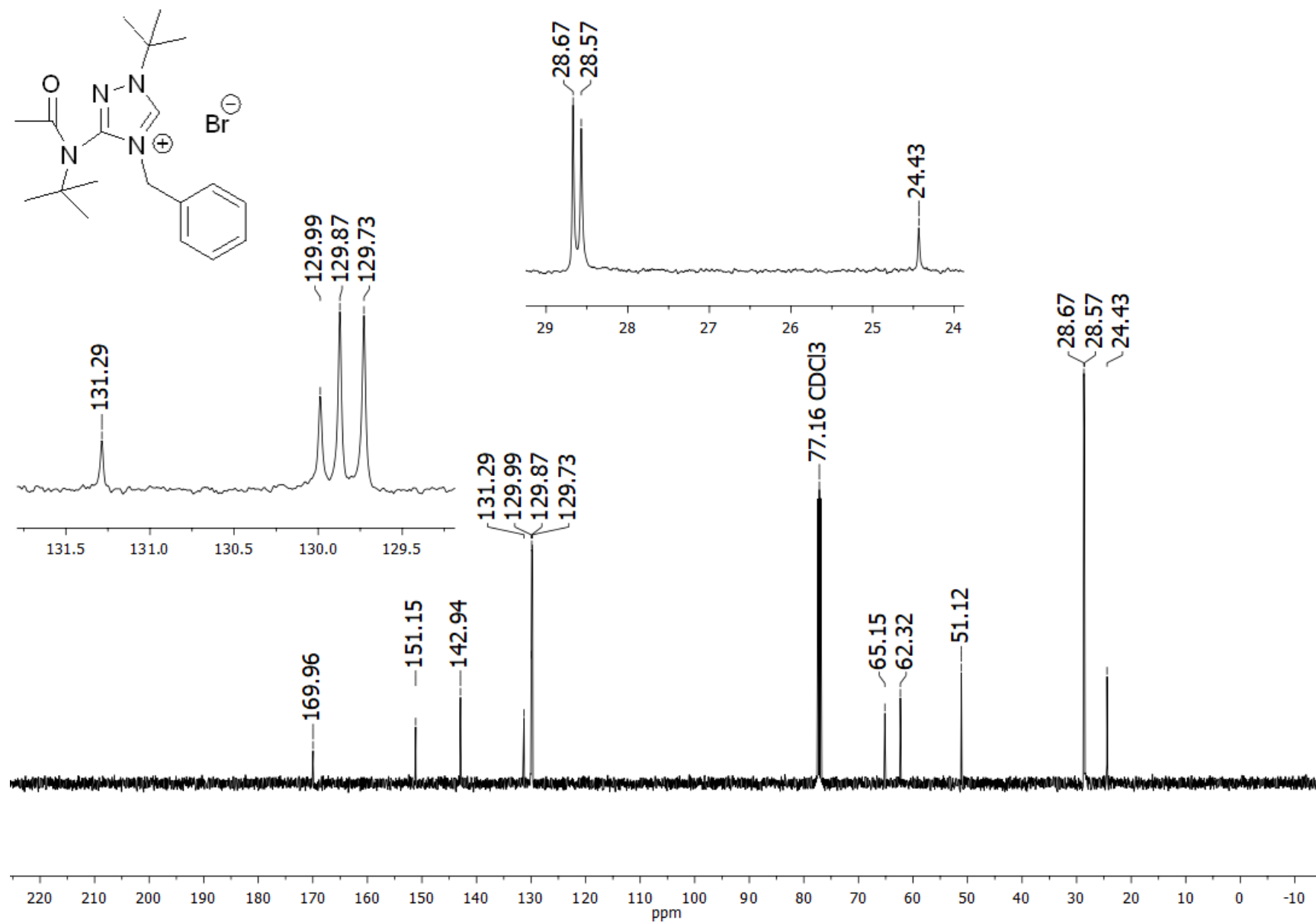
**Figure S47.** $^{13}$C NMR spectrum of compound **1k** (CDCl$_3$, 125 MHz)
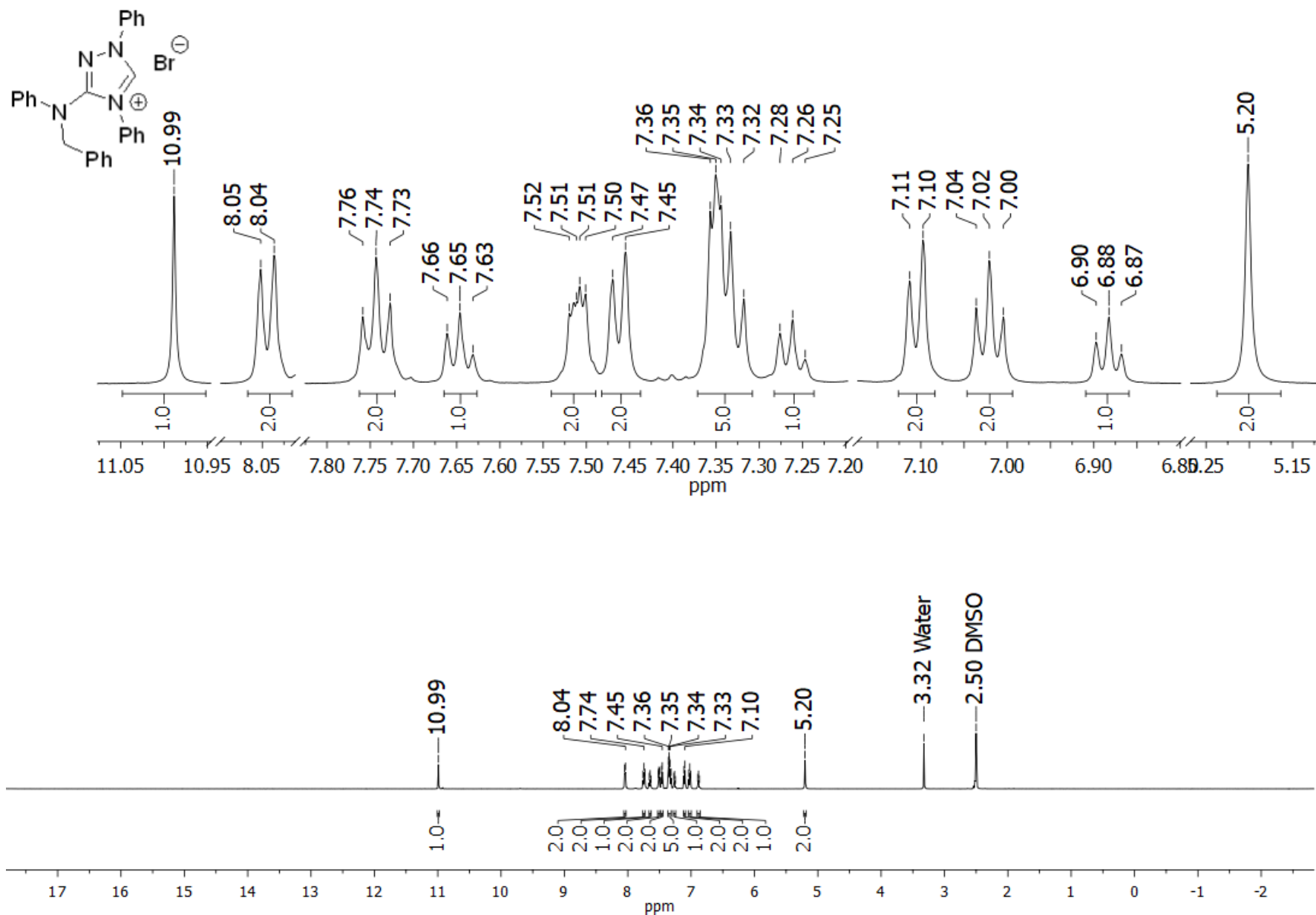
**Figure S48.** $^1H$ NMR spectrum of compound **1l** (DMSO-$d_6$, 500 MHz)
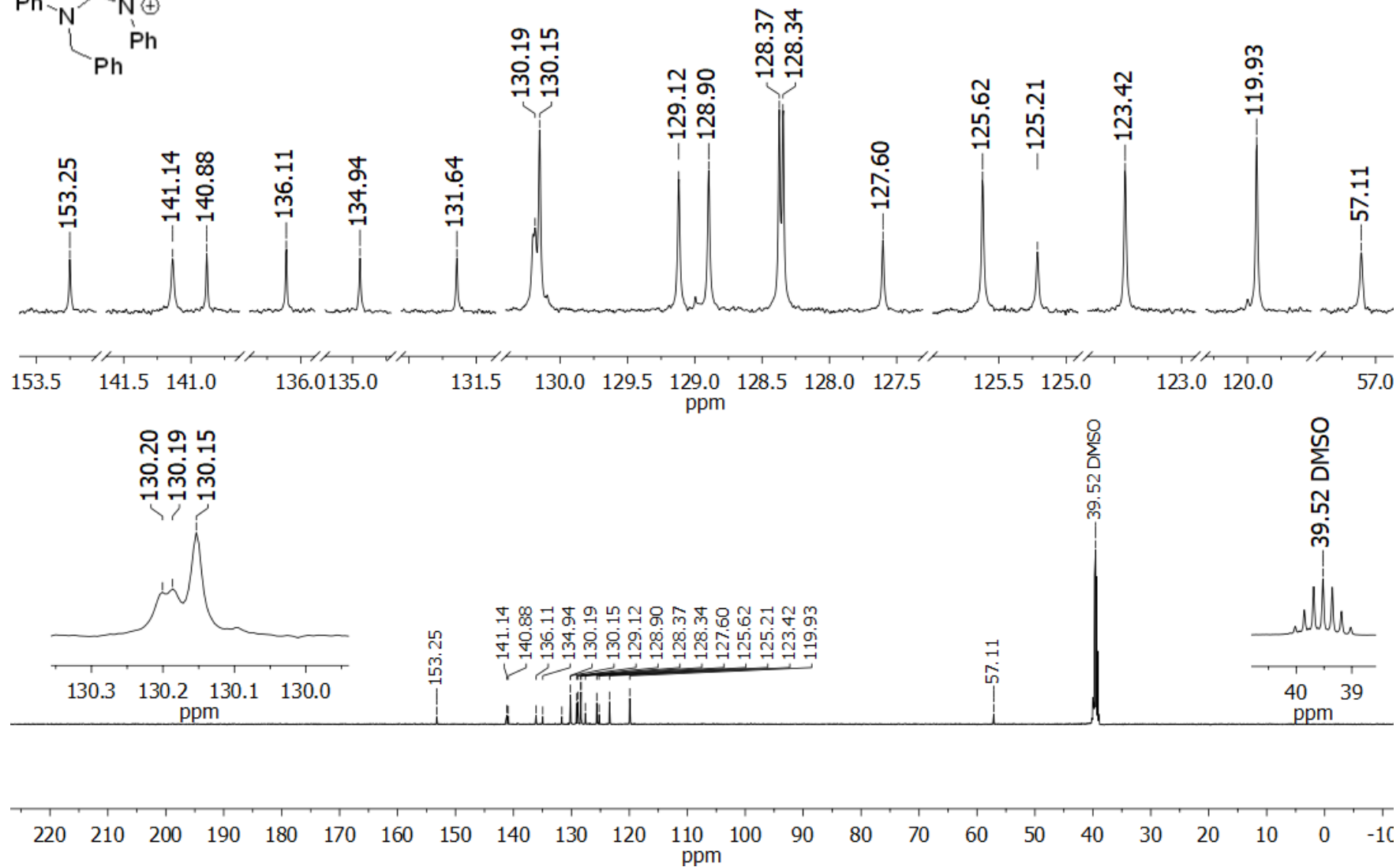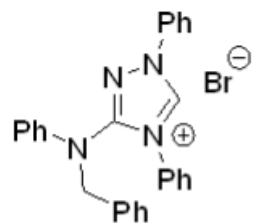
**Figure S49.** $^{13}$C NMR spectrum of compound **1l** (DMSO-$d_6$, 125 MHz)
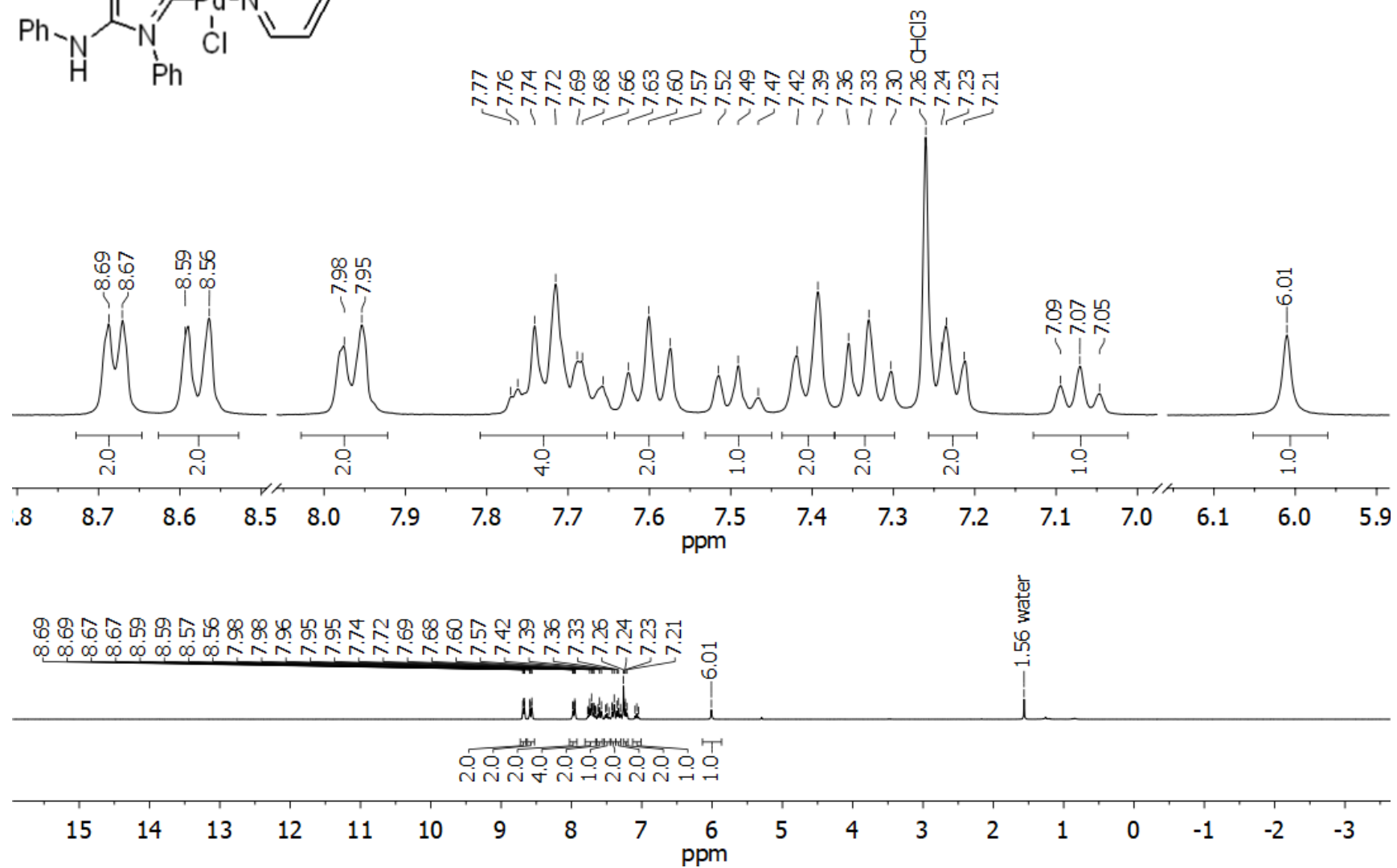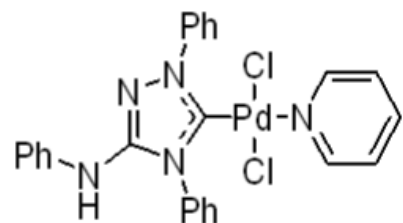
**Figure S50.** $^1$H NMR spectrum of compound **2a** (CDCl$_3$, 300 MHz)
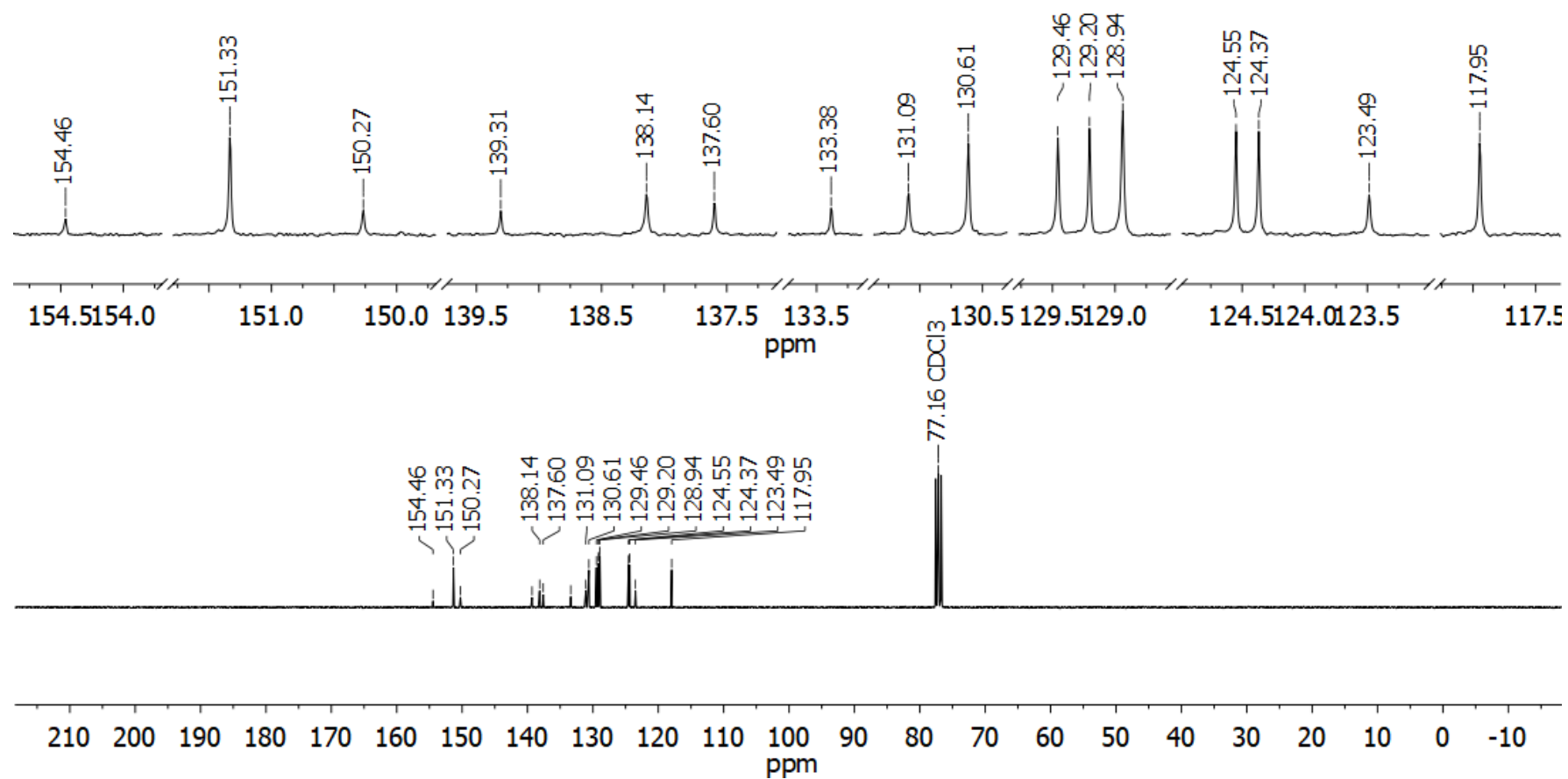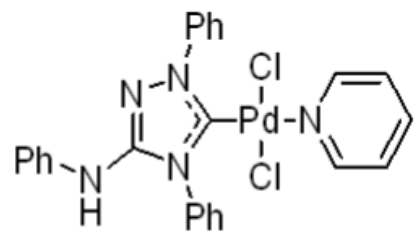
**Figure S51.** $^{13}$C NMR spectrum of compound **2a** (CDCl$_3$, 75 MHz)
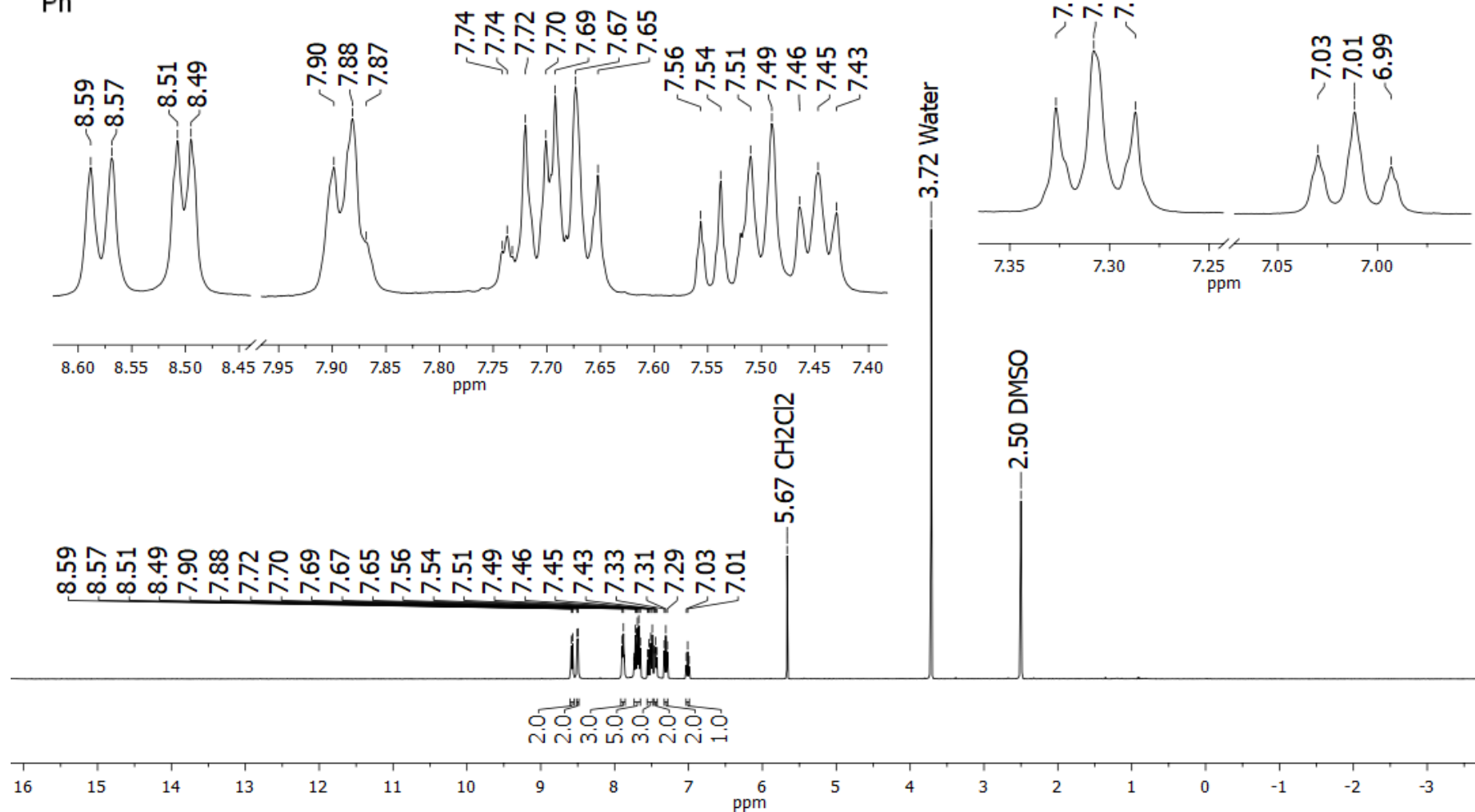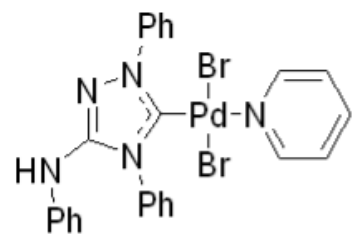
**Figure S52.** $^1$H NMR spectrum of compound **2b** (DMSO-$d_6$, 400 MHz)
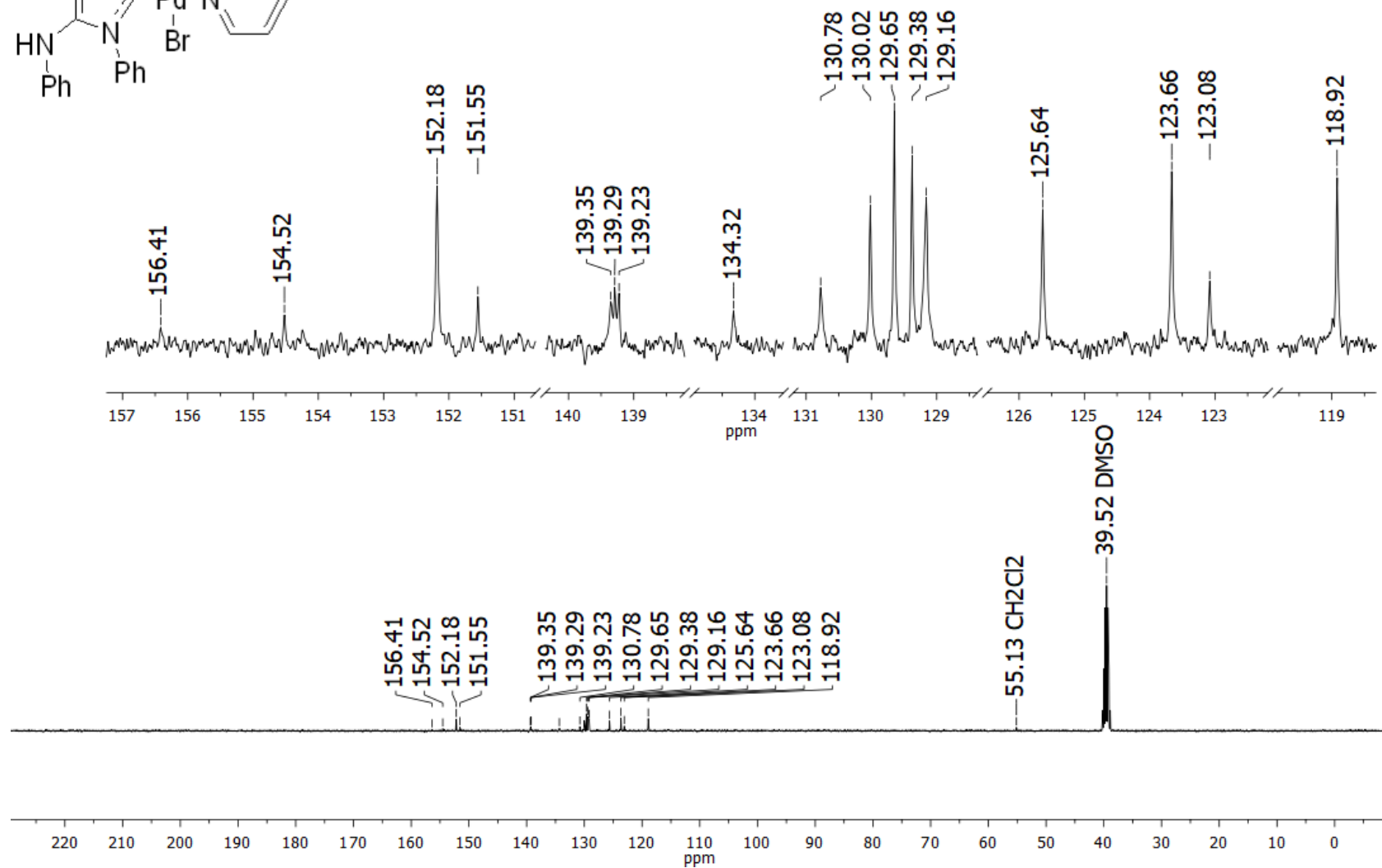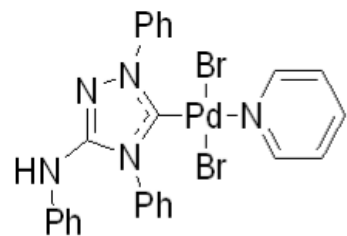
**Figure S53.** $^{13}$C NMR spectrum of compound **2b** (DMSO-$d_6$, 100 MHz)
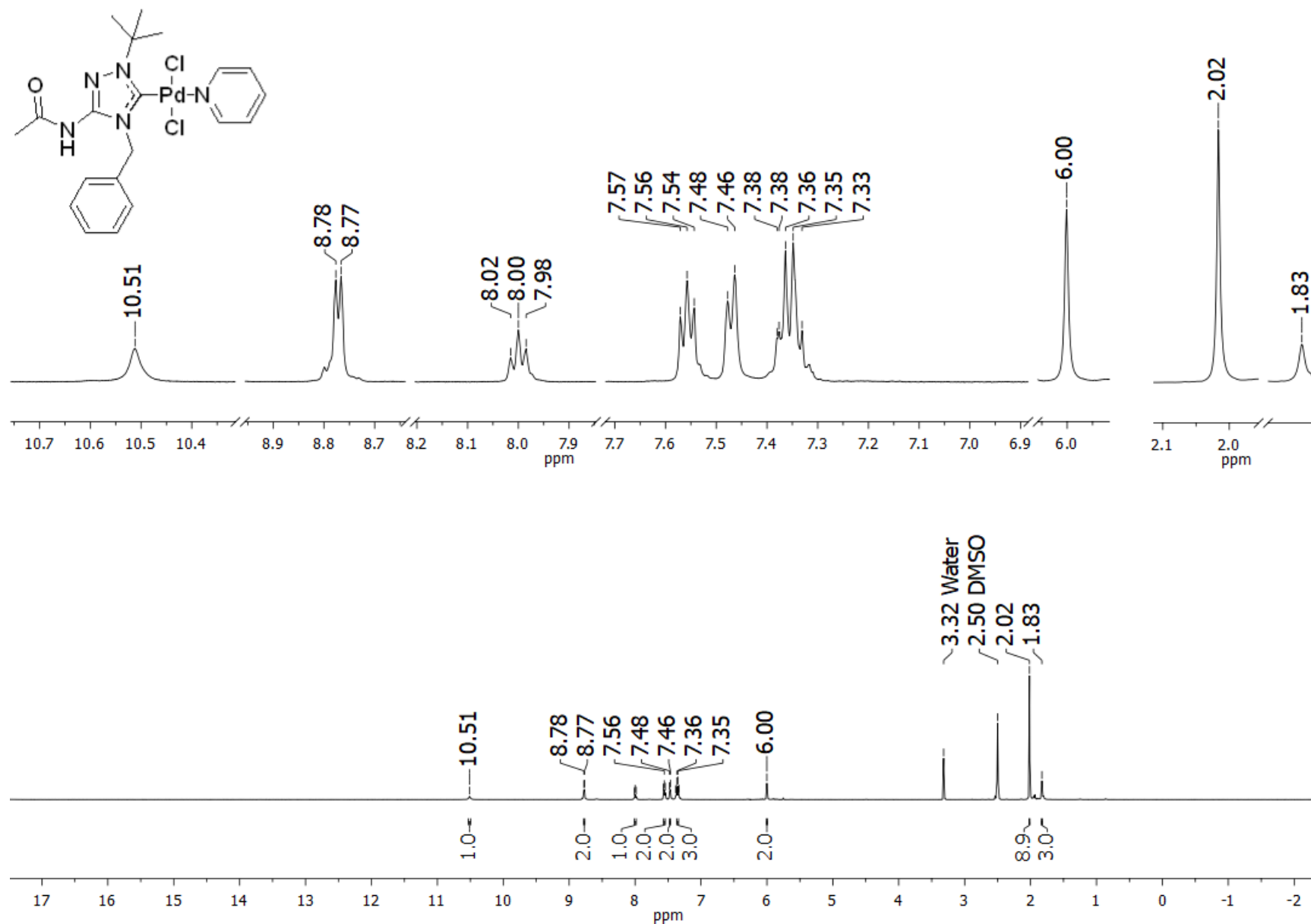
**Figure S54.** $^1$H NMR spectrum of compound **2c** (DMSO-$d_6$, 500 MHz)
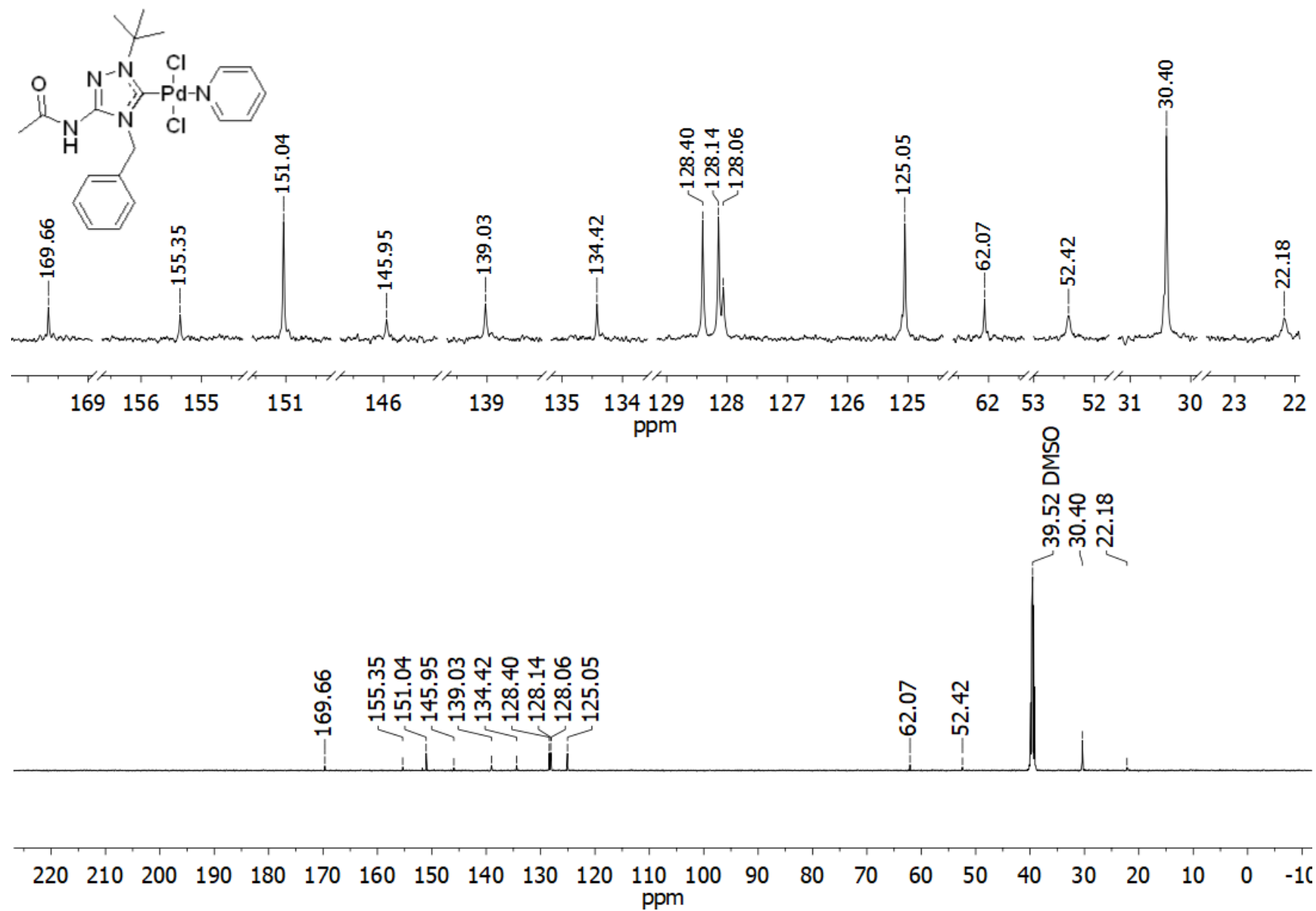
**Figure S55.** $^{13}C$ NMR spectrum of compound **2c** (DMSO-$d_6$, 125 MHz)
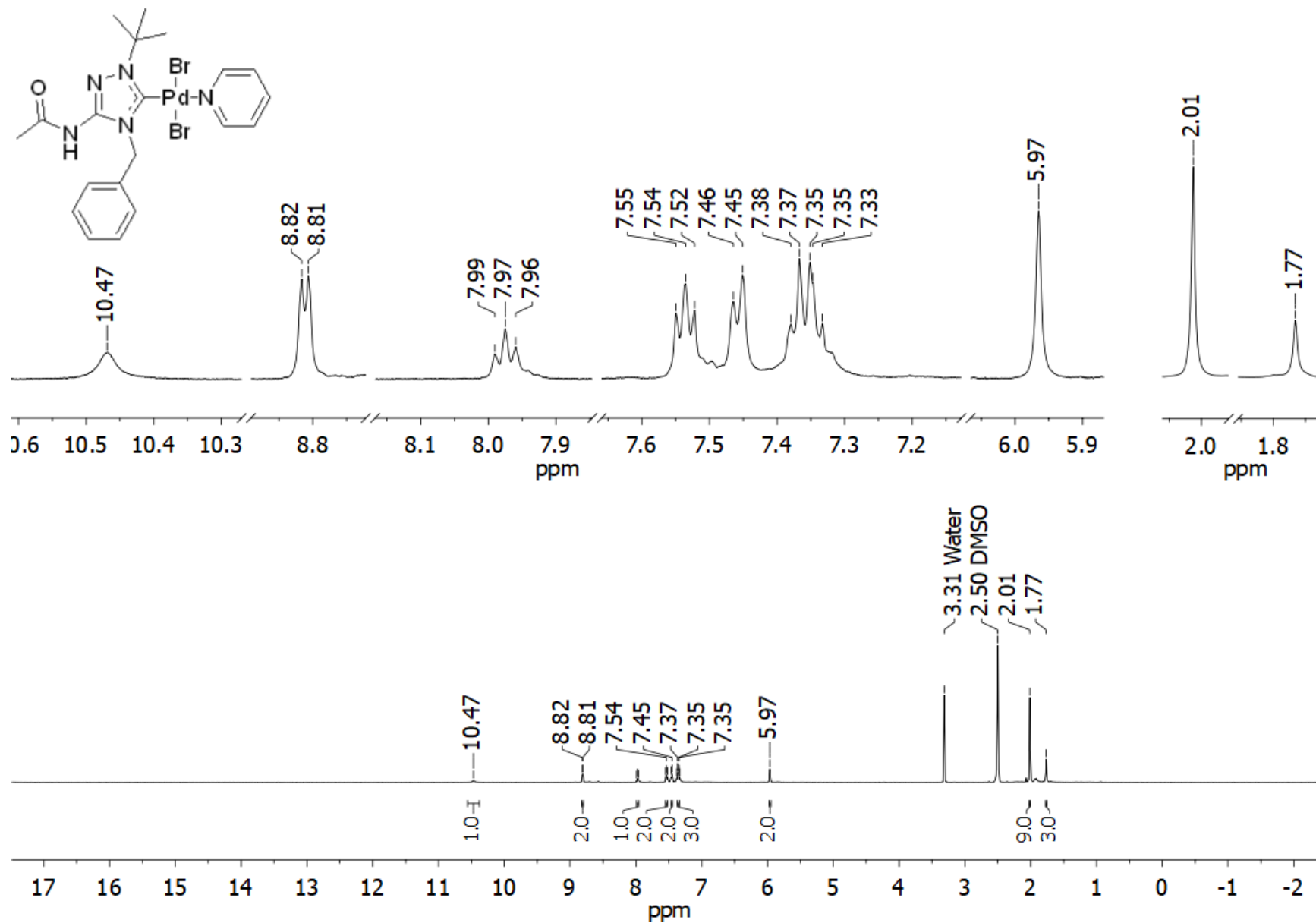
**Figure S56.** $^1$H NMR spectrum of compound **2d** (DMSO-$d_6$, 500 MHz)
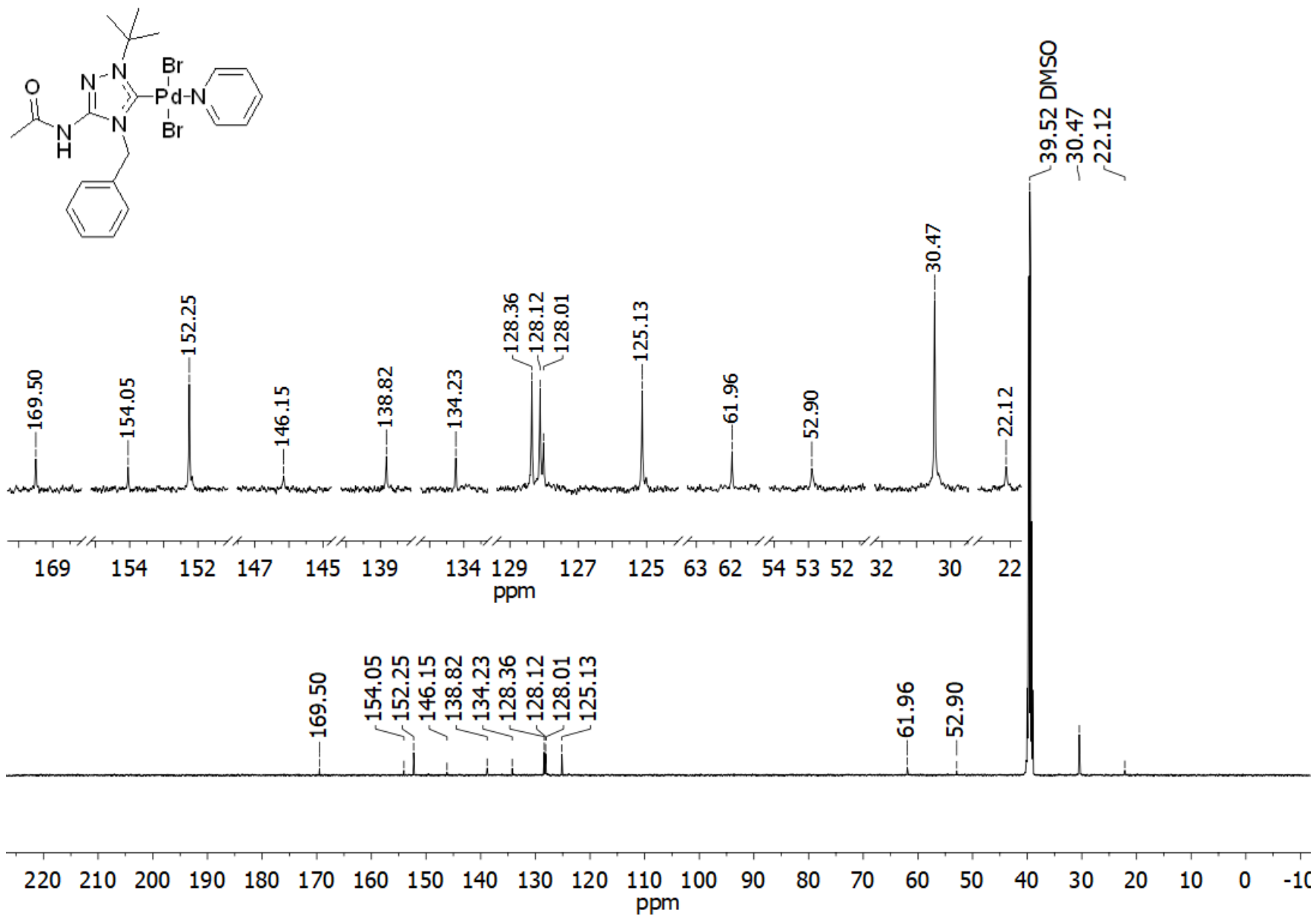
**Figure S57.** $^{13}C$ NMR spectrum of compound **2d** (DMSO-$d_6$, 125 MHz)
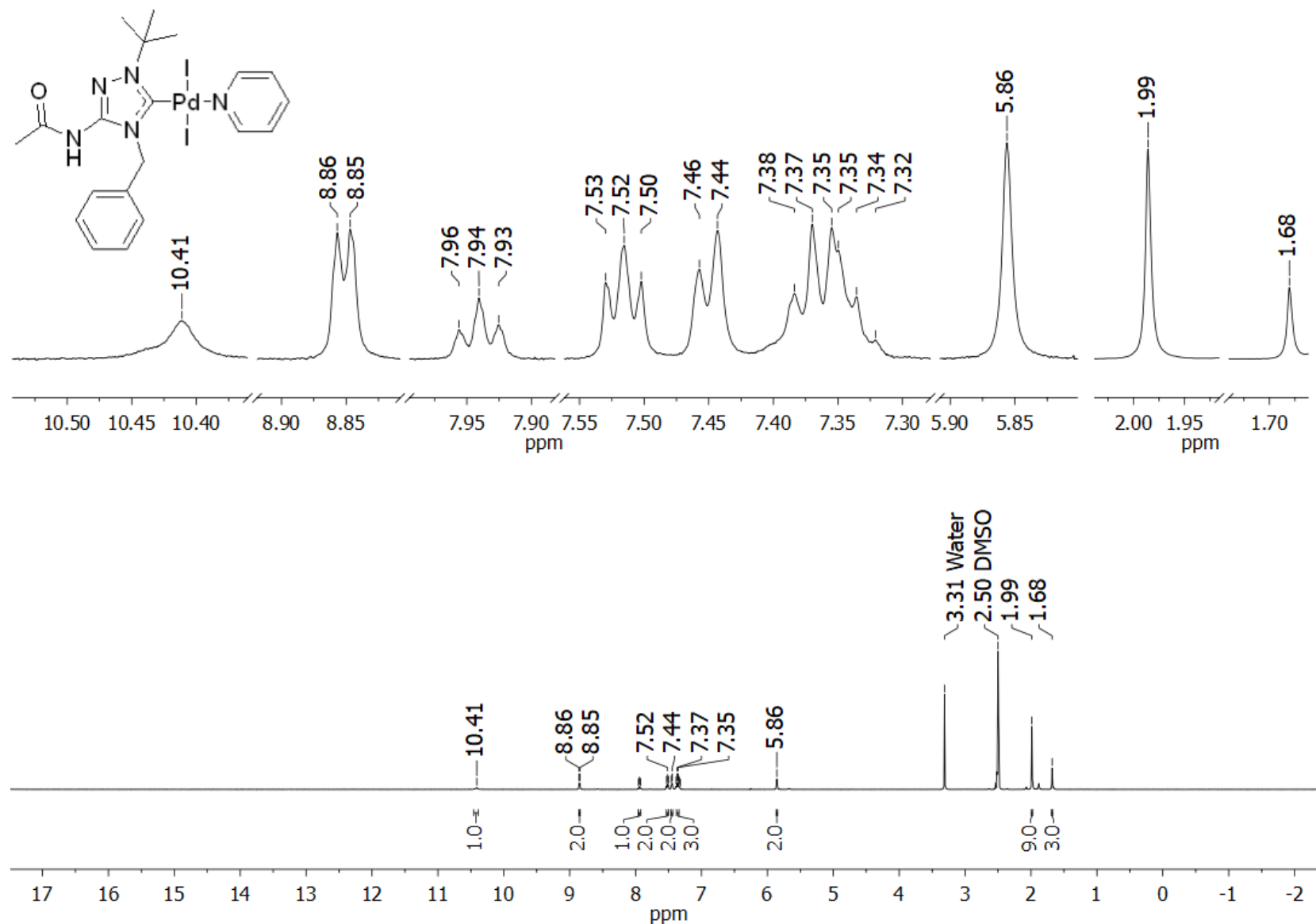
**Figure S58.** $^1$H NMR spectrum of compound **2e** (DMSO-$d_6$, 500 MHz)
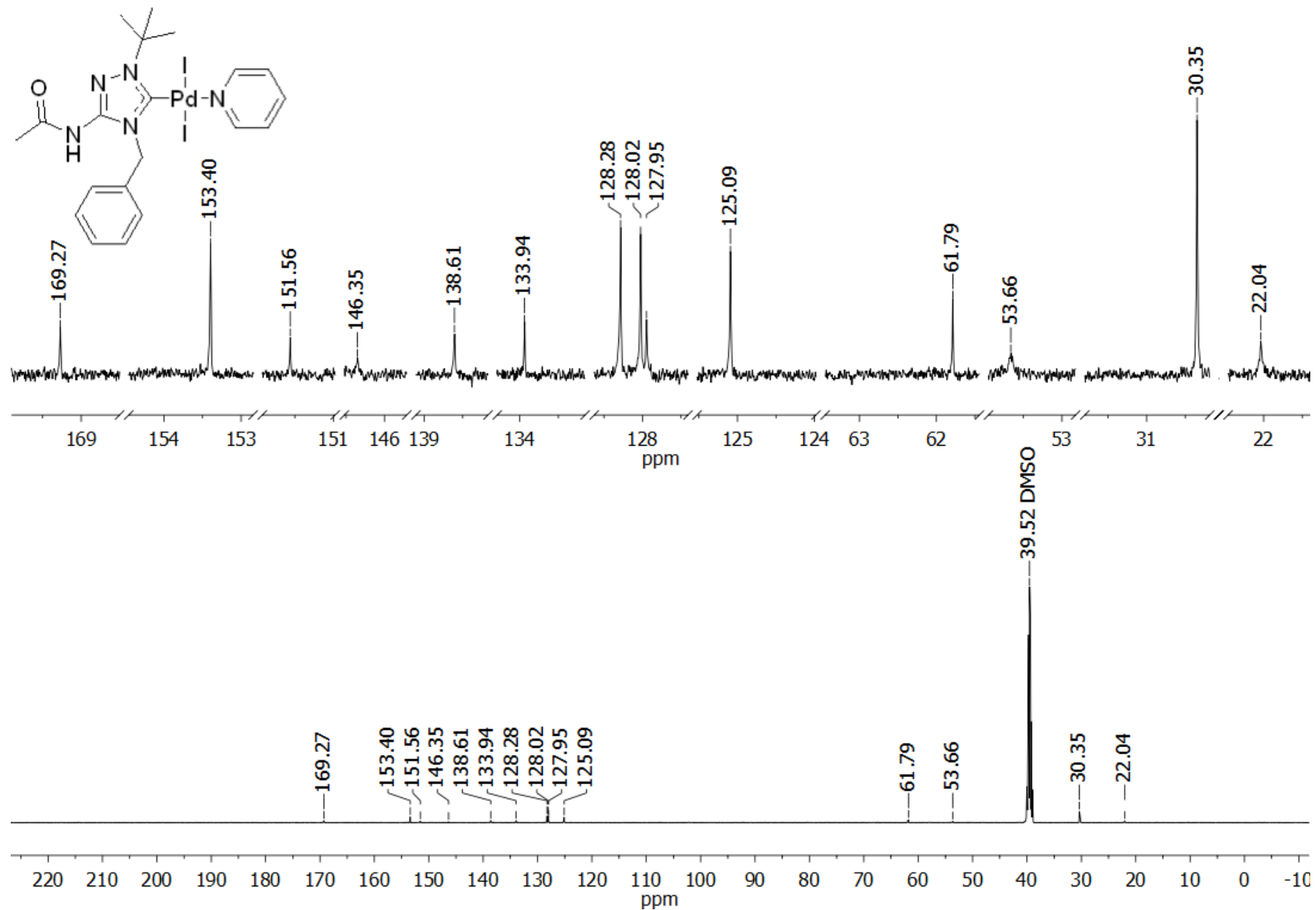
**Figure S59.** $^{13}C$ NMR spectrum of compound **2e** (DMSO-$d_6$, 125 MHz)
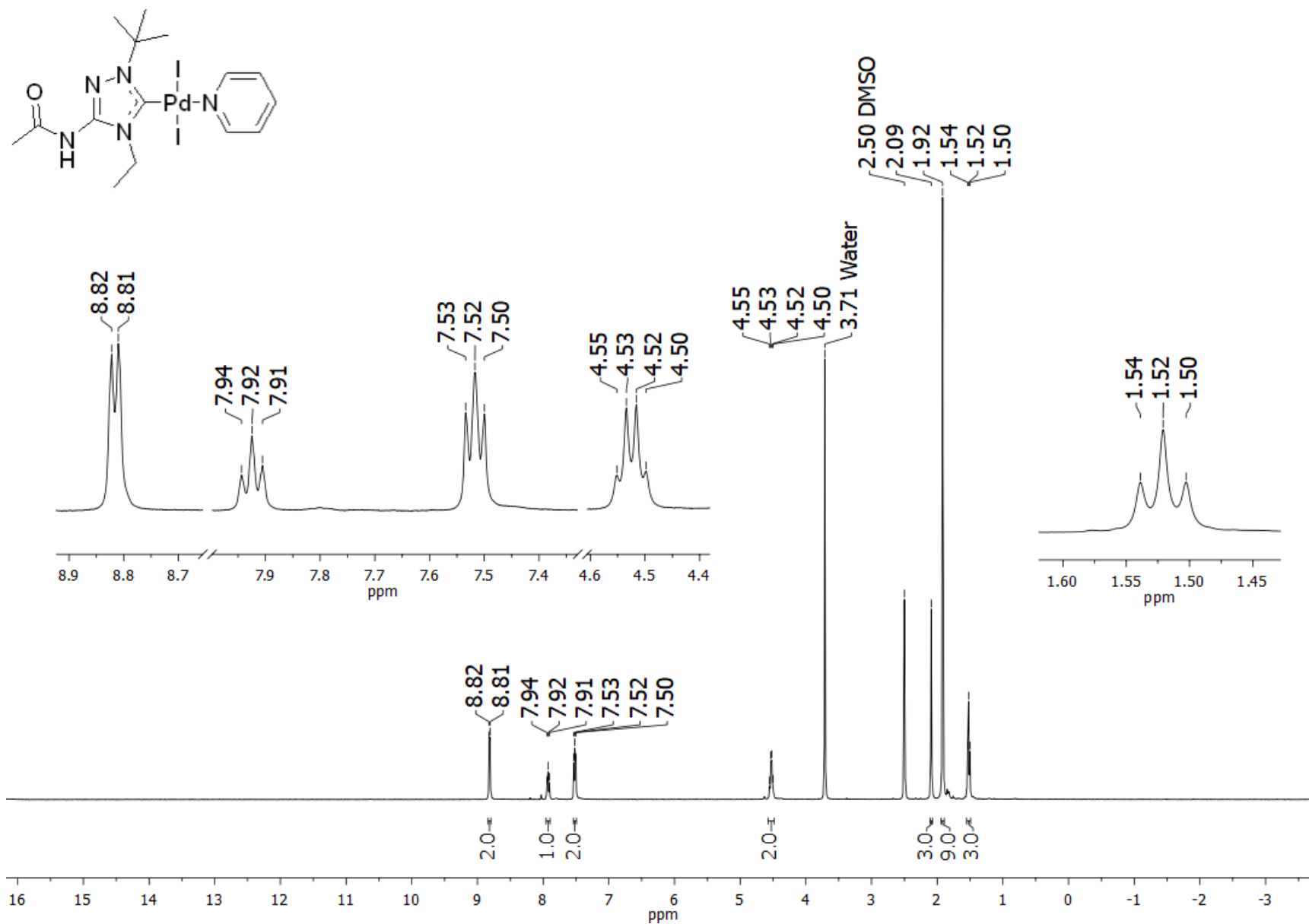
**Figure S60.** $^1$H NMR spectrum of compound **2f** (DMSO-$d_6$, 400 MHz)
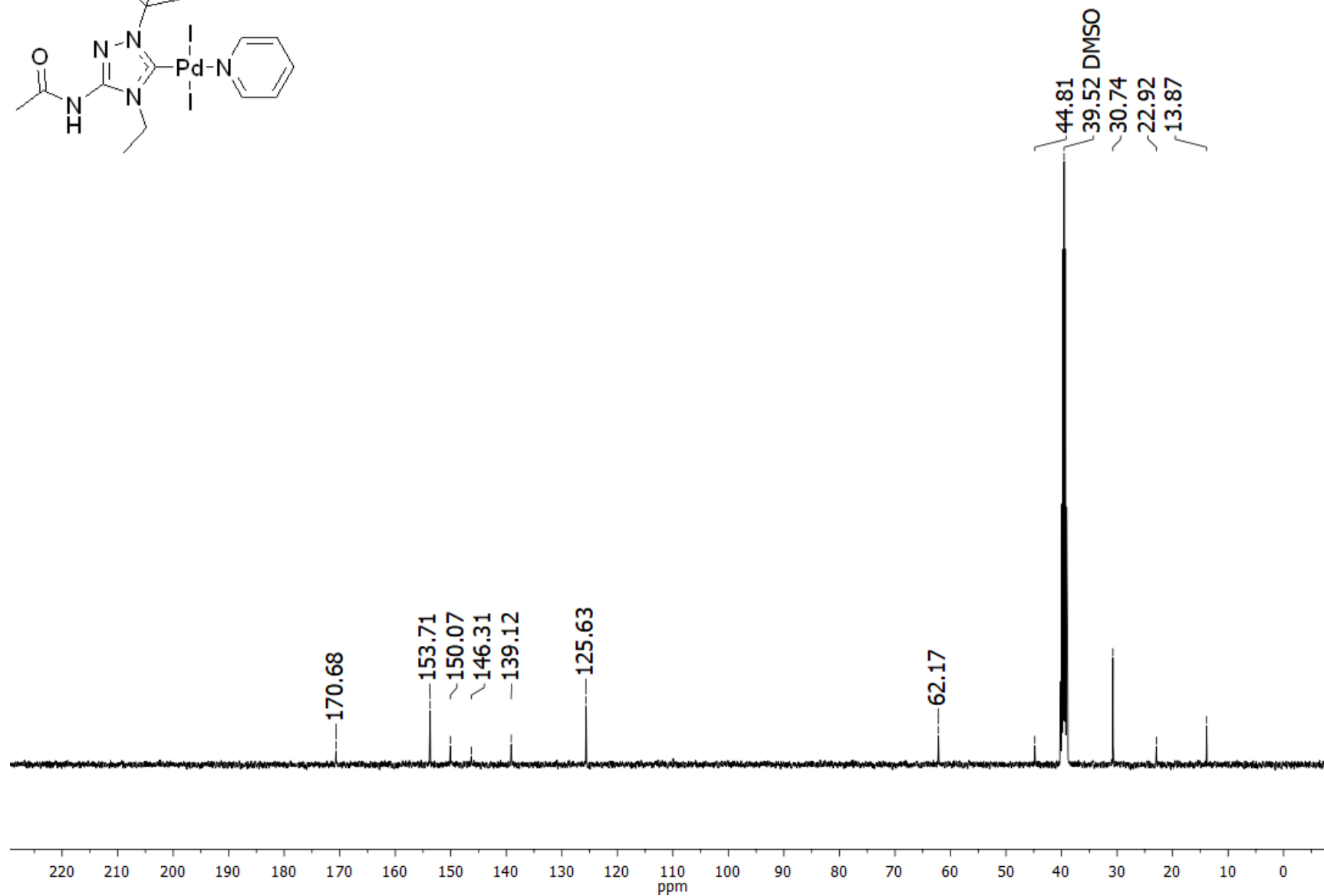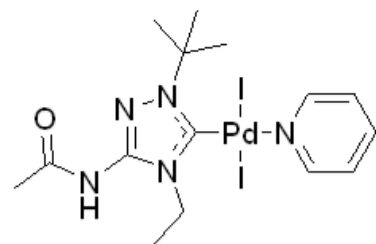
**Figure S61.** $^{13}$C NMR spectrum of compound **2f** (DMSO-$d_6$, 100 MHz)
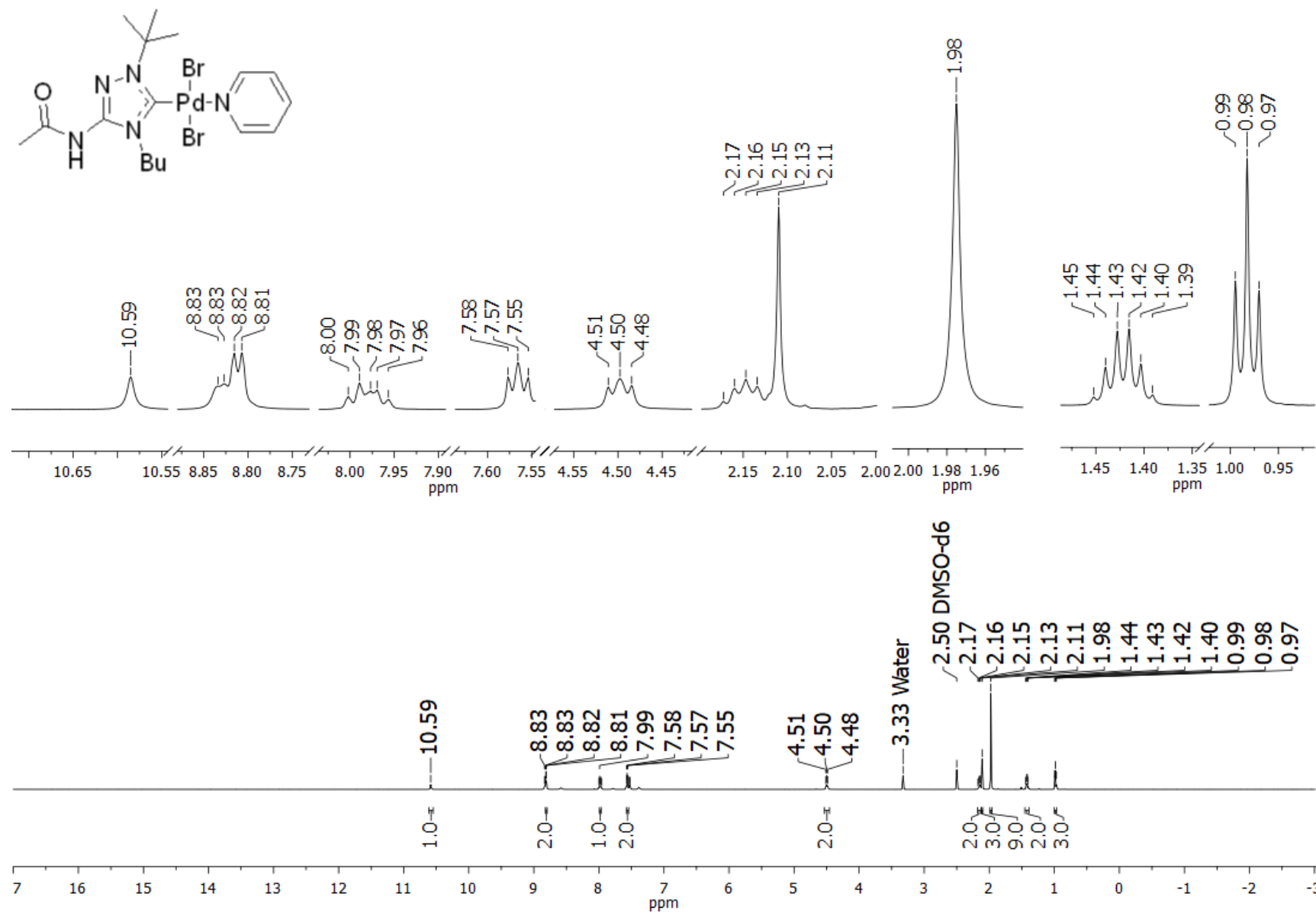
**Figure S62.** $^1$H NMR spectrum of compound **2g** (DMSO-$d_6$, 600 MHz)
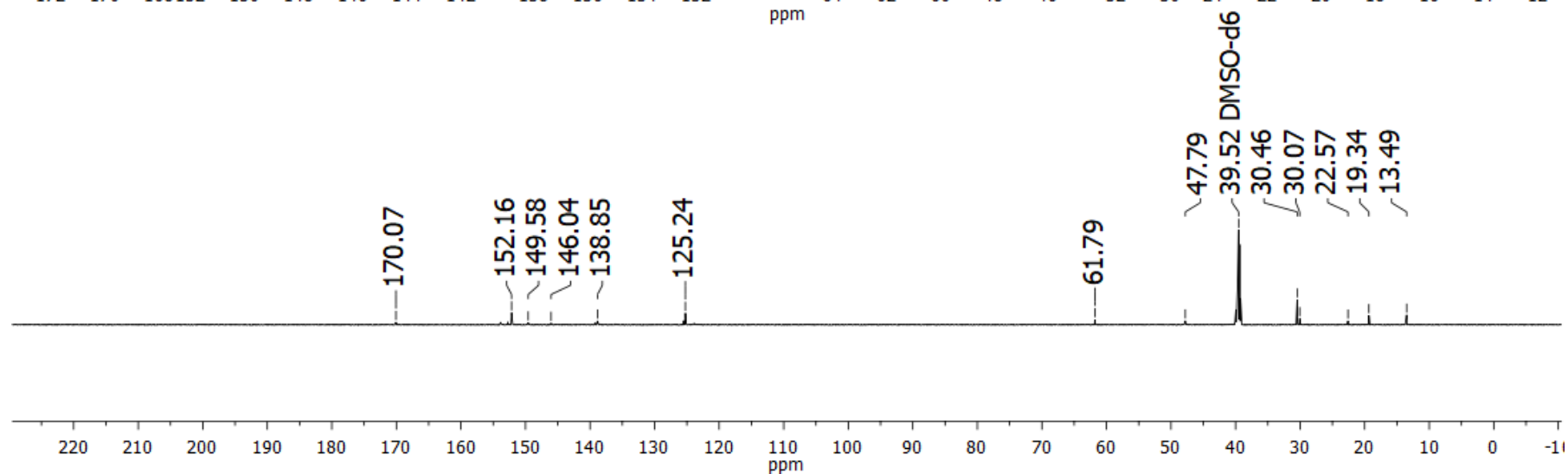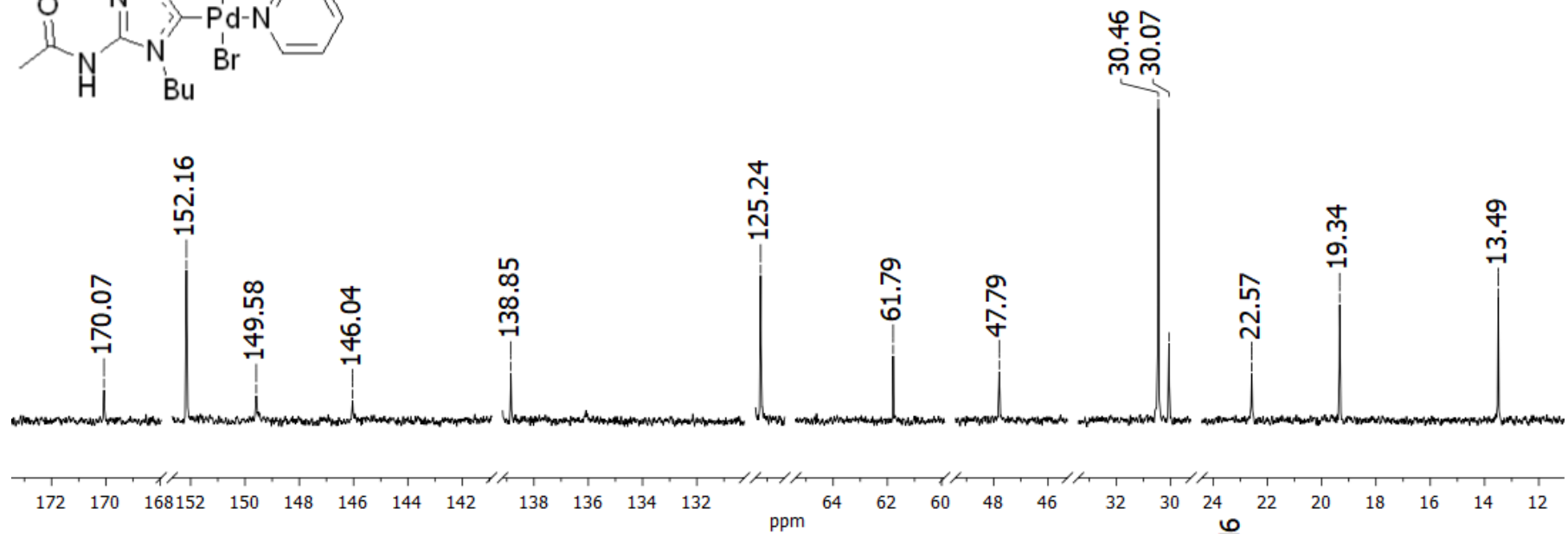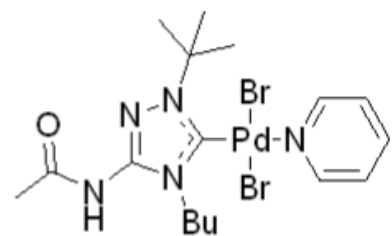
**Figure S63.** $^{13}C$ NMR spectrum of compound **2g** (DMSO-$d_6$, 150 MHz)
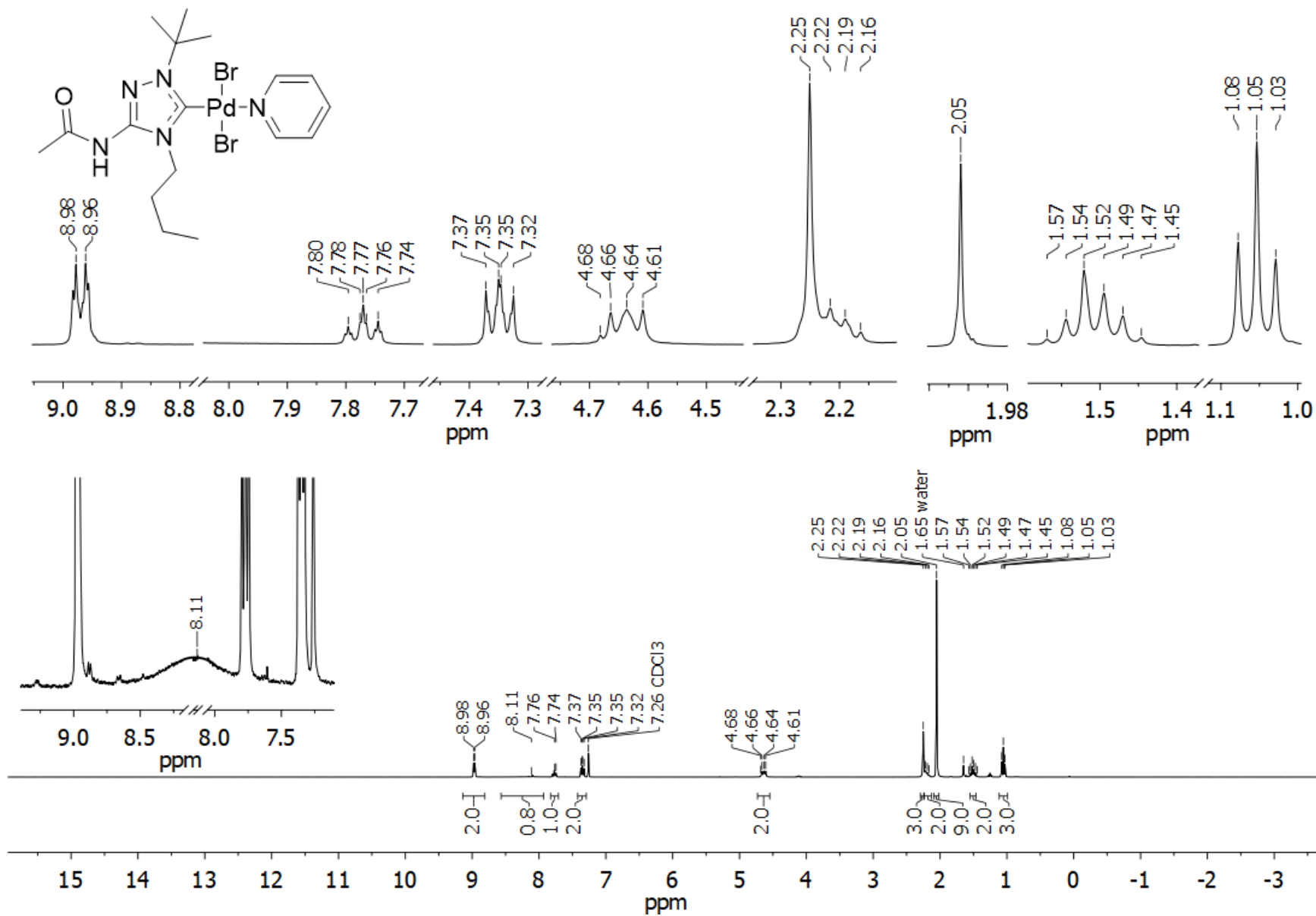
**Figure S64.** $^1$H NMR spectrum of compound **2g** (CDCl$_3$, 300 MHz)
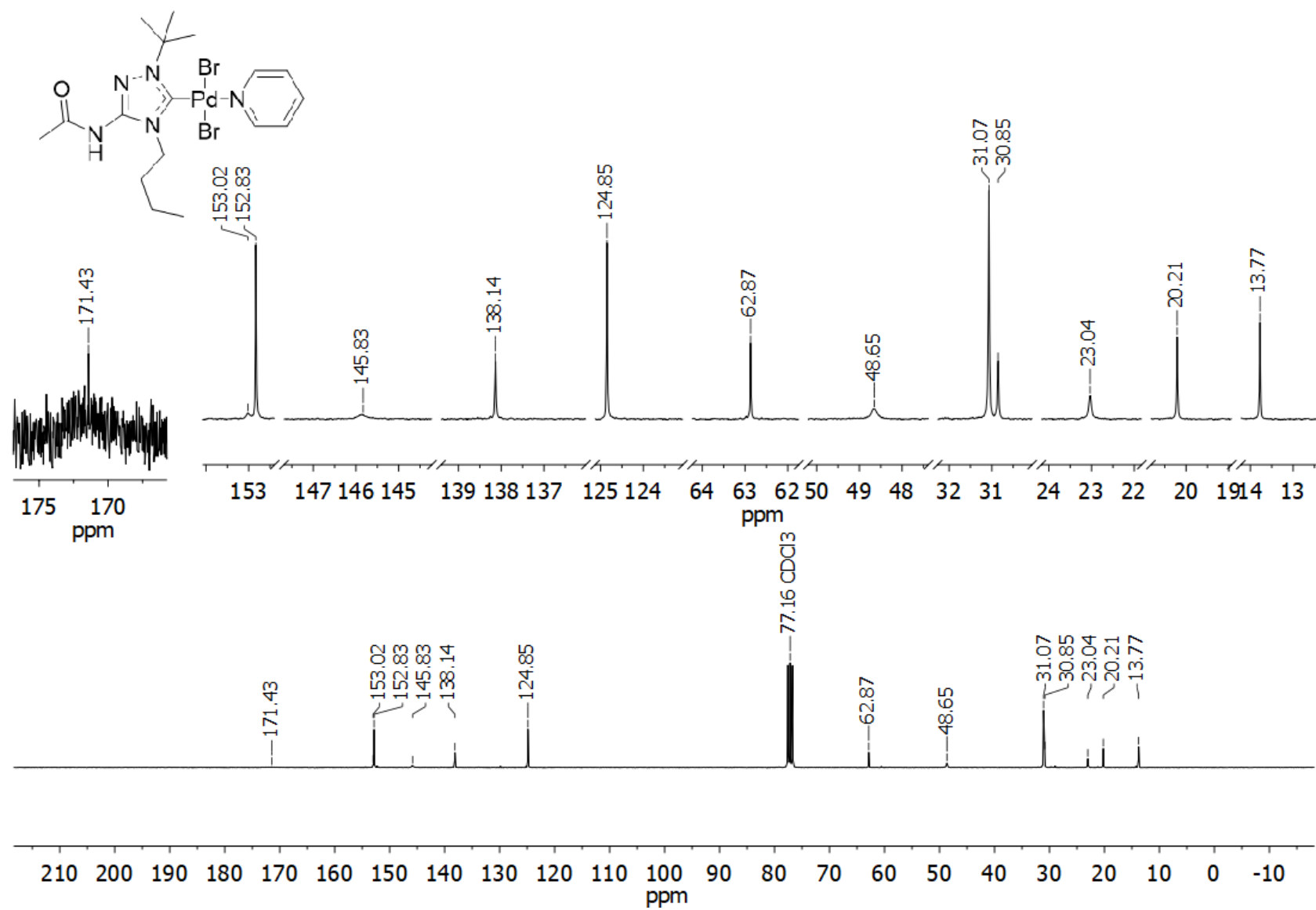
**Figure S65.** $^{13}C$ NMR spectrum of compound **2g** (CDCl$_3$, 75 MHz)
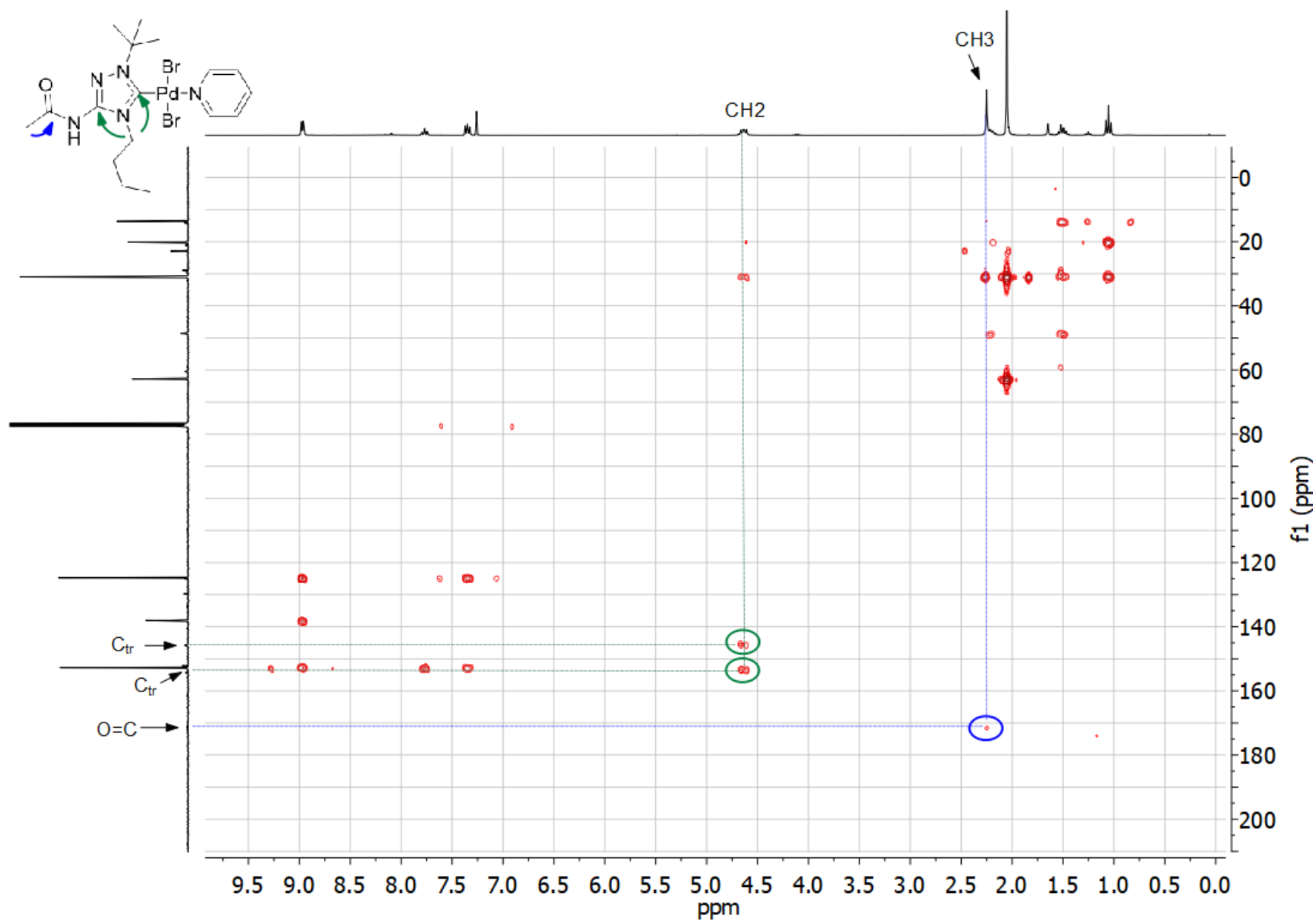
**Figure S66.** $^1$H-$^{13}$C HMBC spectrum of compound **2g** (CDCl$_3$)
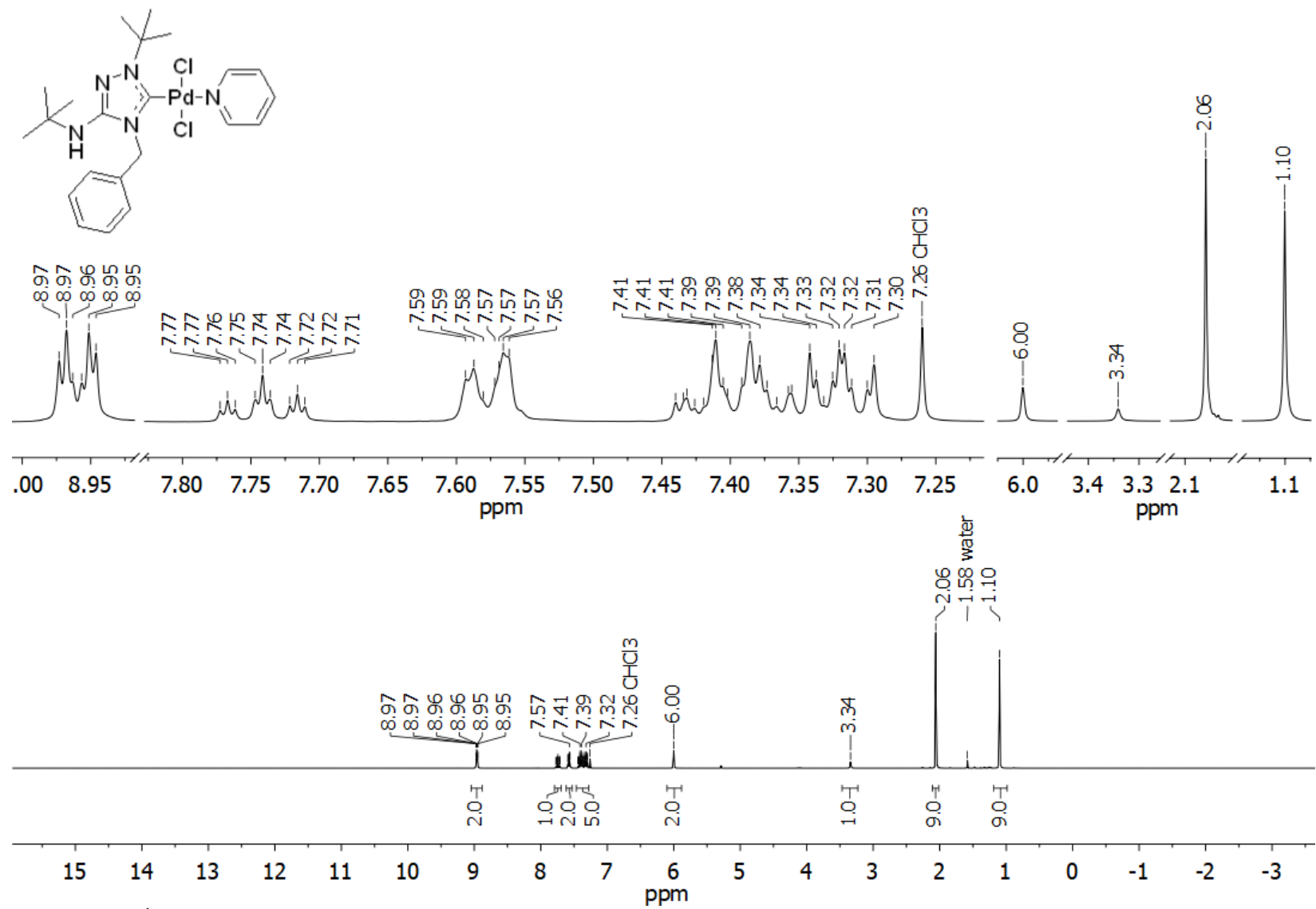
**Figure S67.** $^1$H NMR spectrum of compound **2h** (CDCl$_3$, 300 MHz)
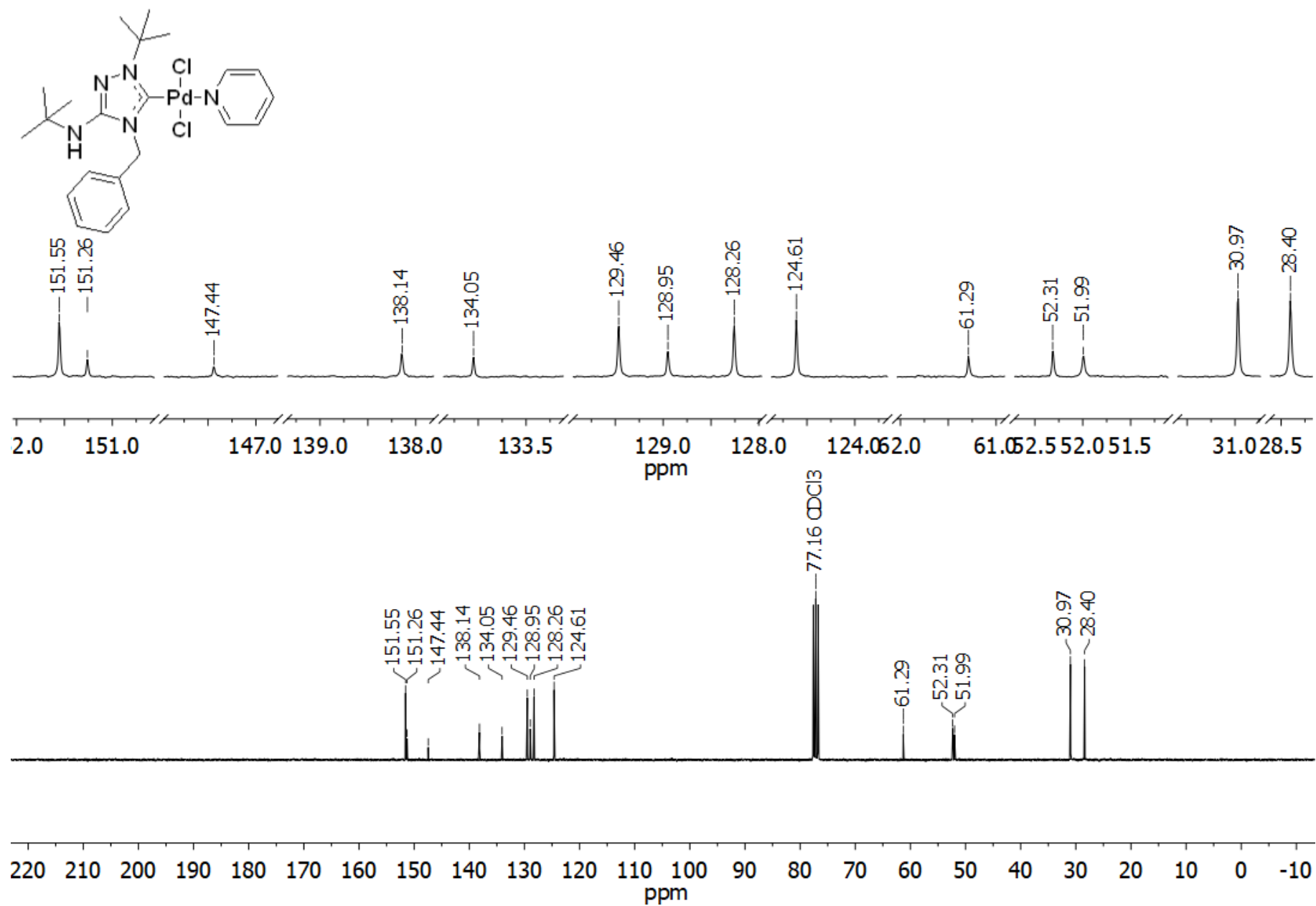
**Figure S68.** $^{13}C$ NMR spectrum of compound **2h** (CDCl$_3$, 75 MHz)
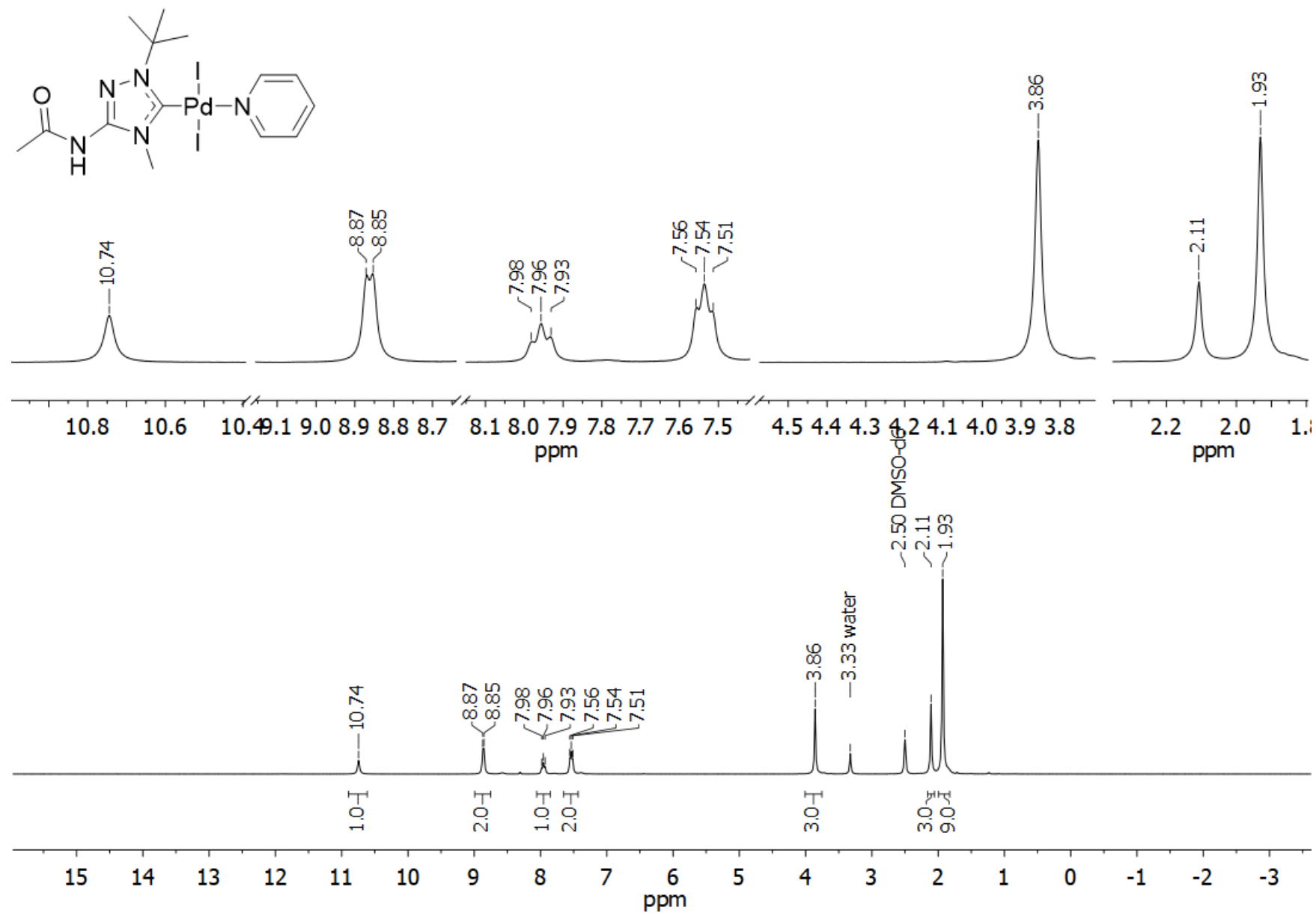
**Figure S69.** $^1$H NMR spectrum of compound **2i** (DMSO-$d_6$, 300 MHz)
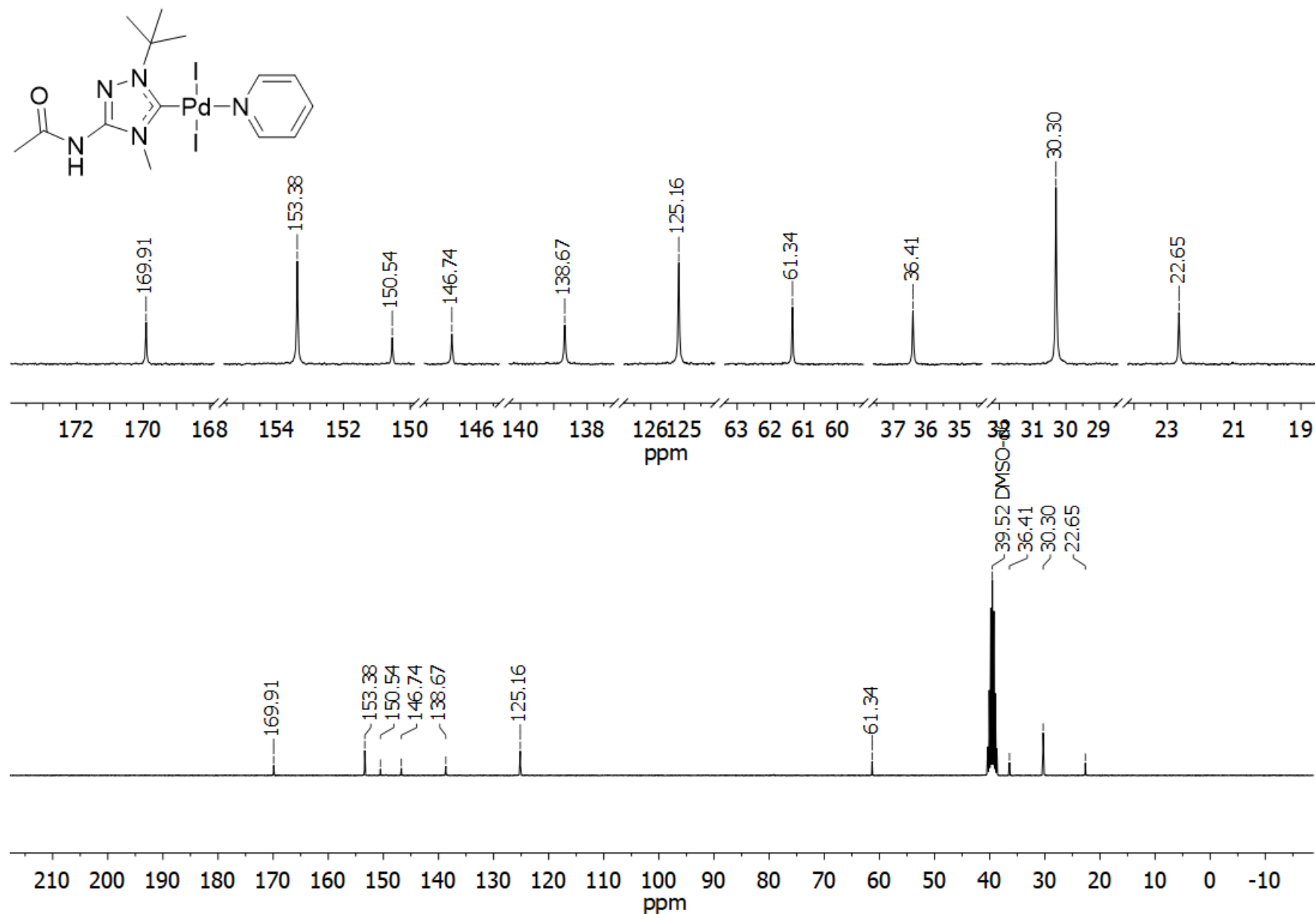
**Figure S70.** $^{13}C$ NMR spectrum of compound **2i** (DMSO-$d_6$, 75 MHz)
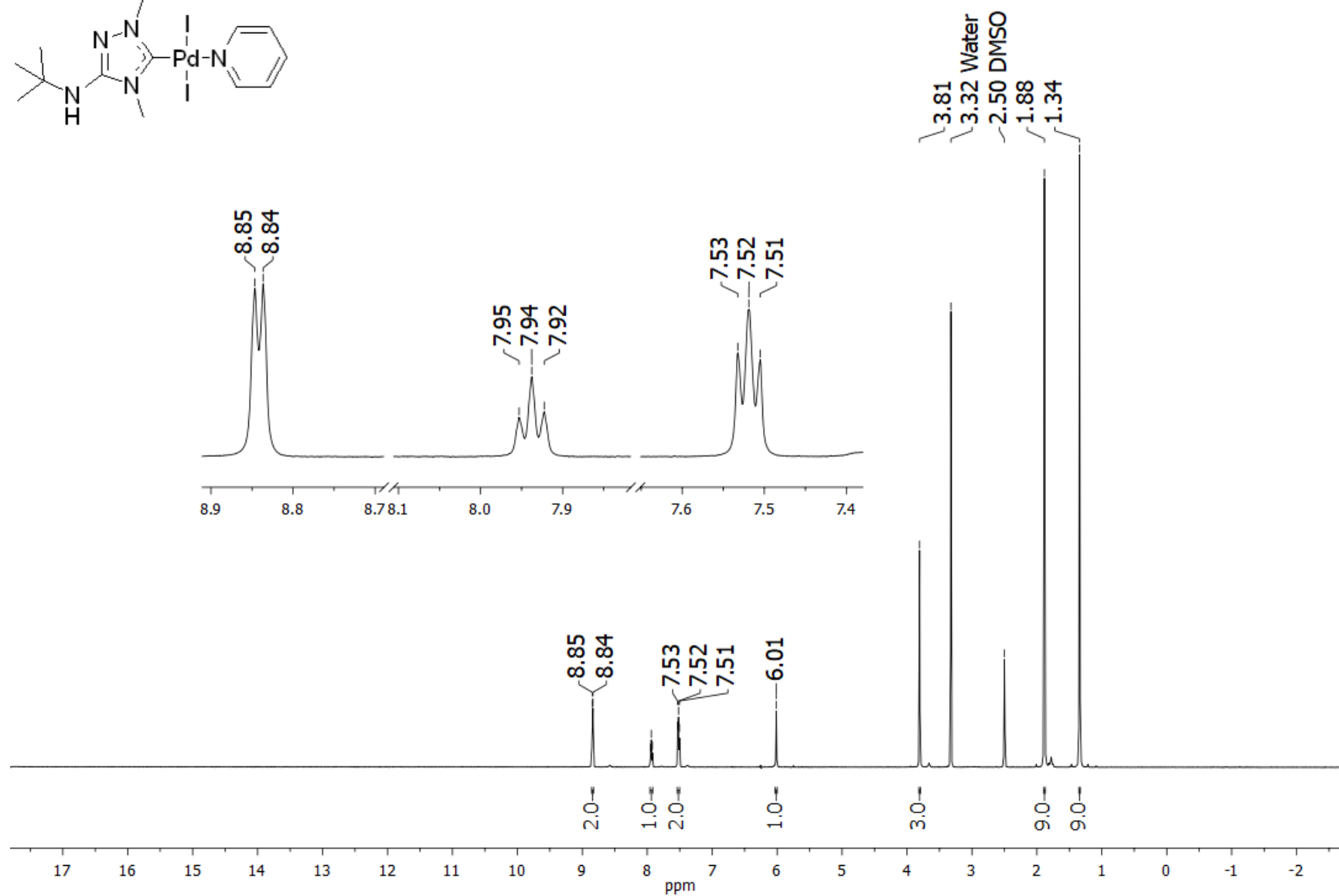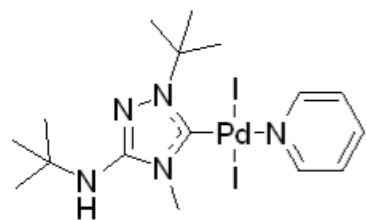
**Figure S71.** $^1$H NMR spectrum of compound **2j** (DMSO-$d_6$, 500 MHz)
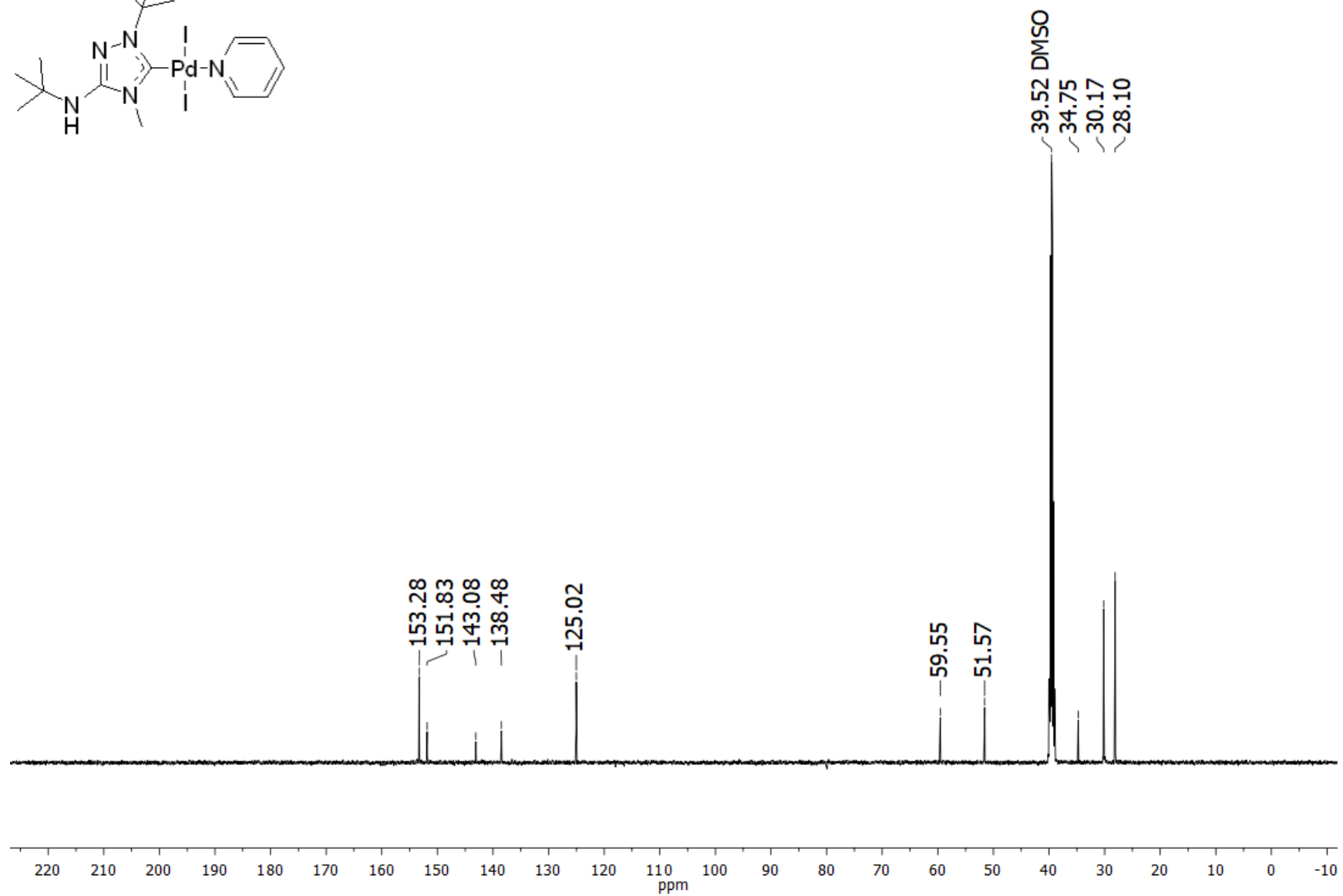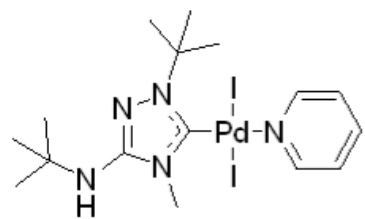
**Figure S72.** $^{13}$C NMR spectrum of compound **2j** (DMSO-$d_6$, 125 MHz)
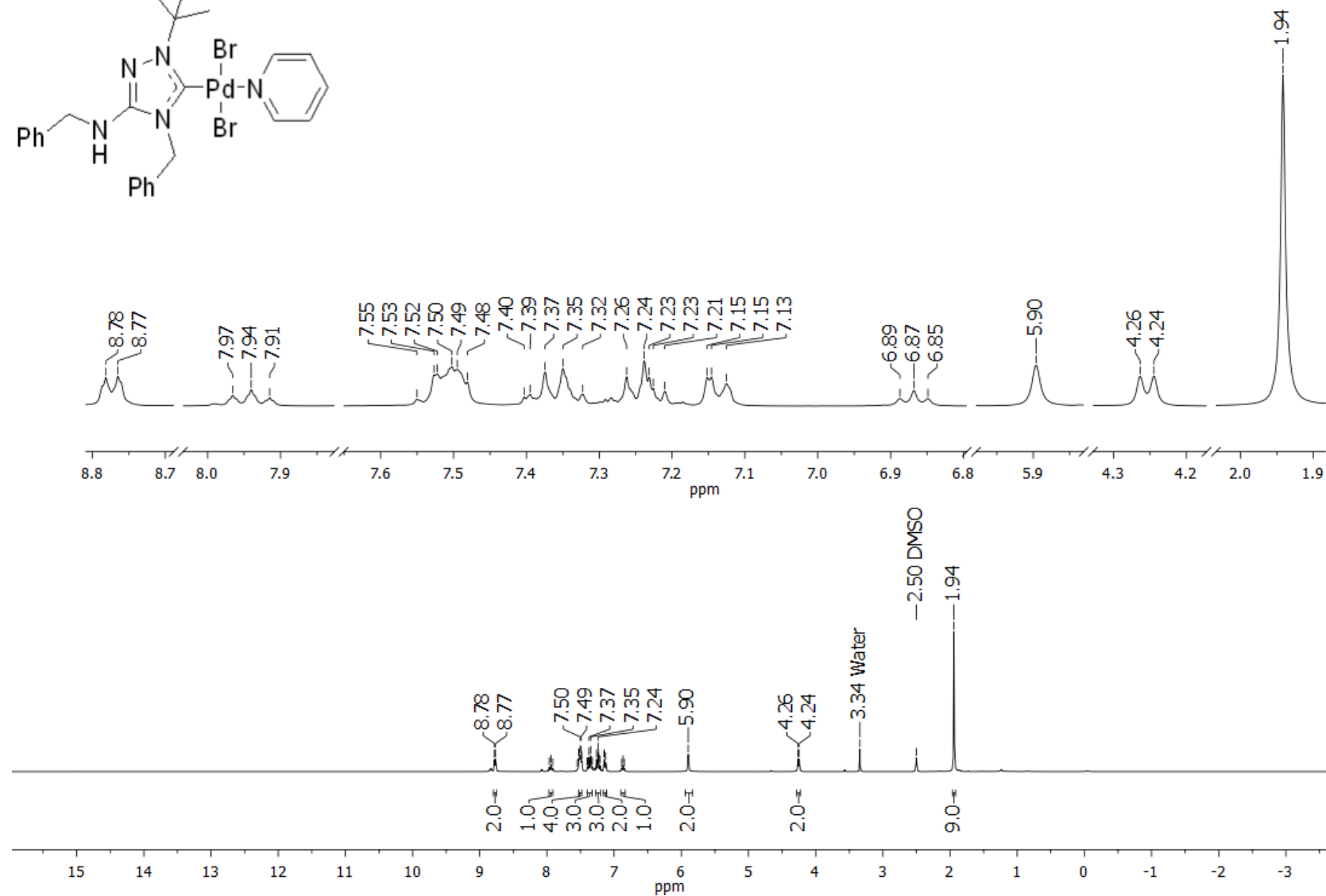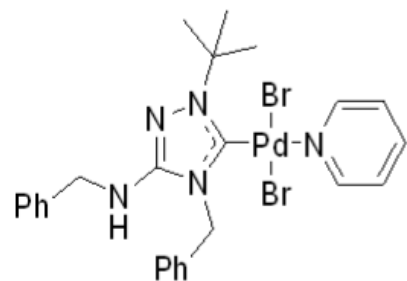
**Figure S73.** $^1$H NMR spectrum of compound **2k** (DMSO-$d_6$, 300 MHz)
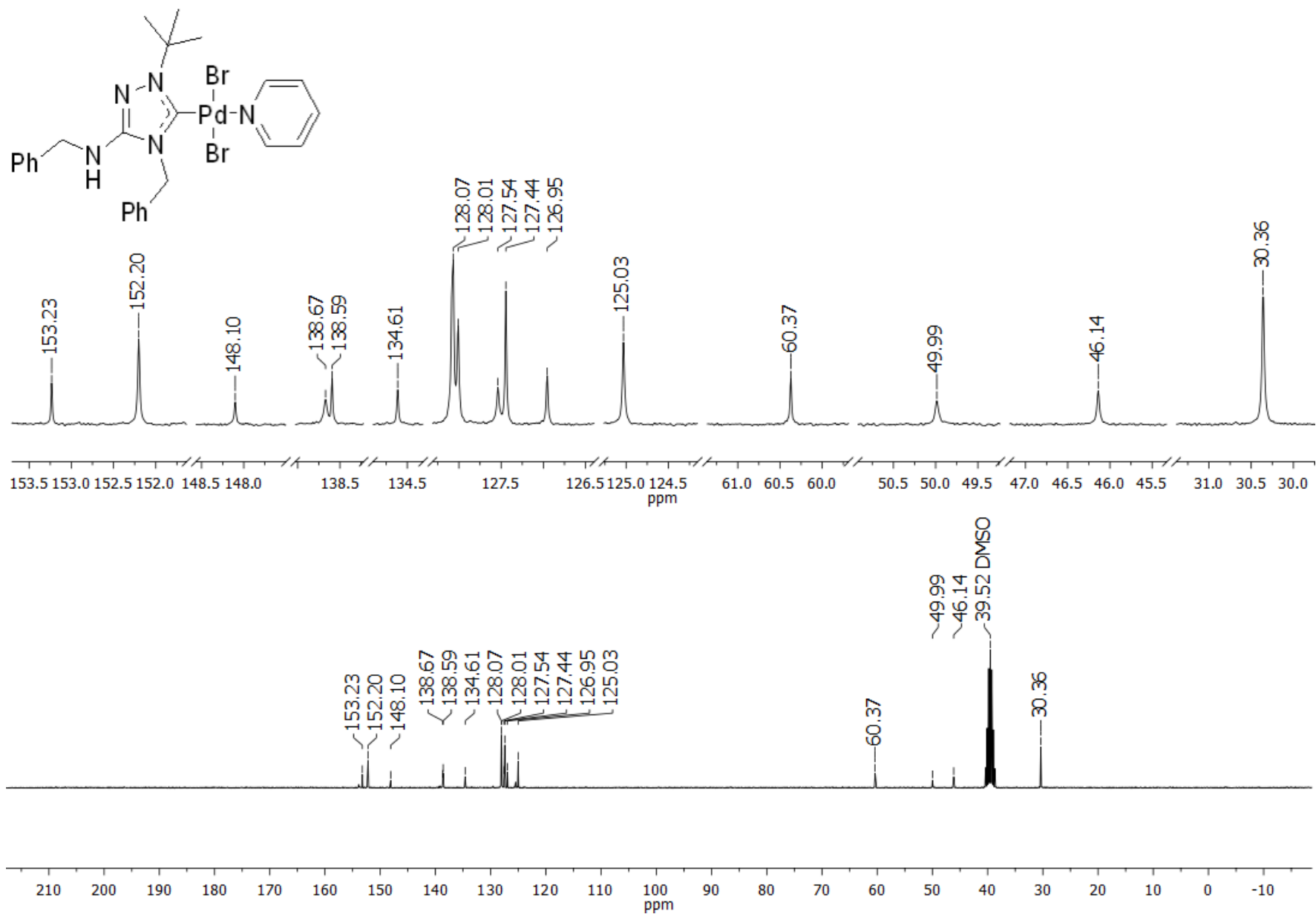
**Figure S74.** $^{13}$C NMR spectrum of compound **2k** (DMSO-$d_6$, 75 MHz)
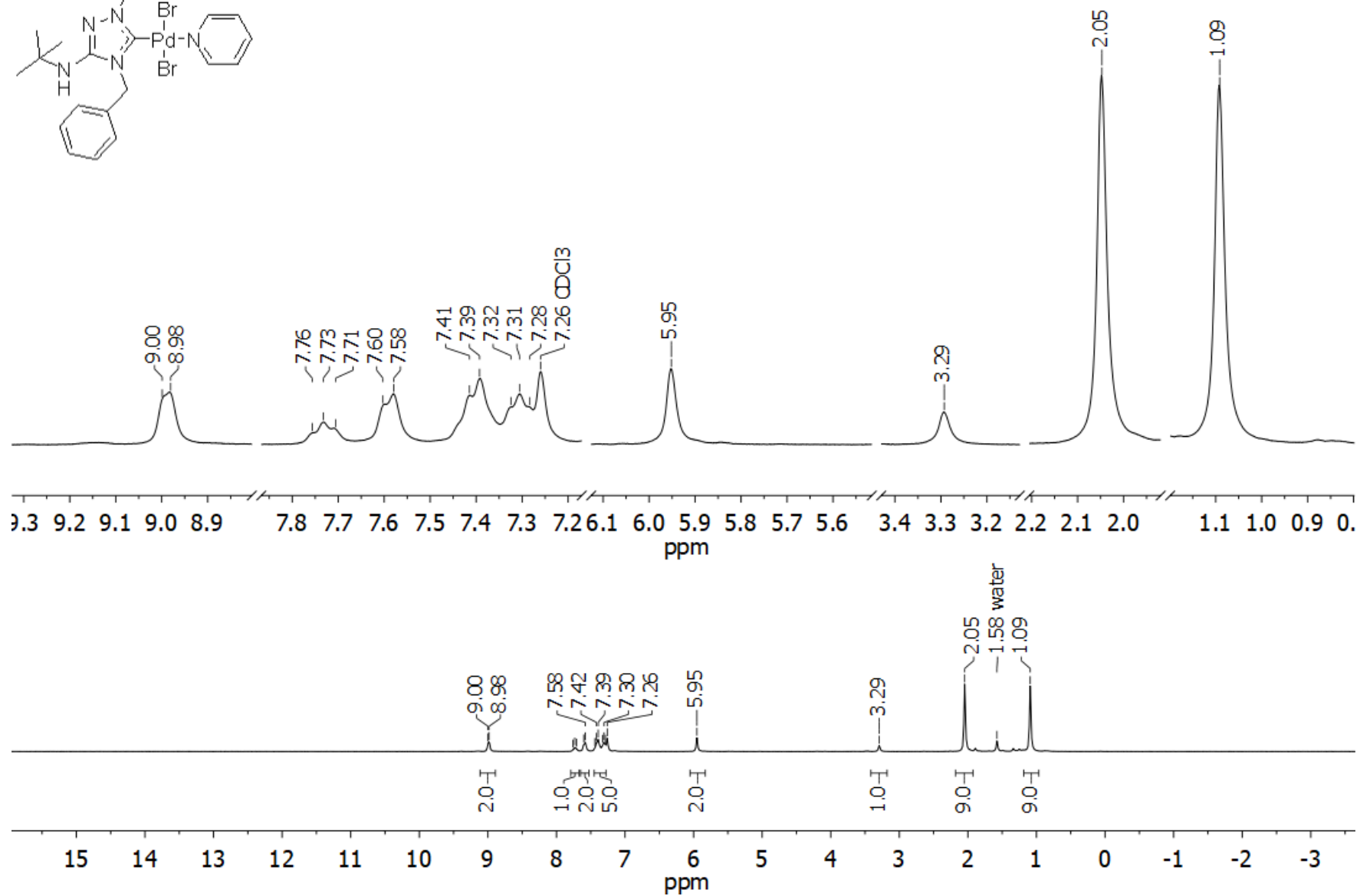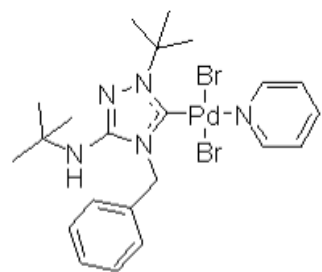
**Figure S75.** $^1H$ NMR spectrum of compound **2l** (CDCl$_3$, 300 MHz)

85
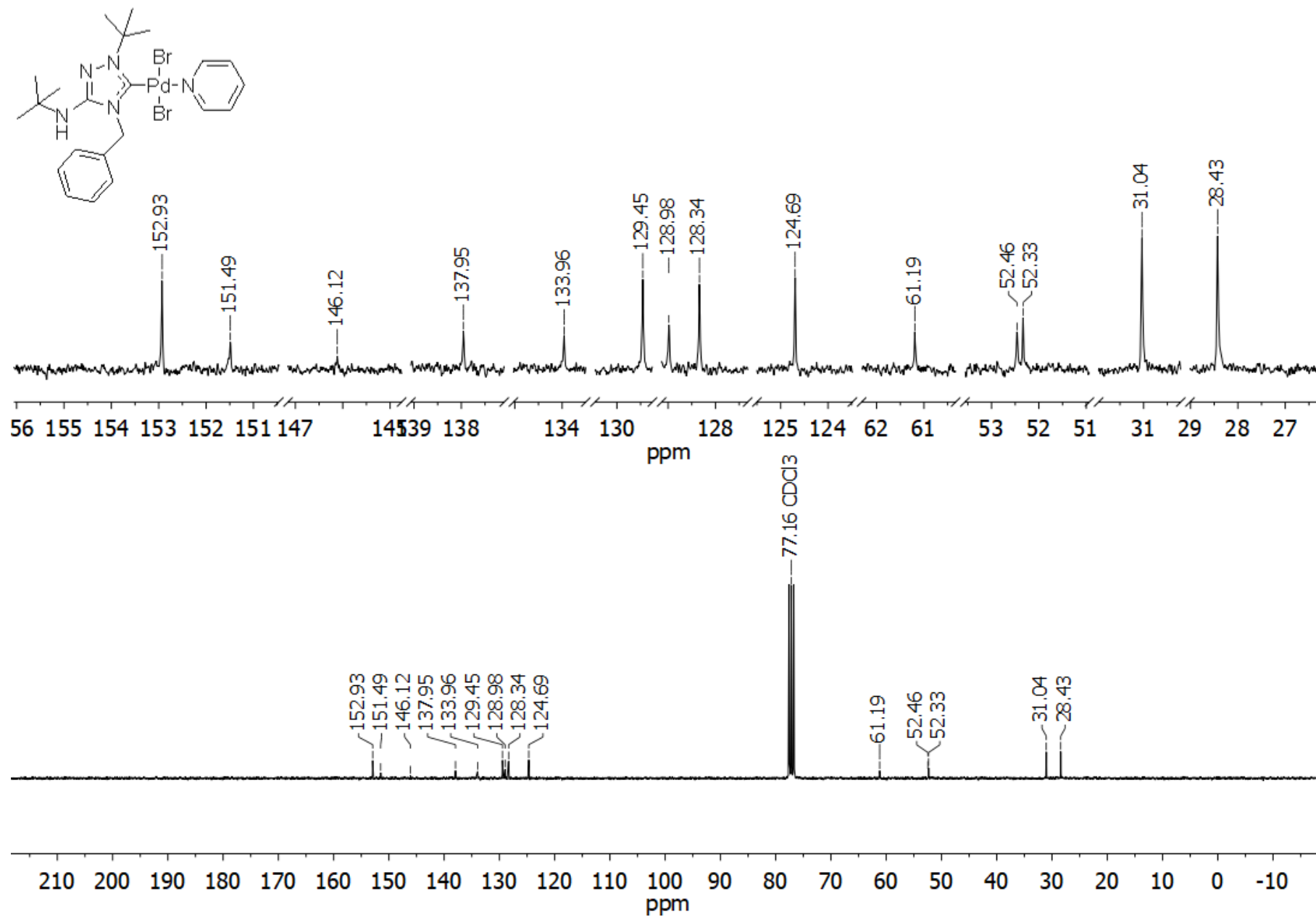
**Figure S76.** ¹³C NMR spectrum of compound **2l** (CDCl₃, 75 MHz)

**Figure S77.** $^1$H NMR spectrum of compound **2m** (DMSO-$d_6$, 300 MHz)
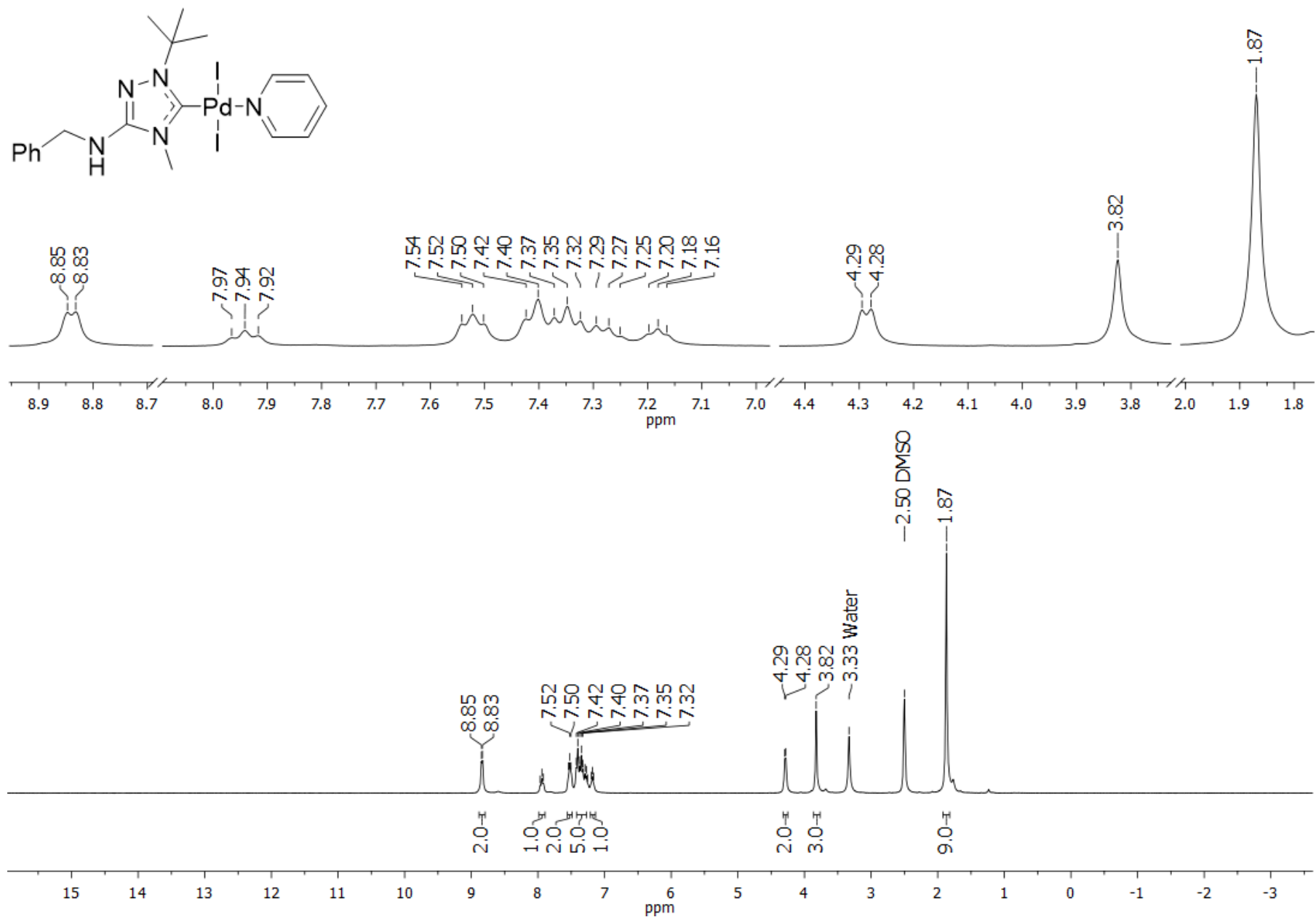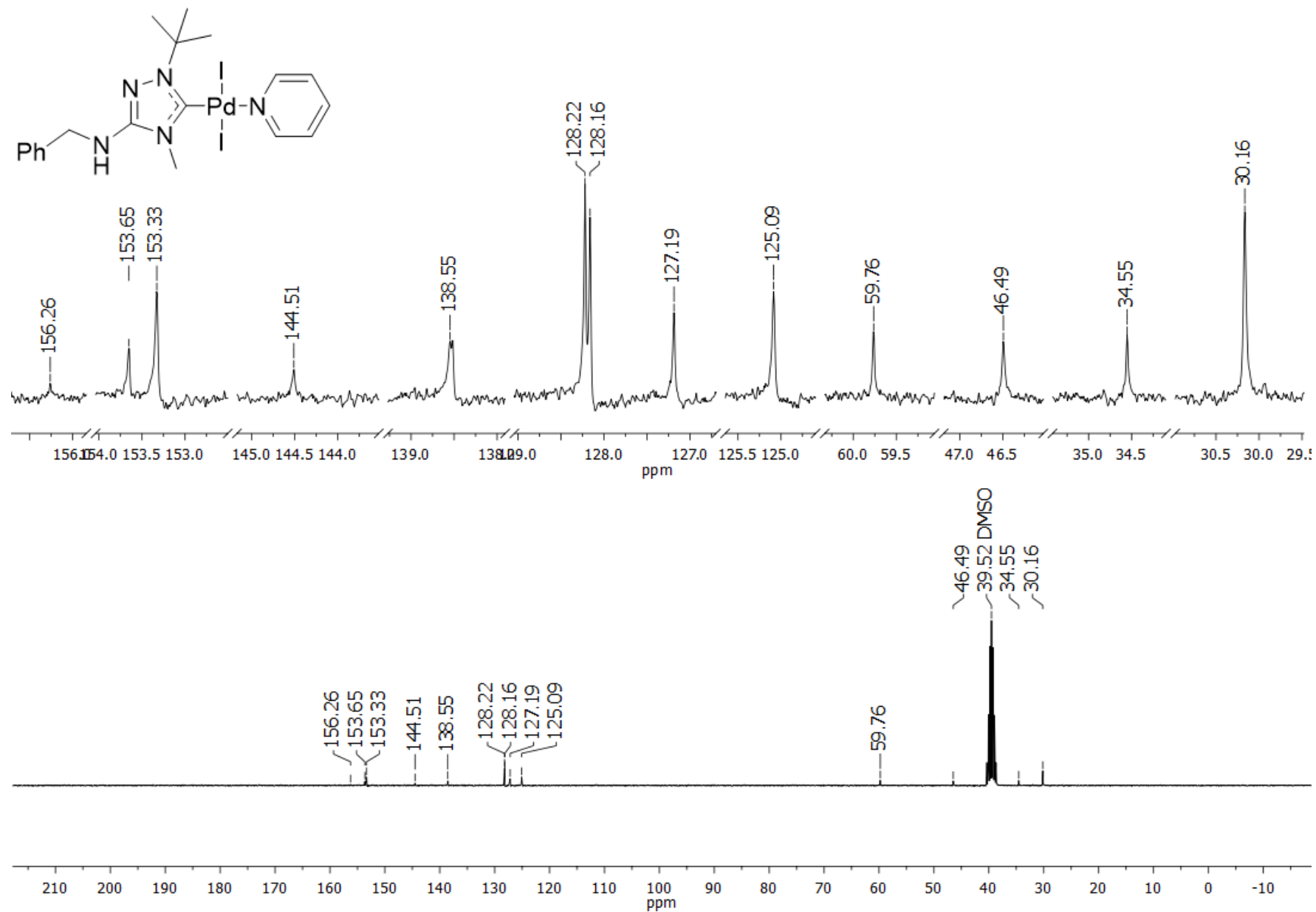
**Figure S78.** $^{13}$C NMR spectrum of compound **2m** (DMSO-$d_6$, 75 MHz)
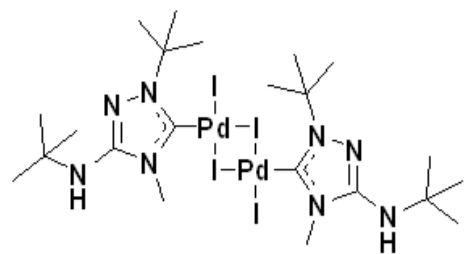
**Figure S79.** $^1$H NMR spectrum of compound **3a** (DMSO-$d_6$, 300 MHz)
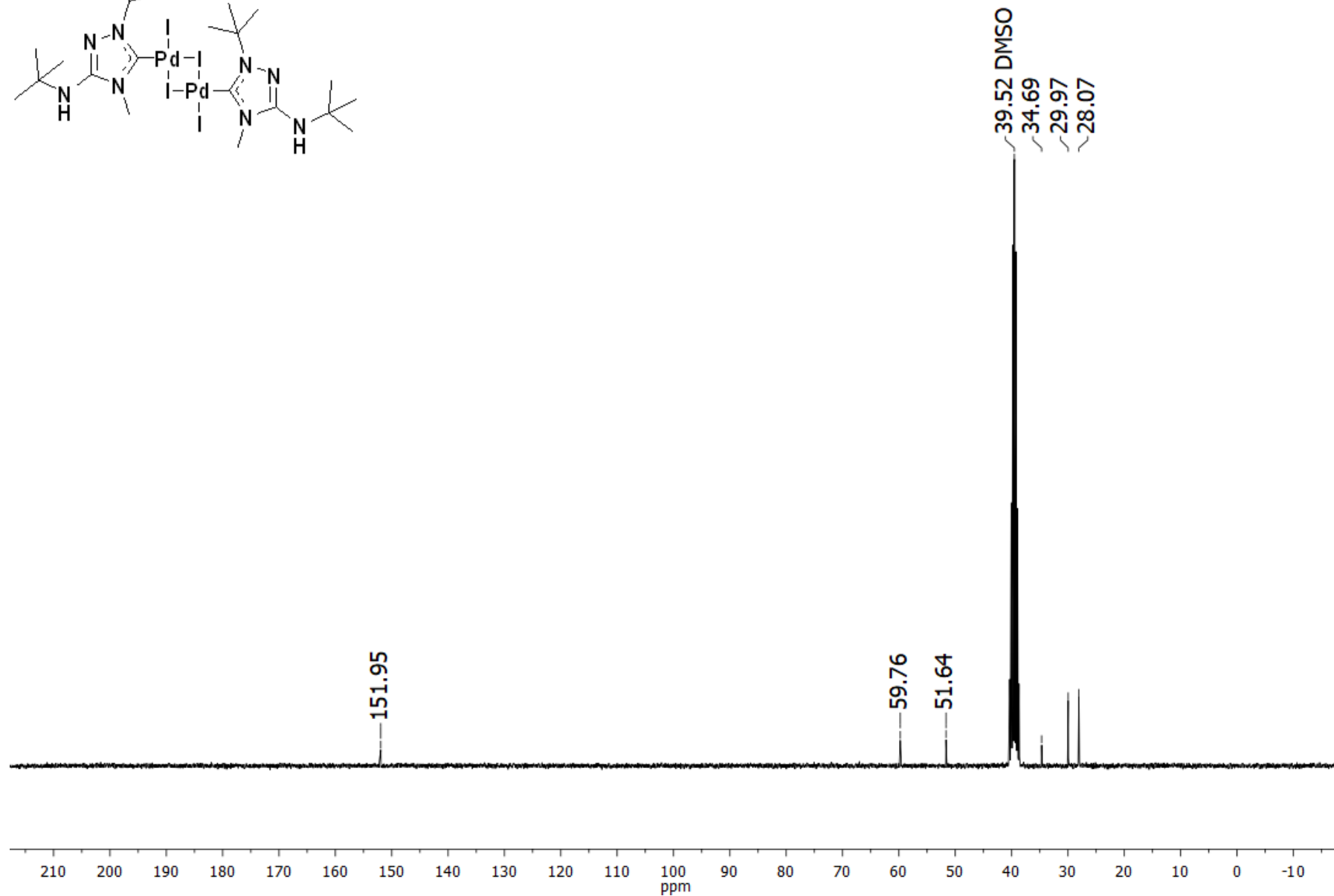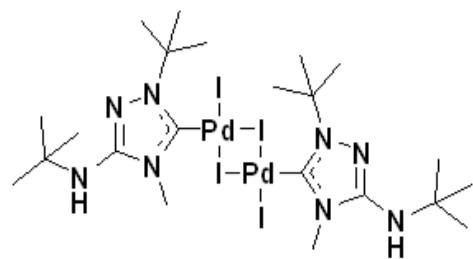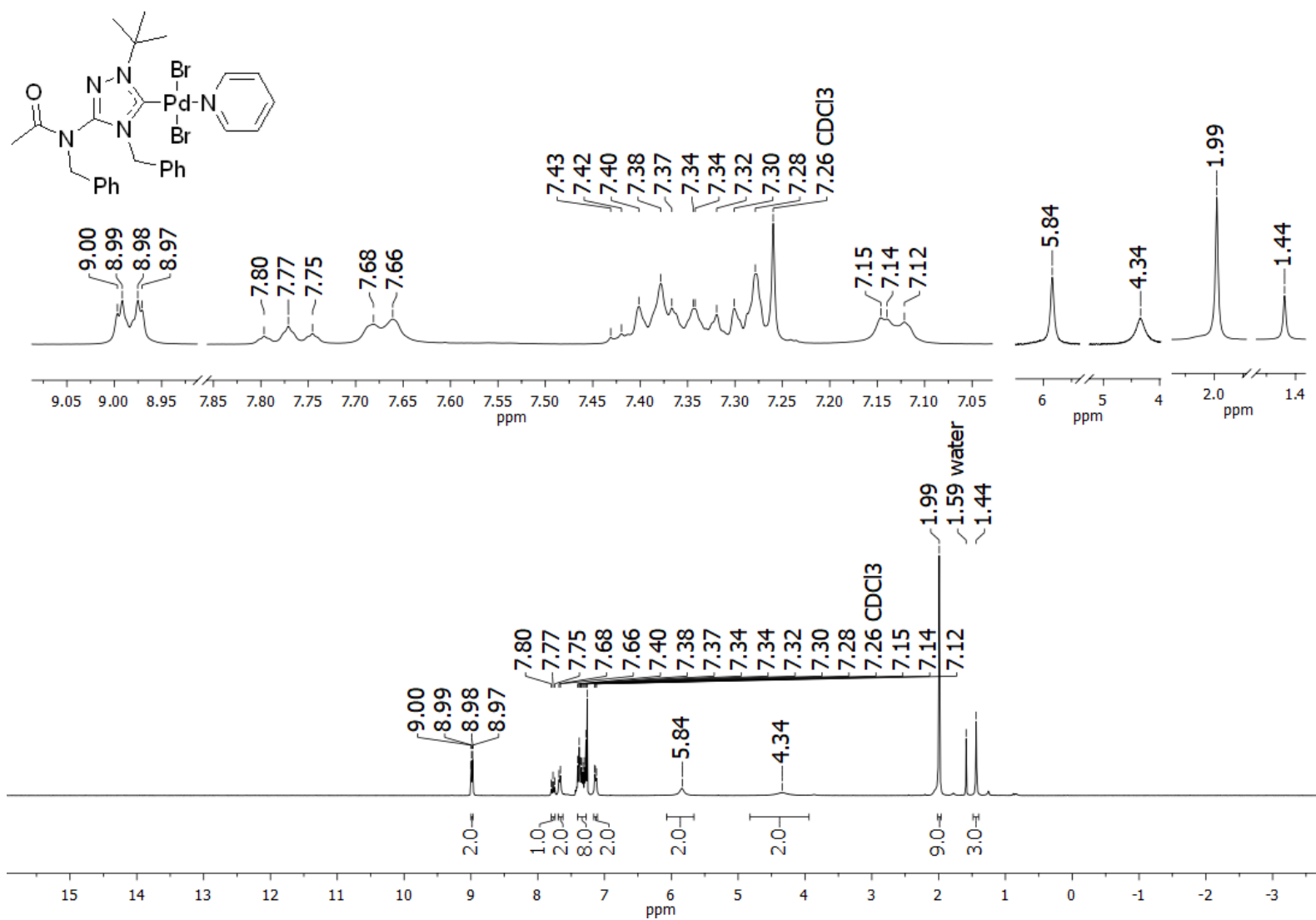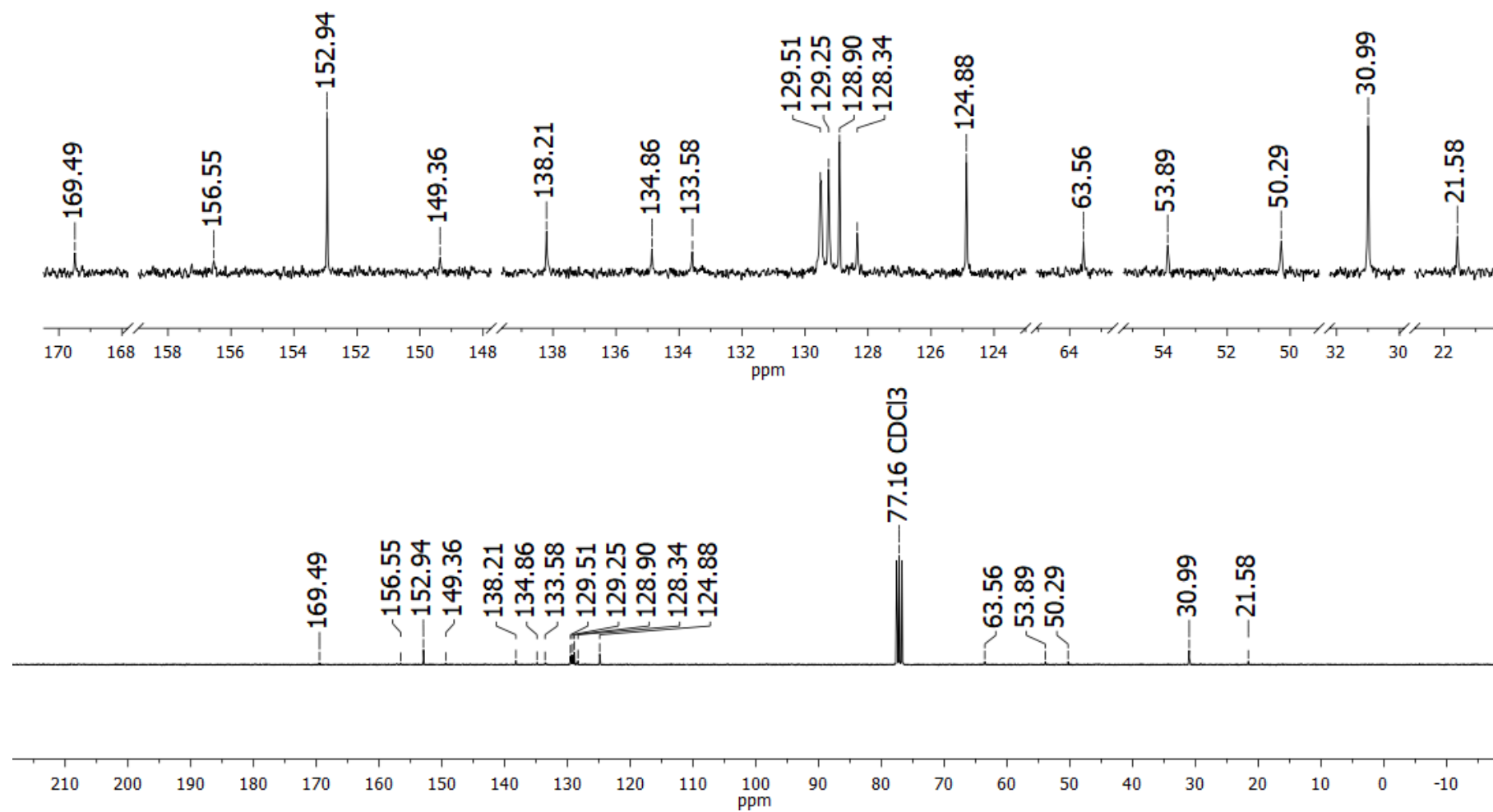
**Figure S80.** $^{13}$C NMR spectrum of compound **3a** (DMSO-$d_6$, 75 MHz)
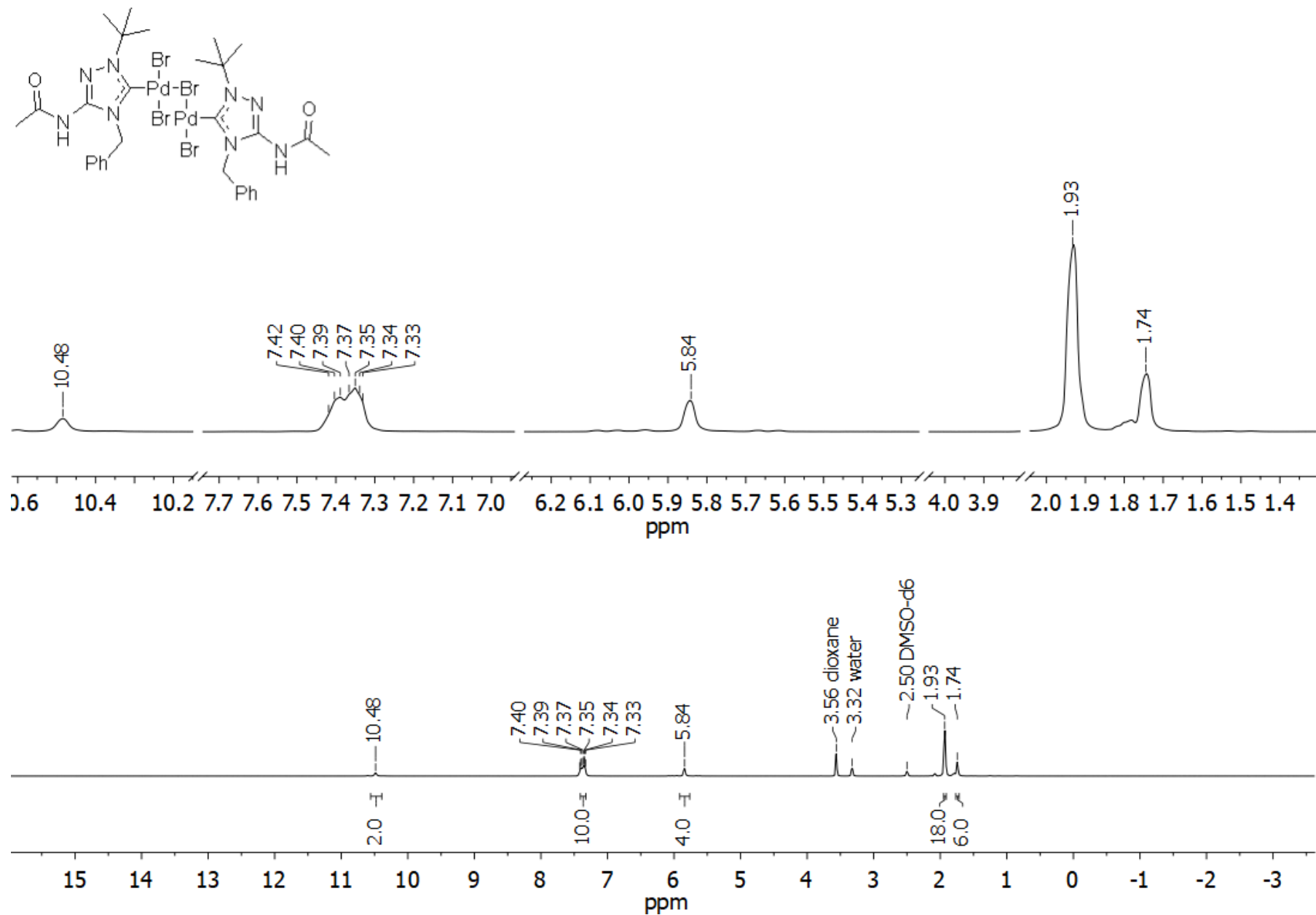
**Figure S81.** $^1$H NMR spectrum of compound **3b** (DMSO-$d_6$, 300 MHz)
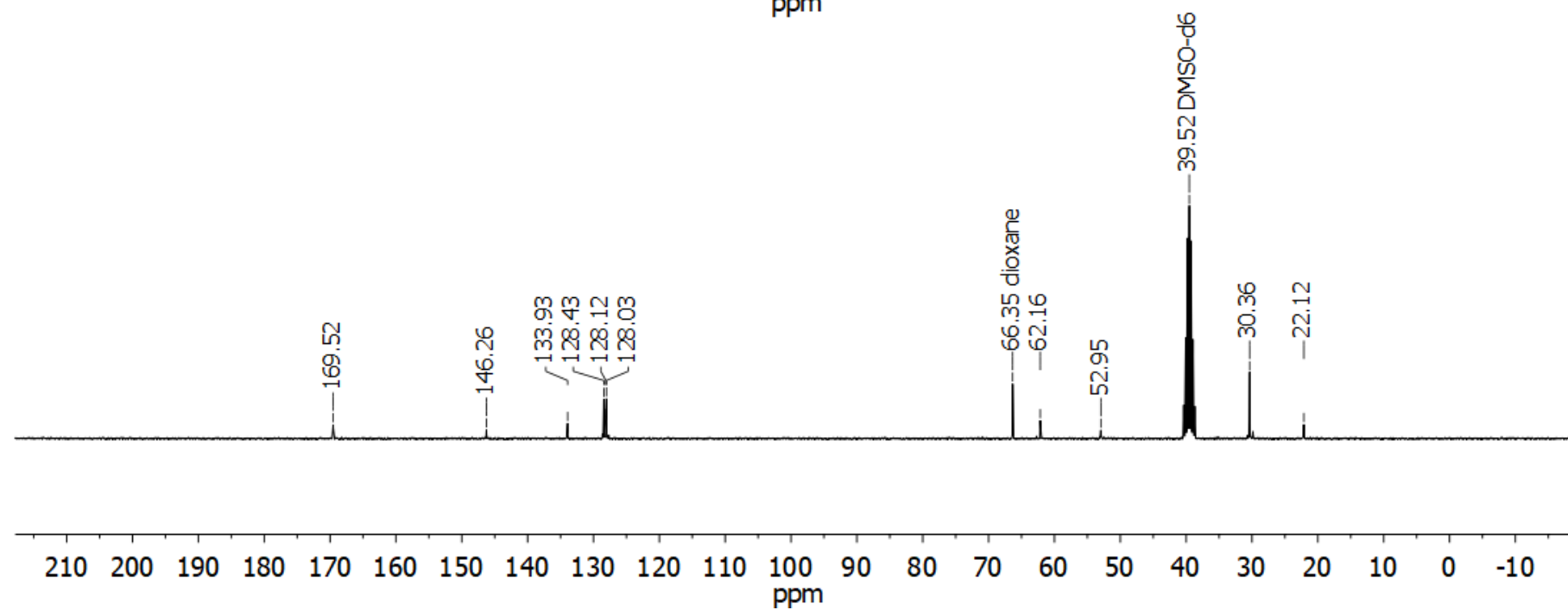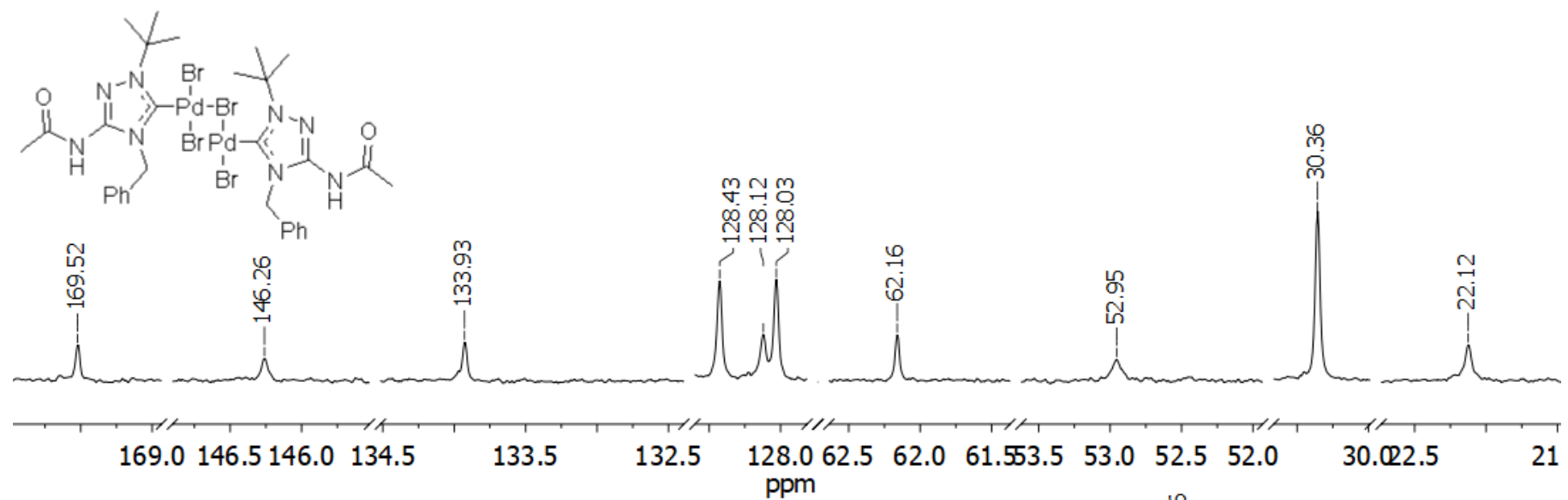
**Figure S82.** $^{13}C$ NMR spectrum of compound **3b** (DMSO-$d_6$, 75 MHz)
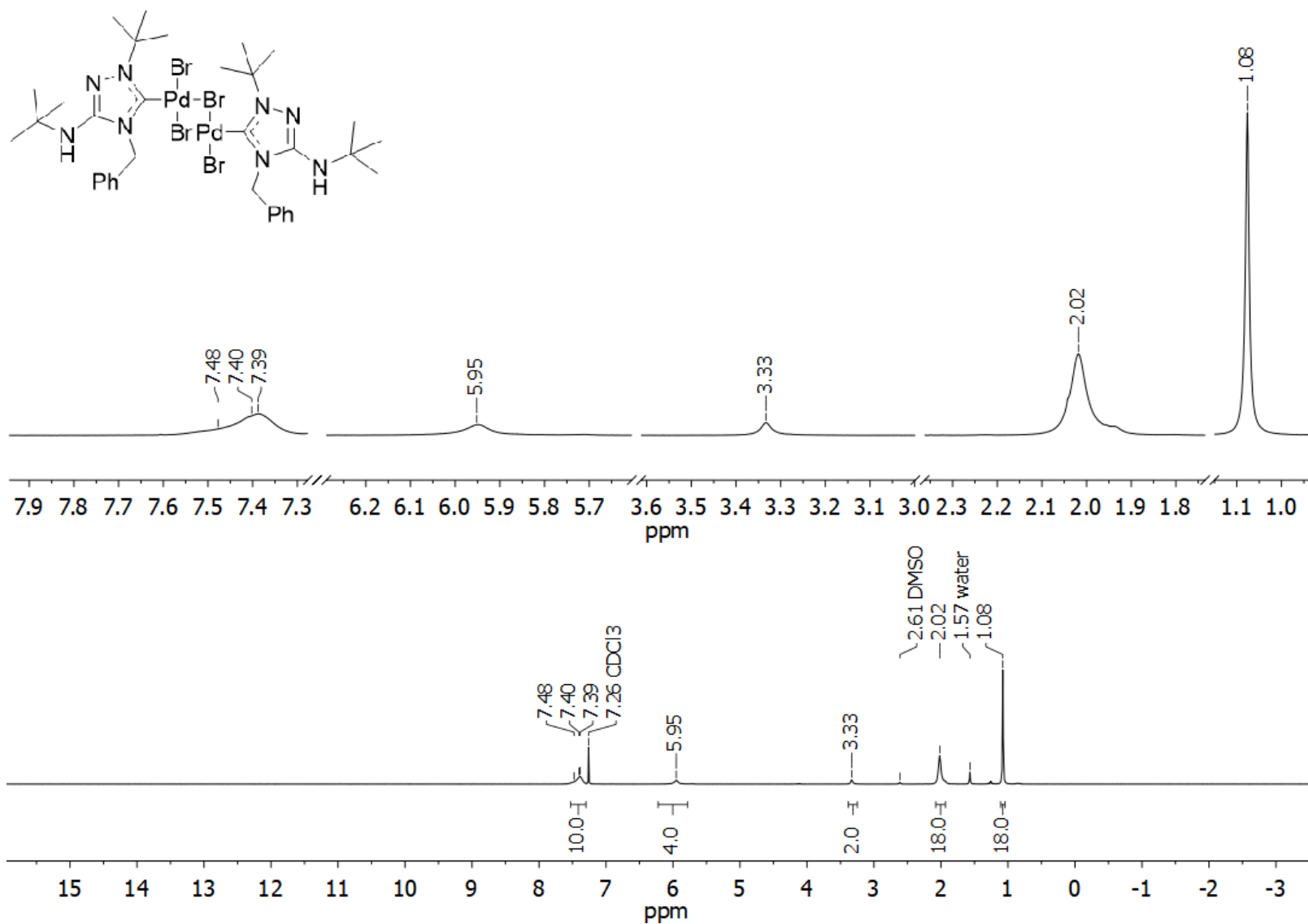
**Figure S83.** $^1$H NMR spectrum of compound **3c** (CDCl$_3$, 300 MHz). Some signals are broadened due to hindered rotation of the corresponding groups.
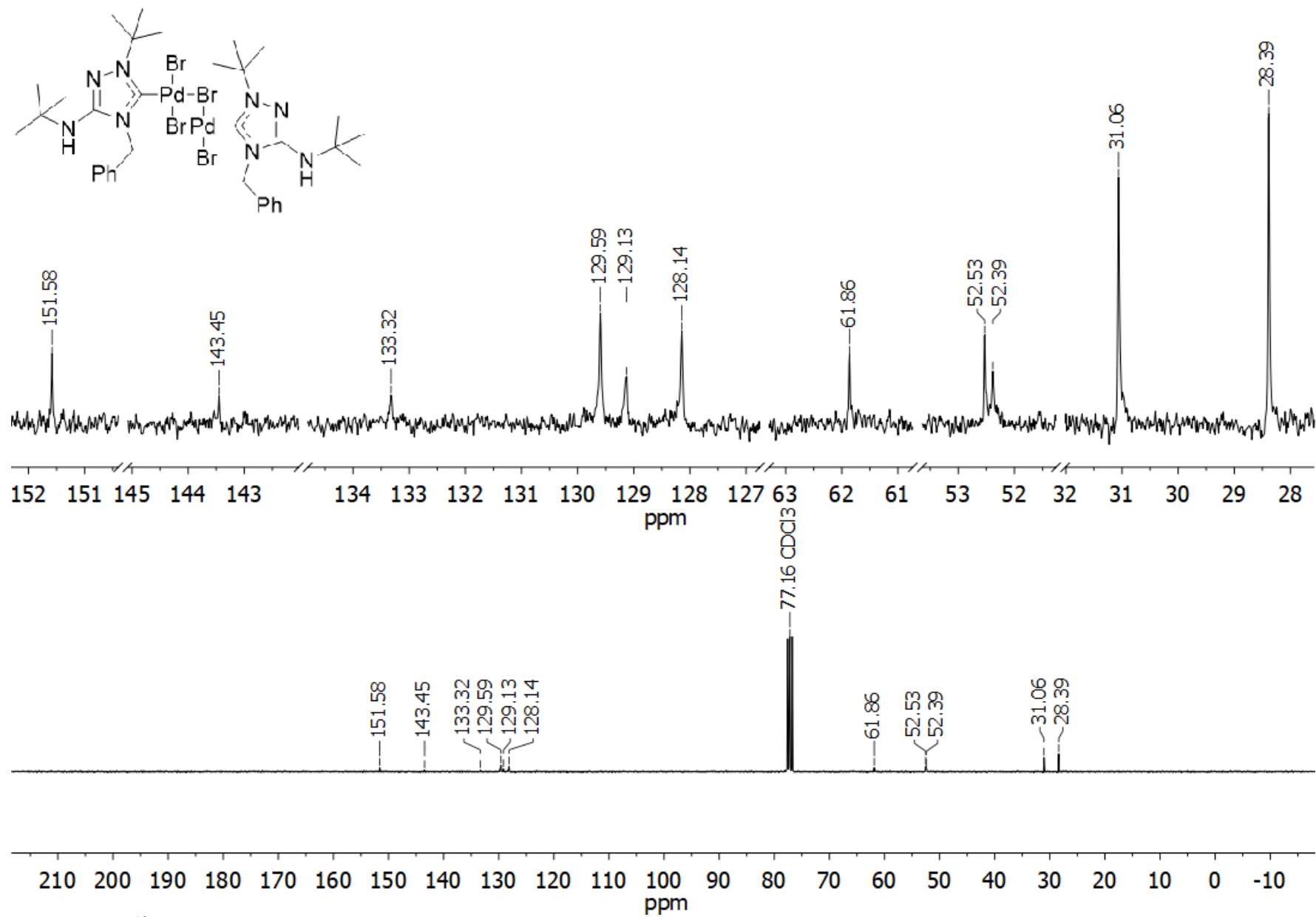
**Figure S84.** $^{13}$C NMR spectrum of compound **3c** (CDCl$_3$, 75 MHz)
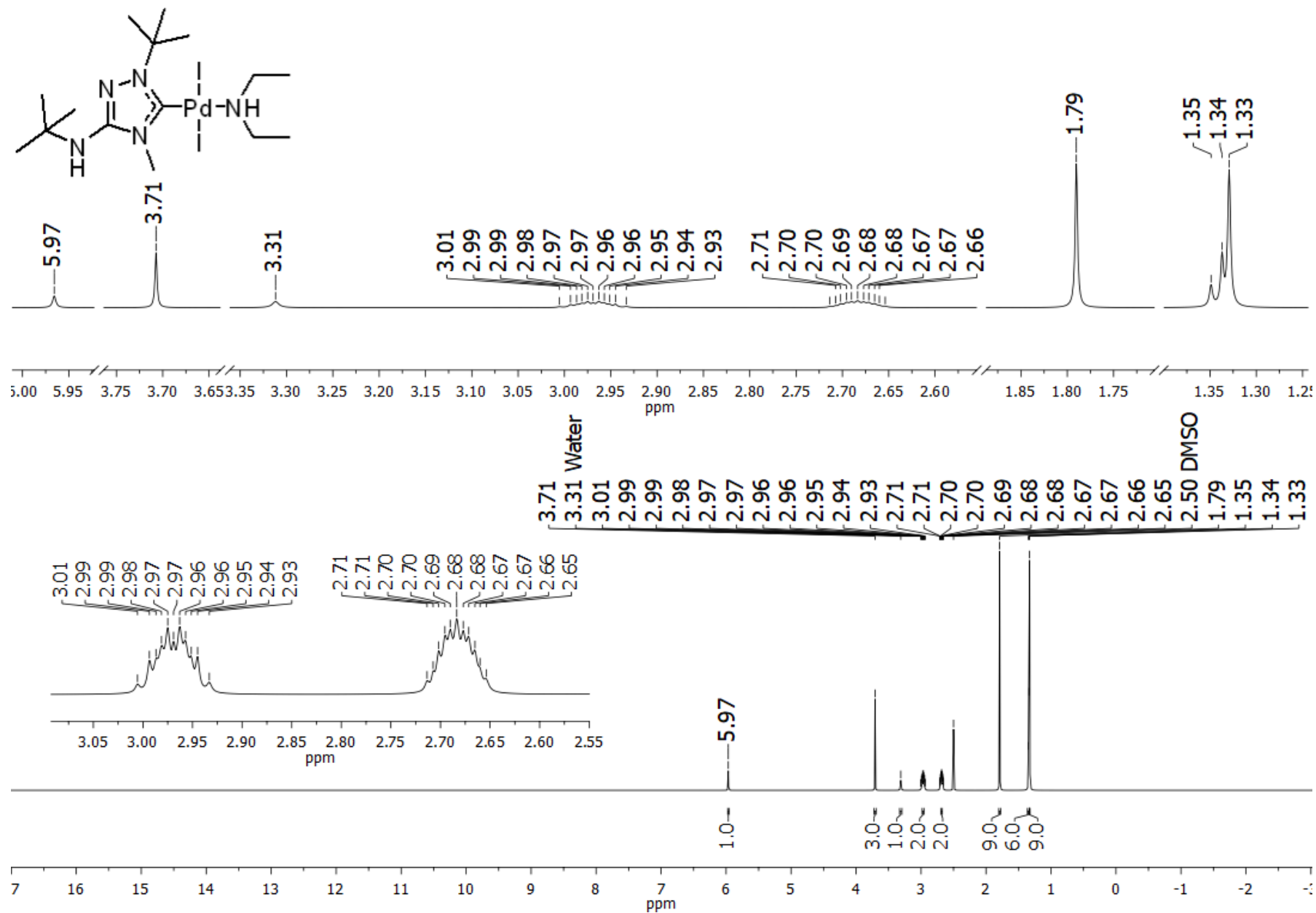
**Figure S85.** $^1$H NMR spectrum of compound **4a** (DMSO-$d_6$, 600 MHz)
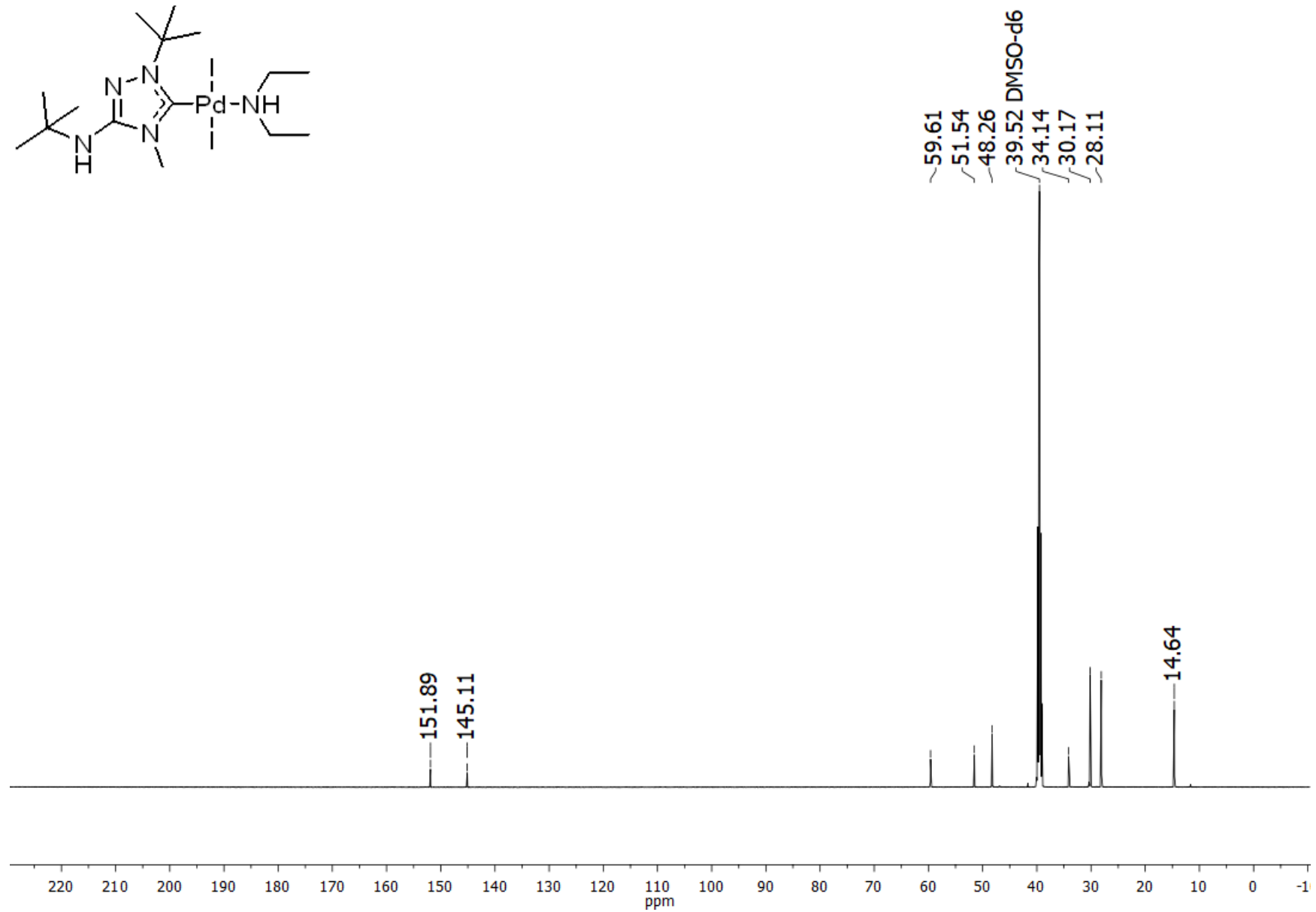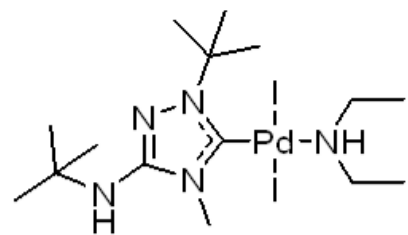
Figure S86. $^{13}$C NMR spectrum of compound **4a** (DMSO-$d_6$, 150 MHz)

Peaks labeled: 151.89, 145.11, 59.61, 51.54, 48.26, 39.52 DMSO-d6, 34.14, 30.17, 28.11, 14.64
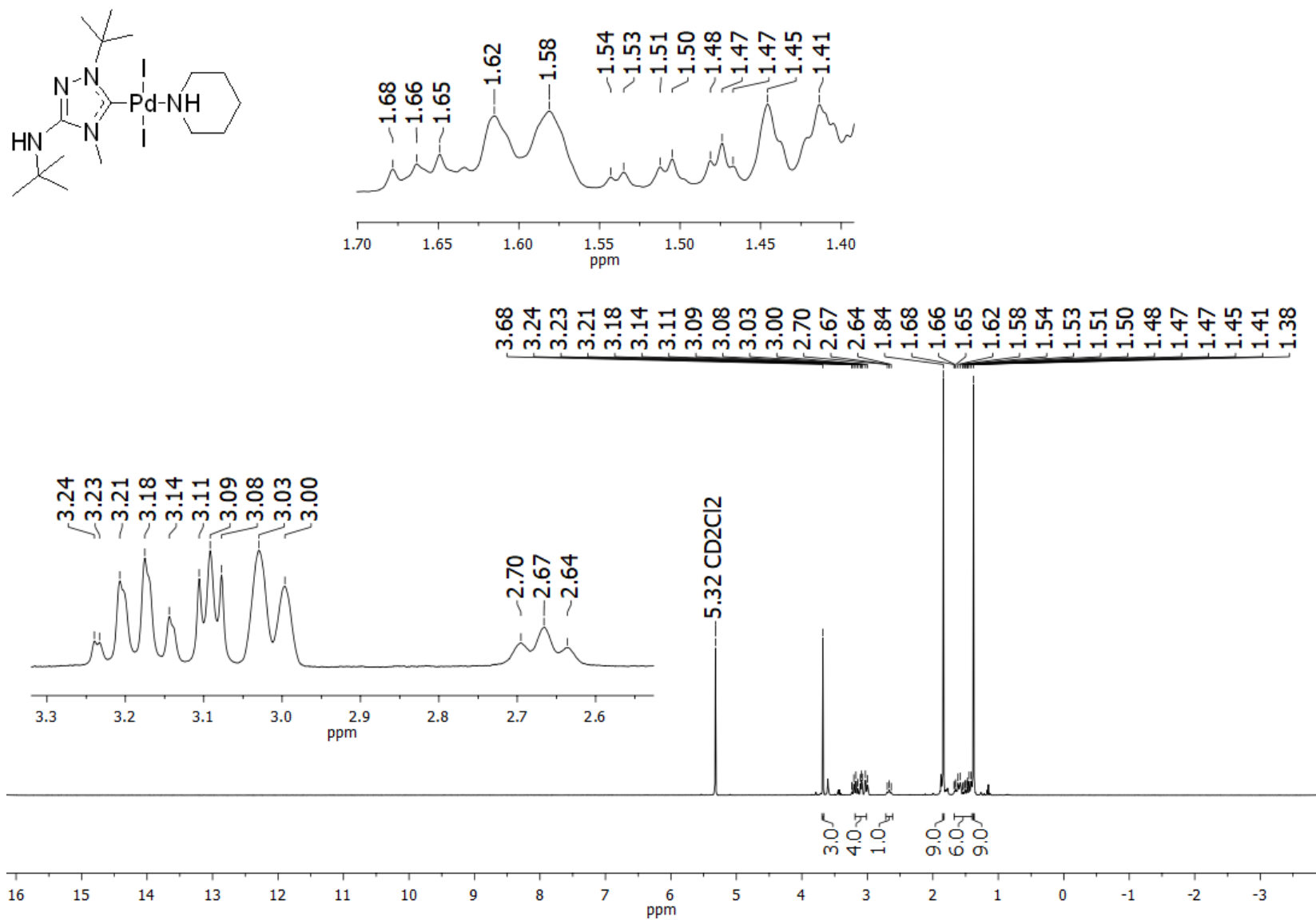
**Figure S87.** $^{1}$H NMR spectrum of compound **4b** (CD$_2$Cl$_2$, 400 MHz)
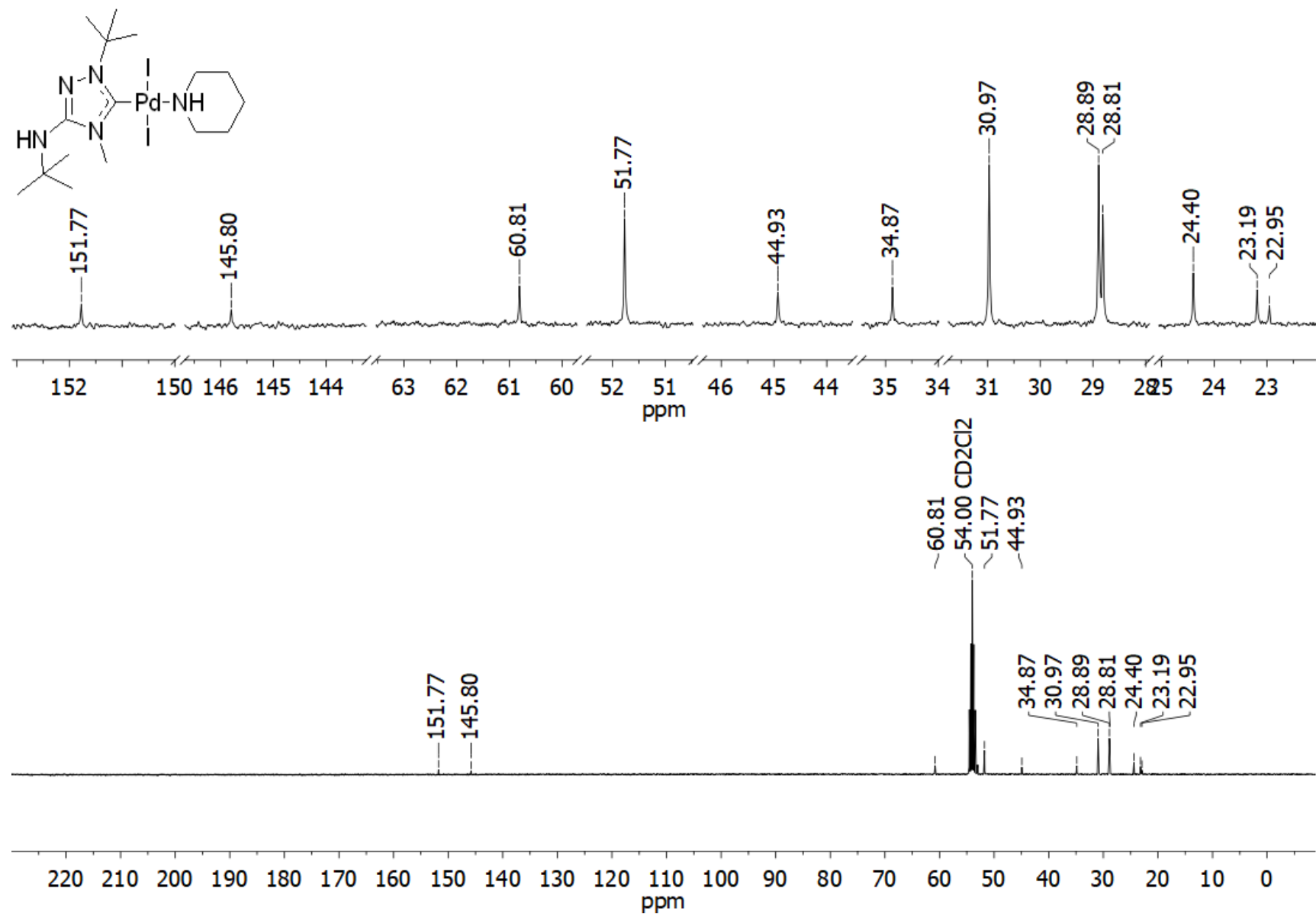
**Figure S88.** $^{13}C$ NMR spectrum of compound **4b** (CD$_2$Cl$_2$, 100 MHz)
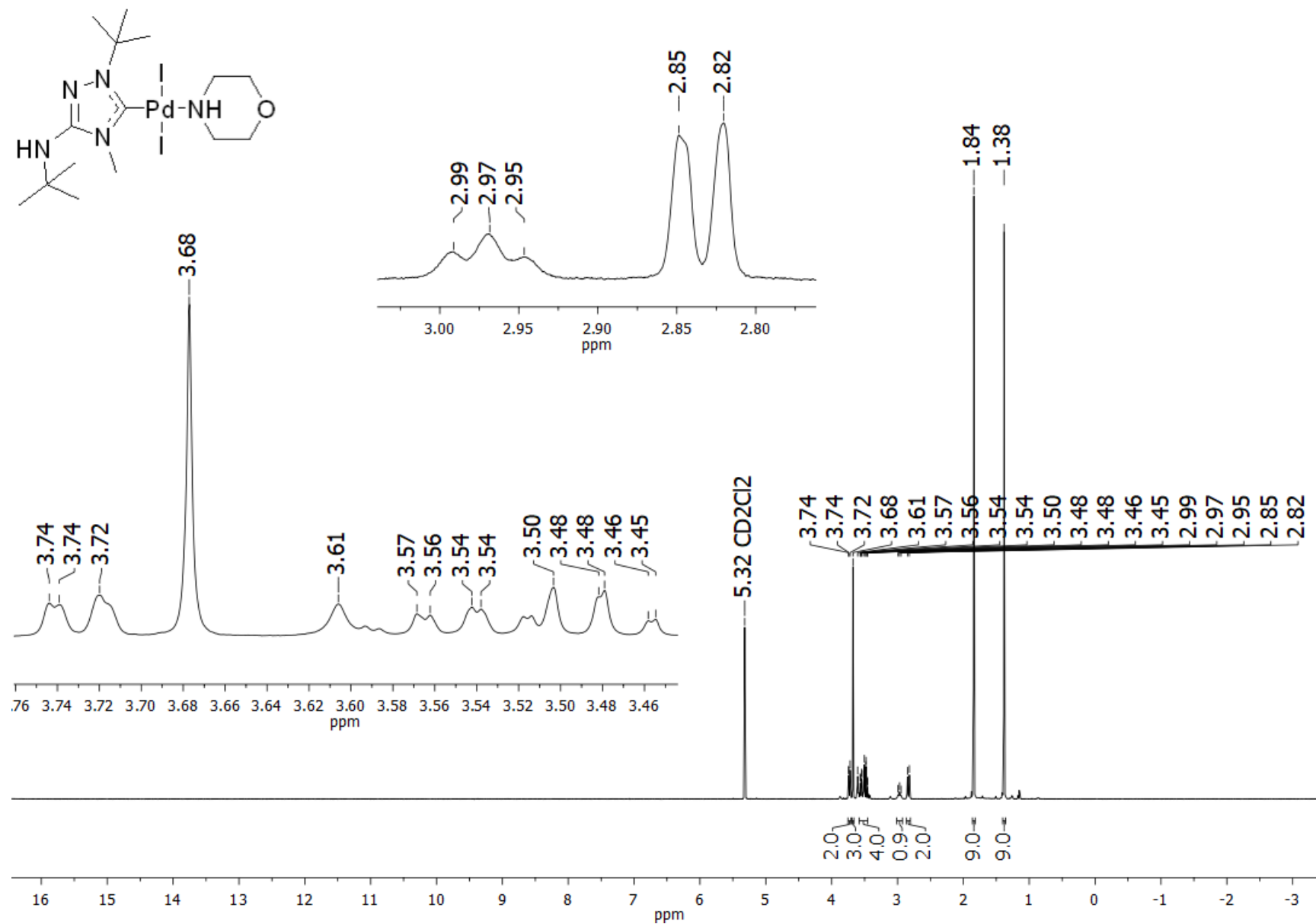
**Figure S89.** $^1$H NMR spectrum of compound **4c** (CD$_2$Cl$_2$, 500 MHz)
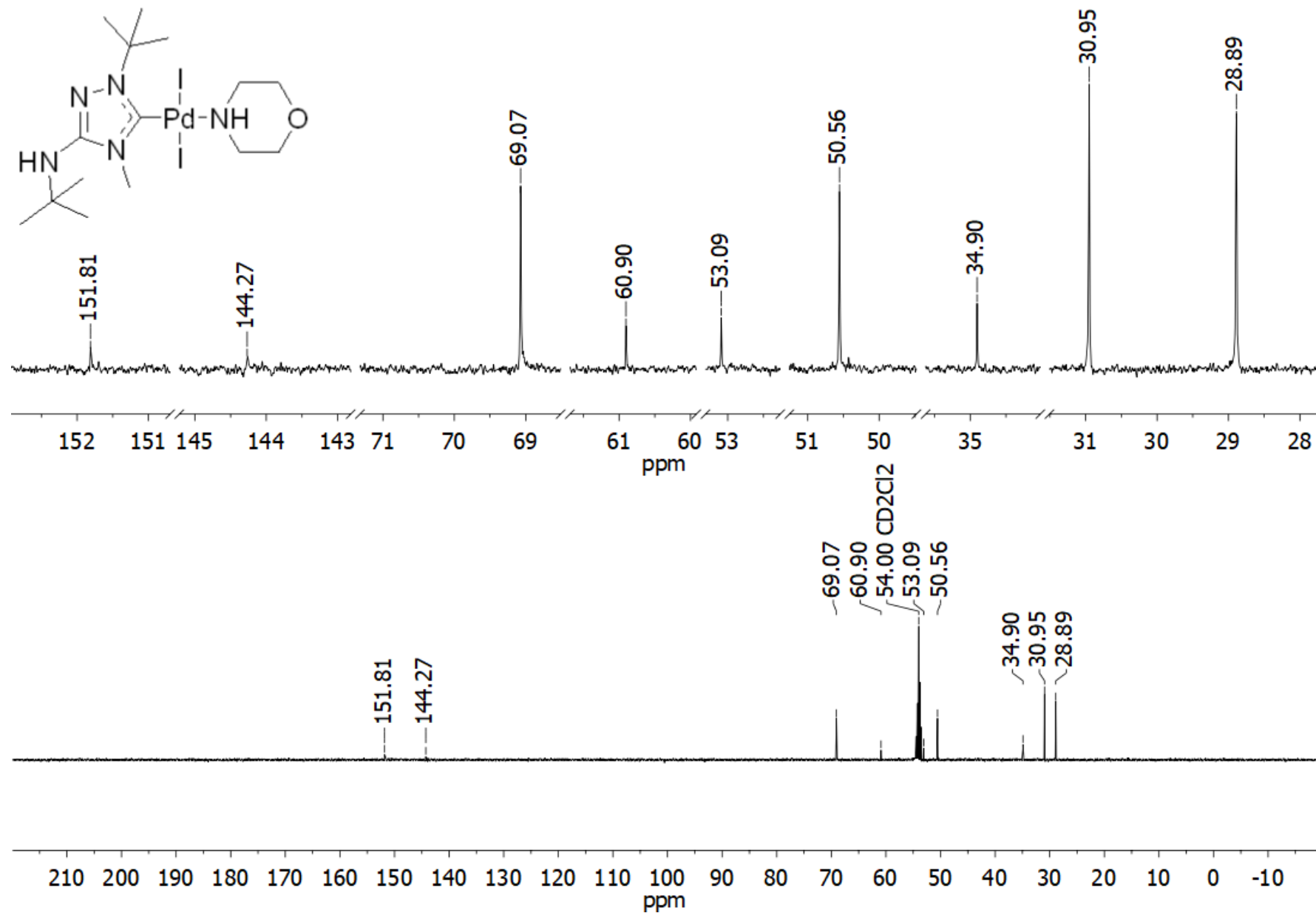
**Figure S90.** $^{13}$C NMR spectrum of compound **4c** (CD$_2$Cl$_2$, 125 MHz)
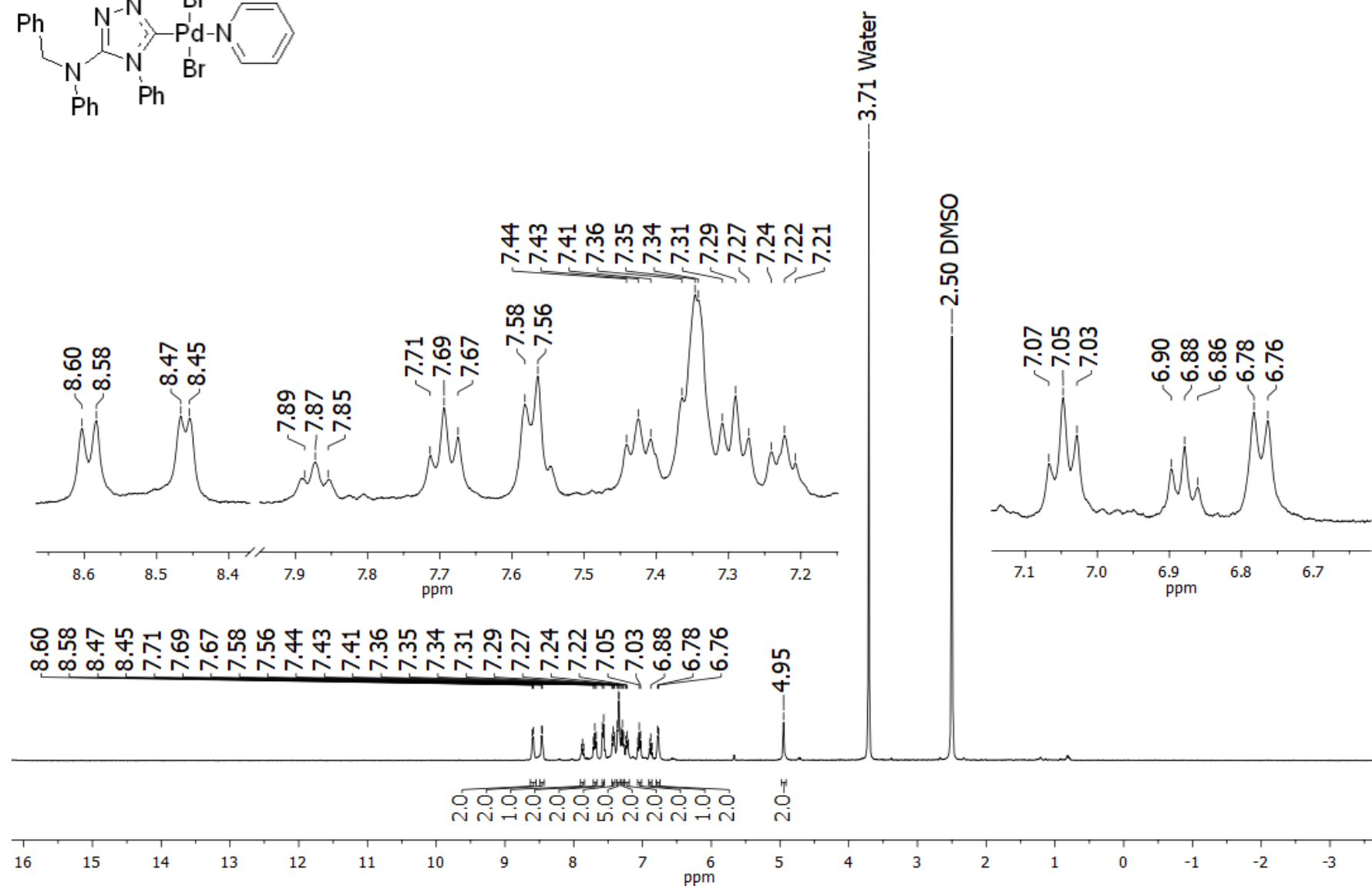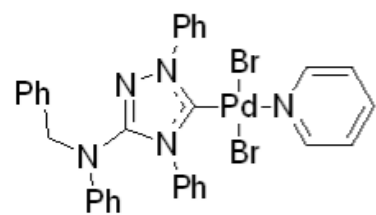
**Figure S91.** $^1$H NMR spectrum of compound **5a** (DMSO-$d_6$, 400 MHz)
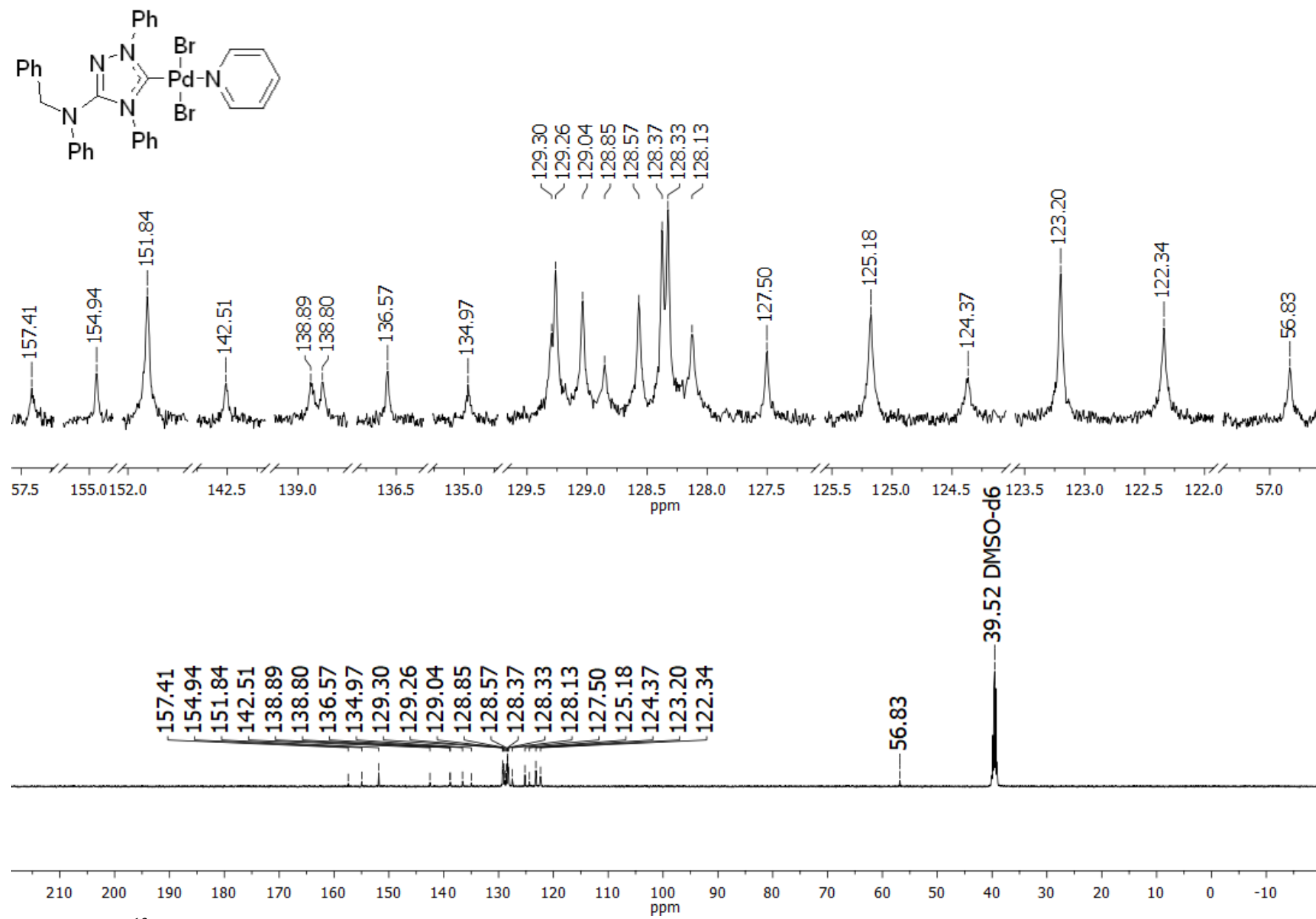
**Figure S92.** $^{13}$C NMR spectrum of compound **5a** (DMSO-$d_6$, 125 MHz)

**Figure S93.** $^1$H NMR spectrum of compound **5b** (CDCl$_3$, 300 MHz)
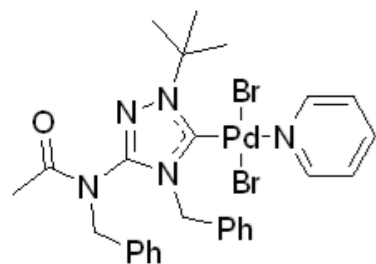
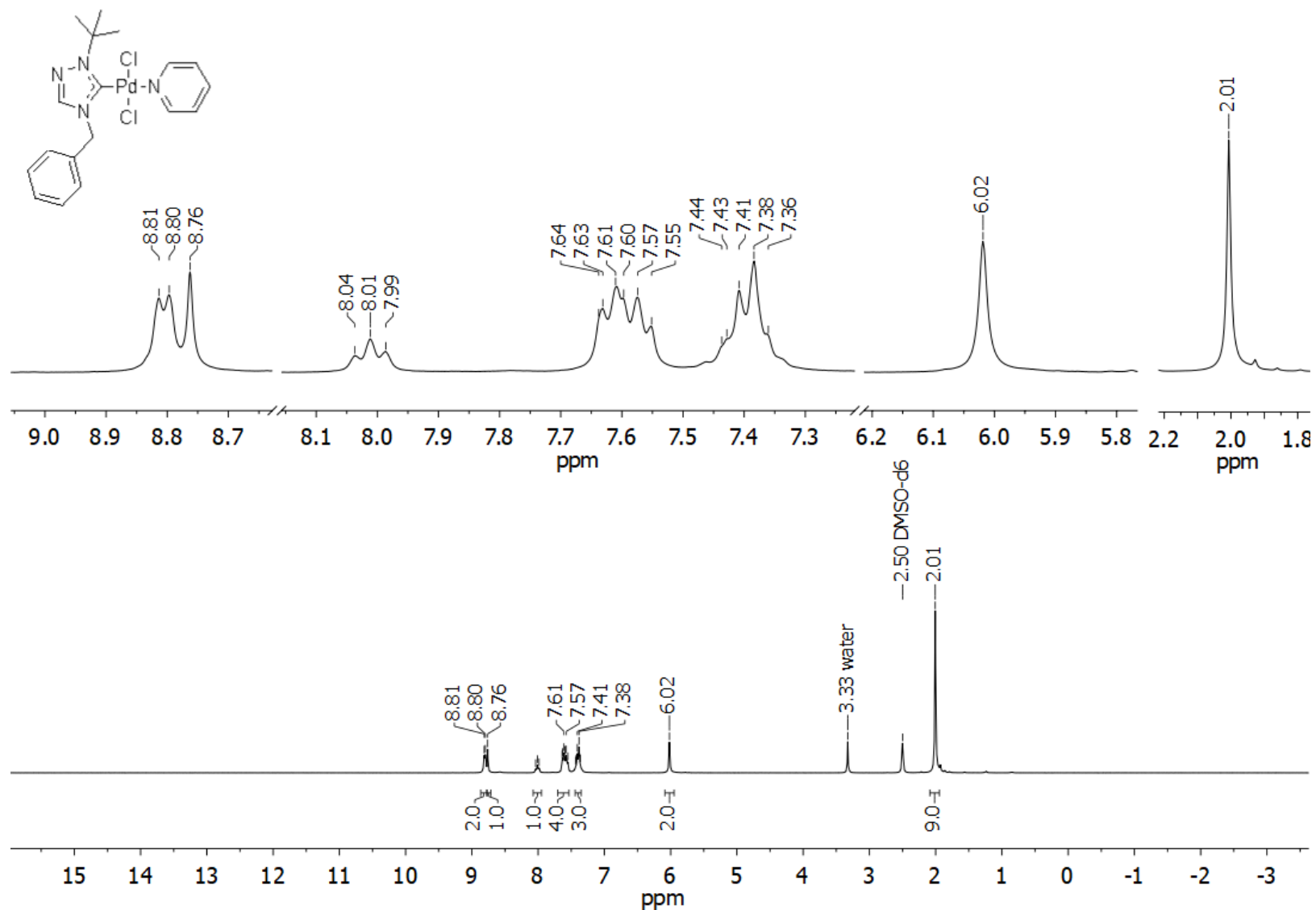**Figure S94.** $^{13}$C NMR spectrum of compound **5b** (CDCl$_3$, 75 MHz)
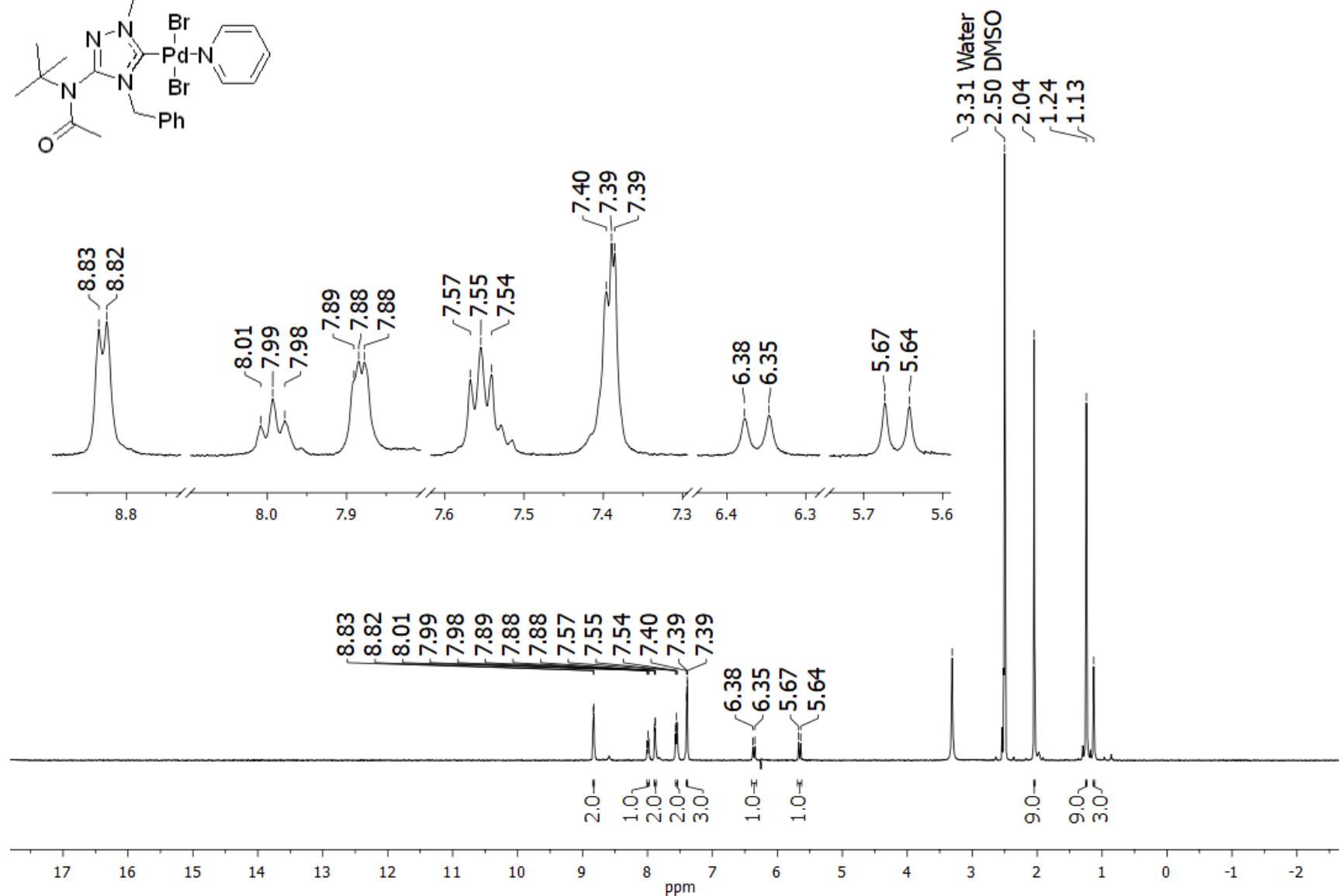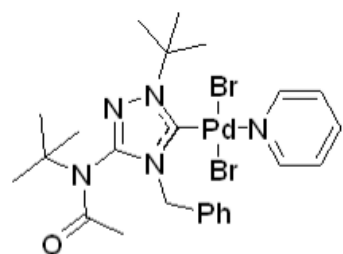
**Figure S95.** $^{1}$H NMR spectrum of compound **5c** (DMSO-$d_6$, 500 MHz)

105
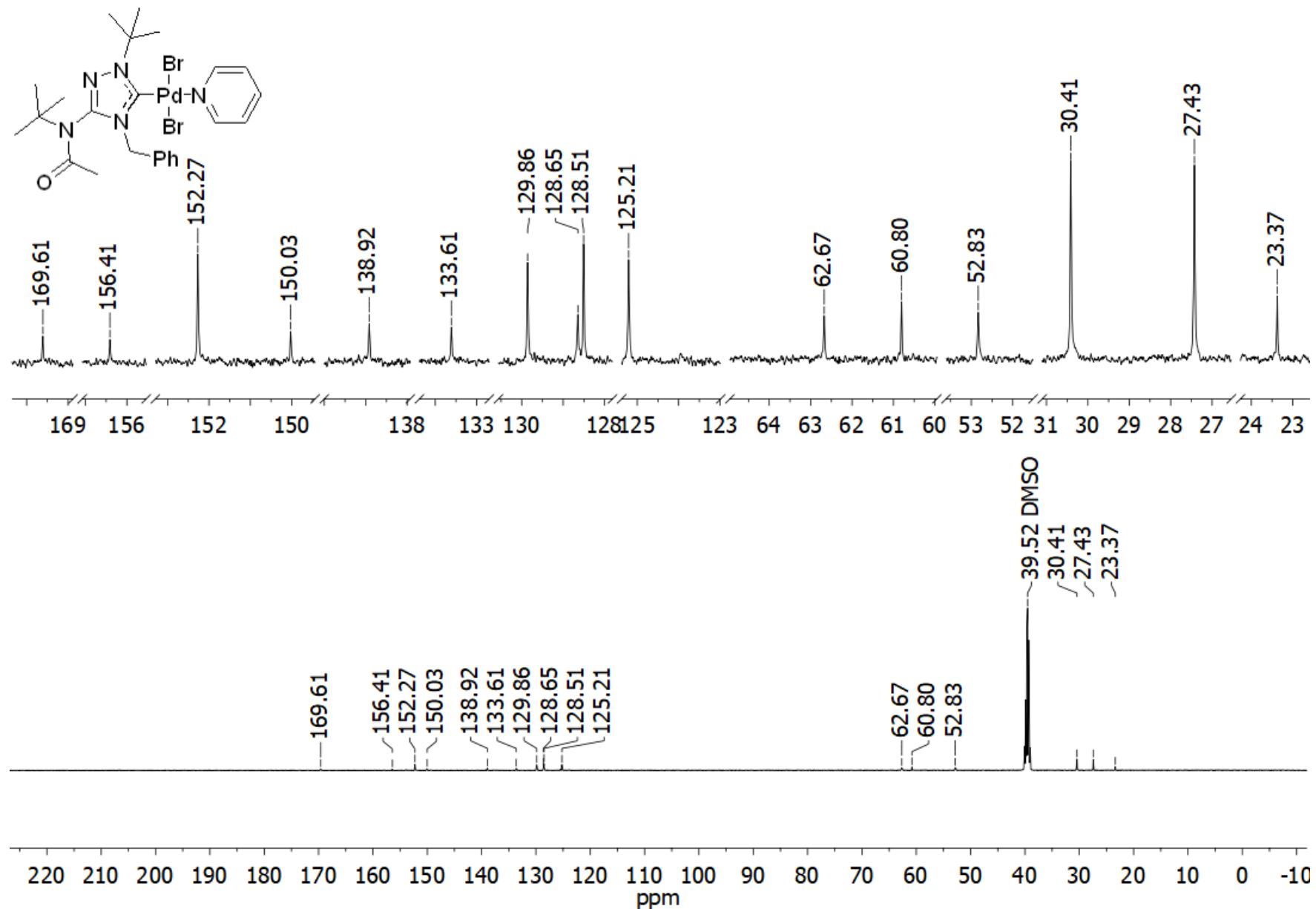
**Figure S96.** $^{13}$C NMR spectrum of compound **5c** (DMSO-$d_6$, 125 MHz)
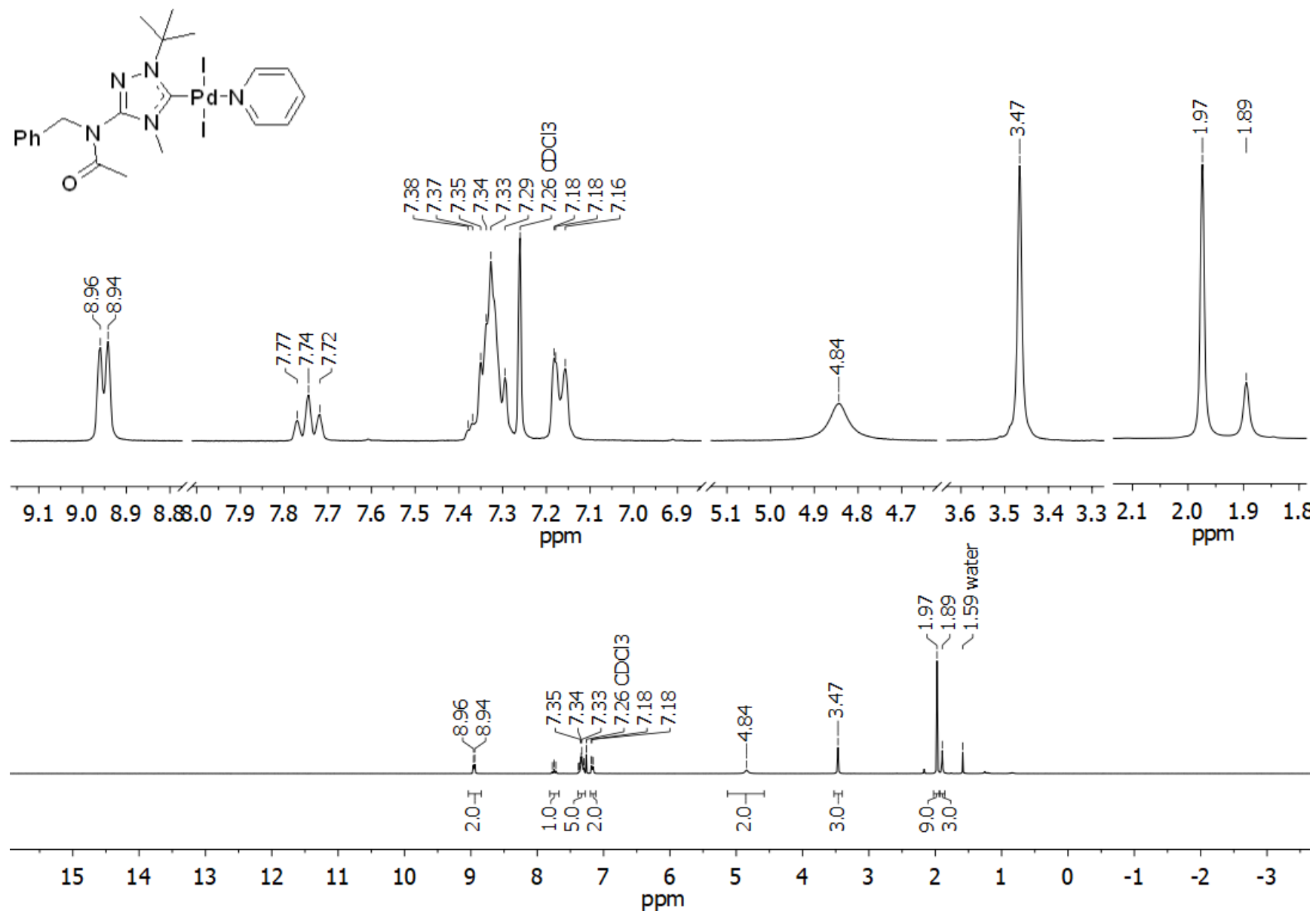
**Figure S97.** $^1$H NMR spectrum of compound **5d** (CDCl$_3$, 300 MHz)
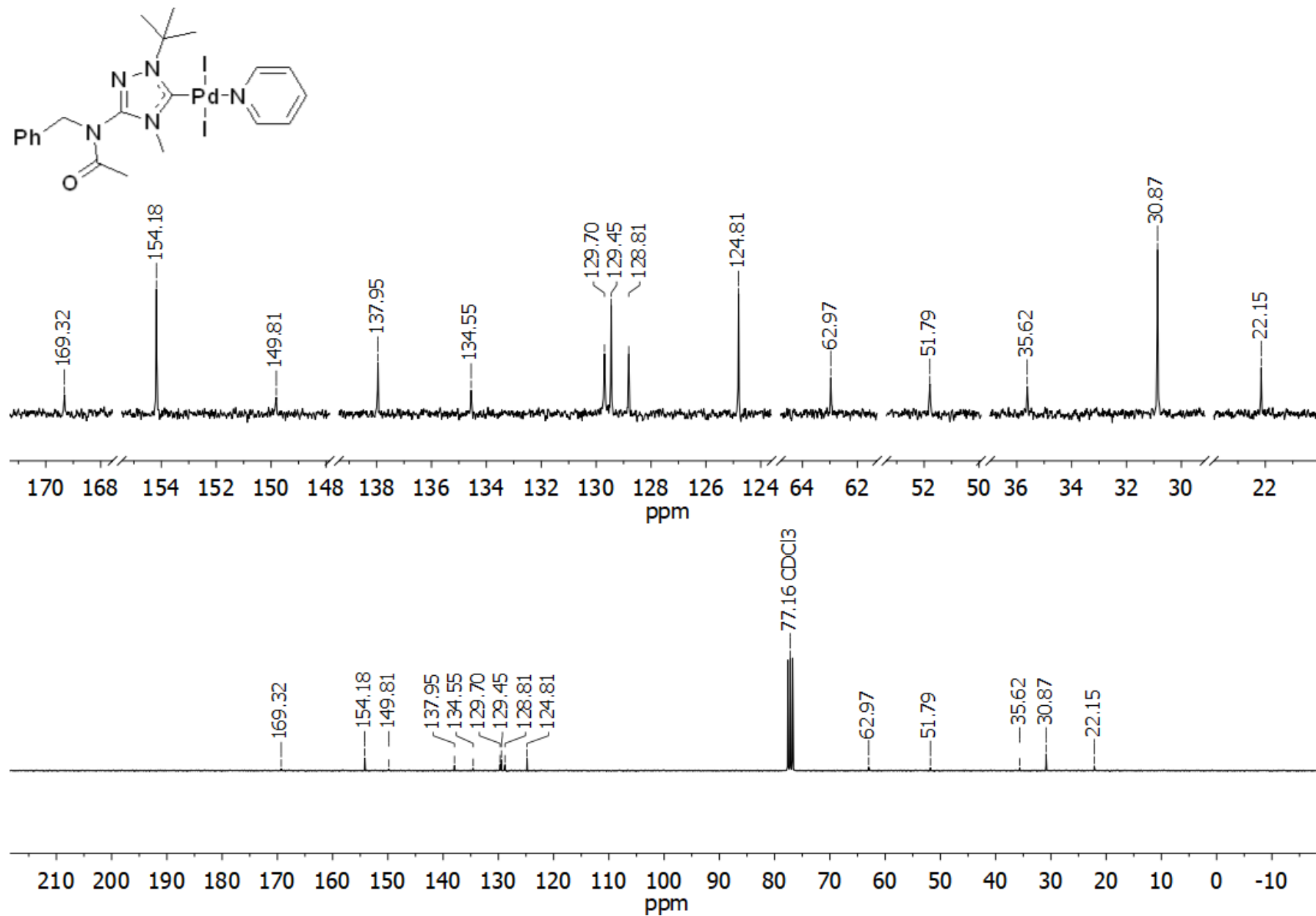
**Figure S98.** $^{13}C$ NMR spectrum of compound **5d** (CDCl$_3$, 75 MHz)

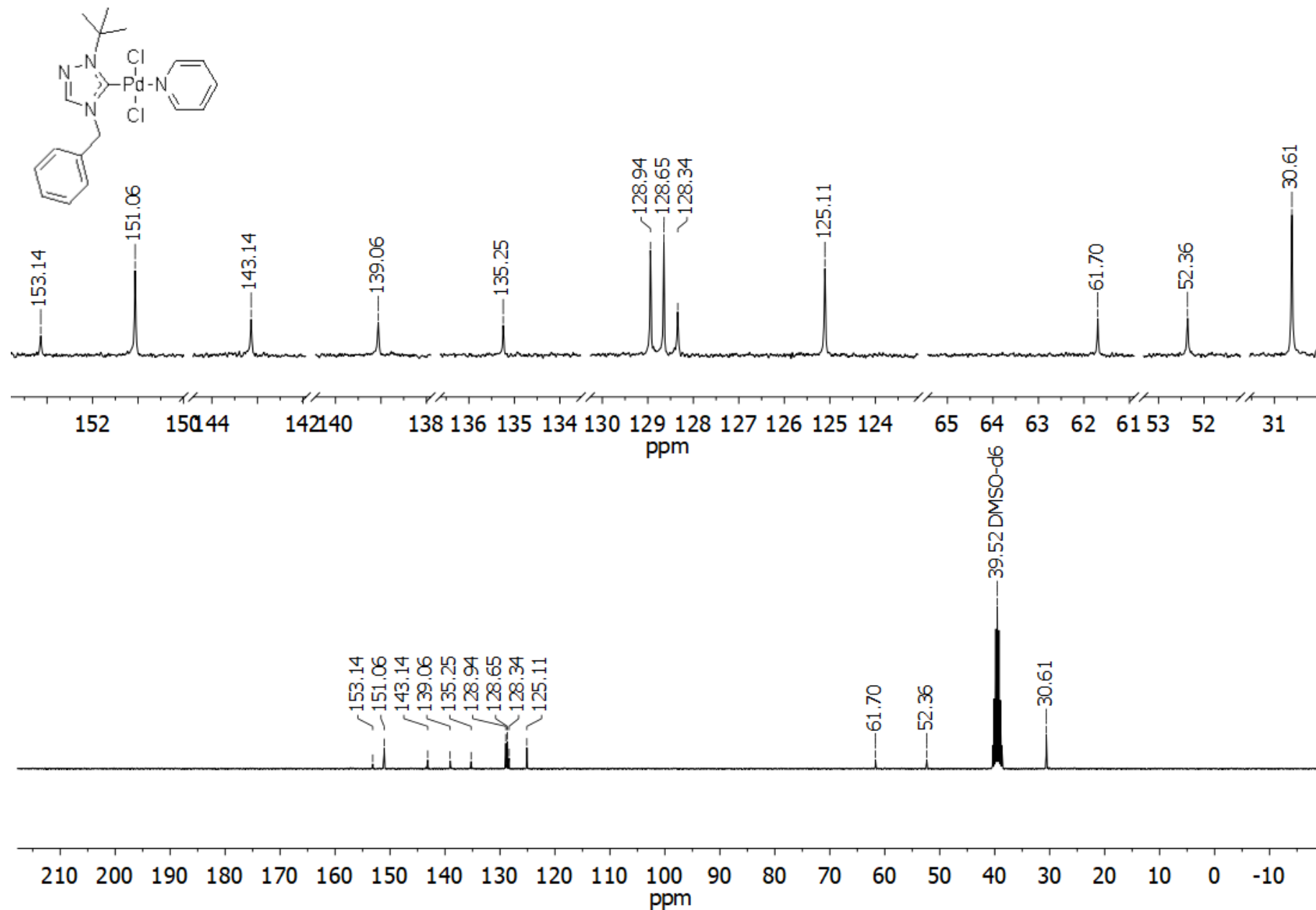**Figure S99.** $^1$H NMR spectrum of compound **6** (DMSO-$d_6$, 300 MHz)

**Figure S100.** $^{13}$C NMR spectrum of compound **6** (DMSO-$d_6$, 75 MHz)
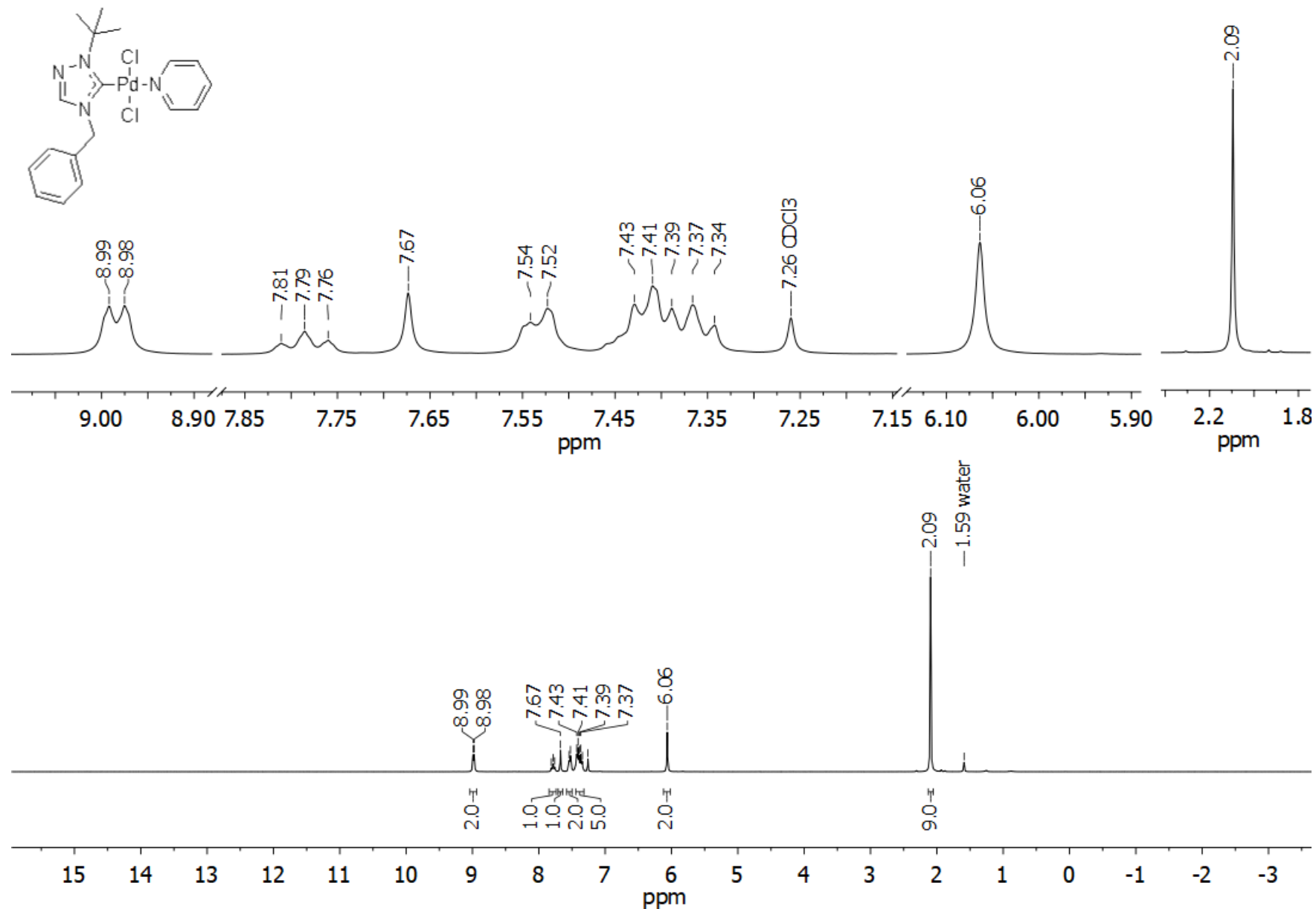
**Figure S101.** $^1$H NMR spectrum of compound **6** (CDCl$_3$, 300 MHz)
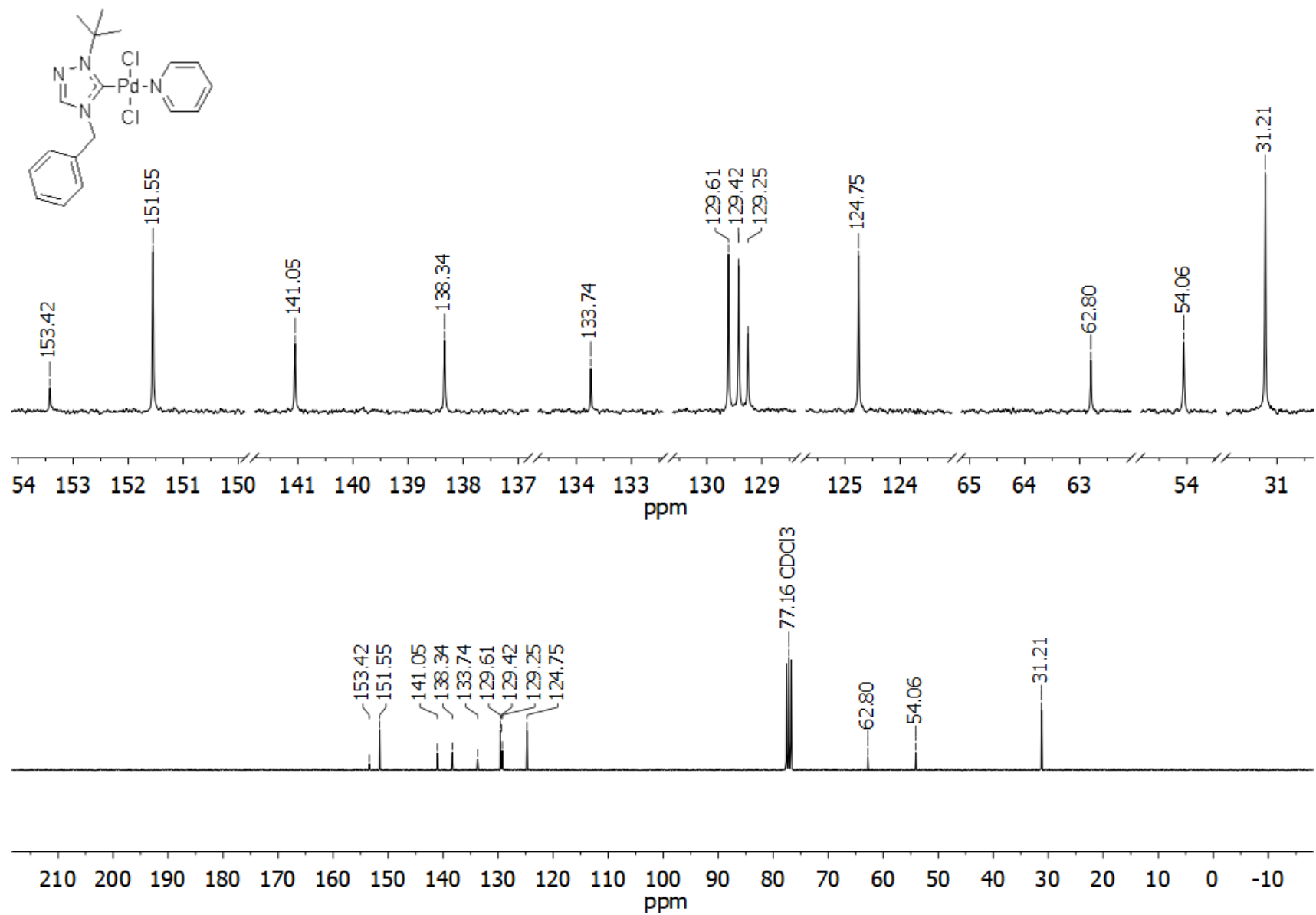
**Figure S102.** $^{13}$C NMR spectrum of compound **6** (CDCl$_3$, 75 MHz)
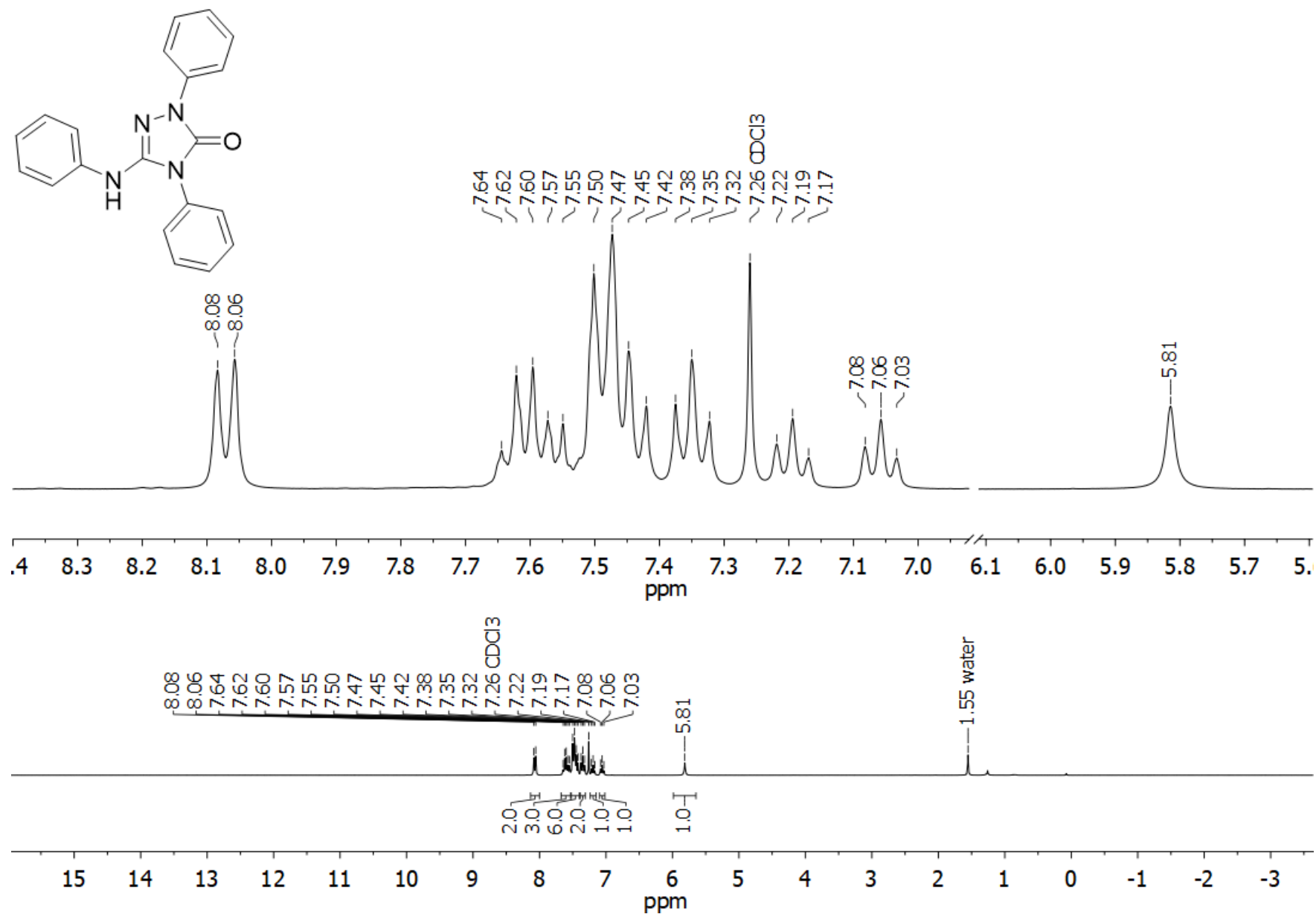
**Figure S103.** $^1$H NMR spectrum of compound **8a** (CDCl$_3$, 300 MHz)

113
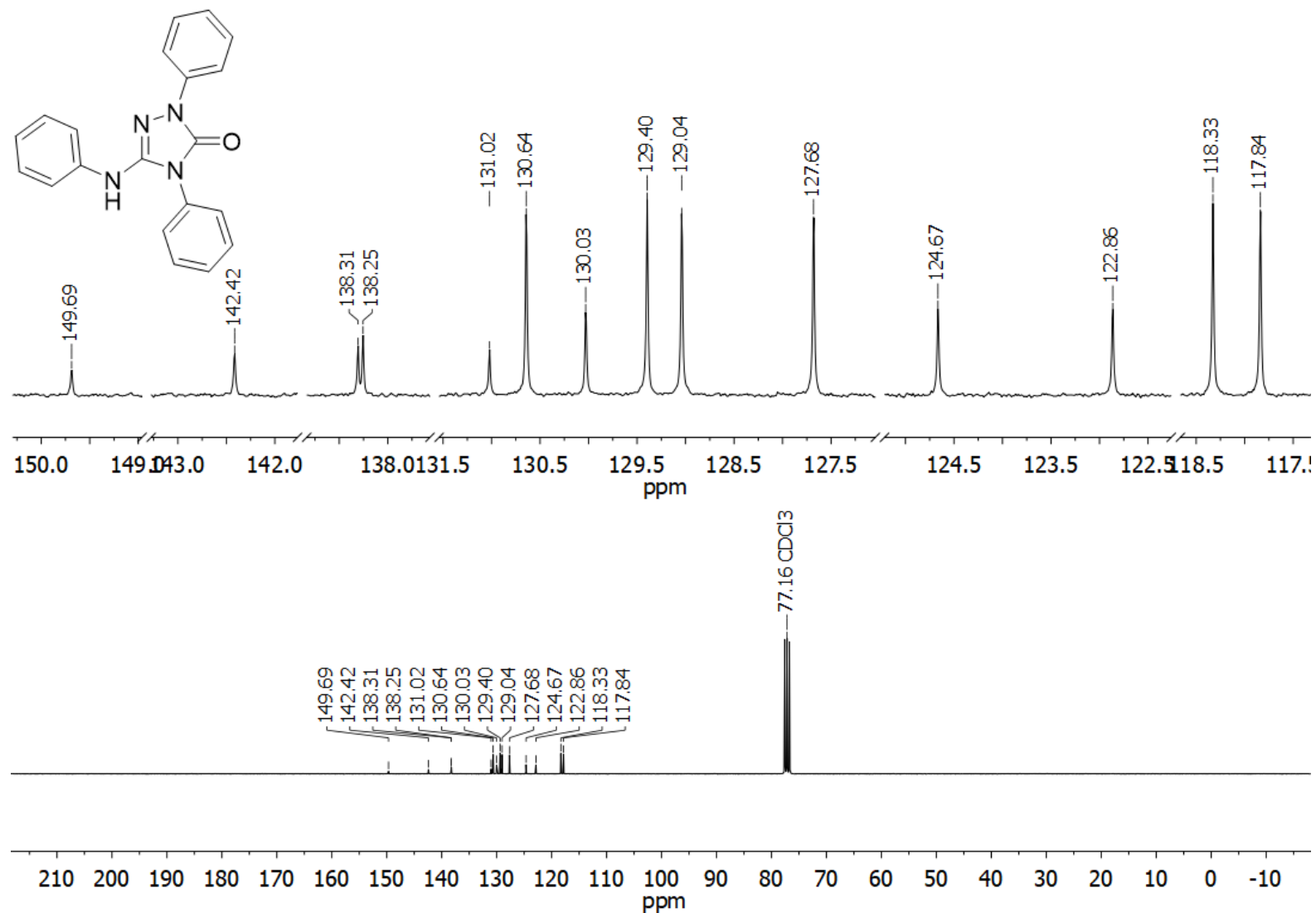
**Figure S104.** $^{13}$C NMR spectrum of compound **8a** (CDCl$_3$, 75 MHz)